Patterning Biological Material: A Microfabrication-Compatible Technique for Guiding the Growth of Neurons and Glia

Evangelos Delivopoulos

A thesis submitted for the degree of Doctor of Philosophy.

The University of Edinburgh.

March 2008

Abstract

This project proposes a novel and simple technique to pattern glia and neurons. The integration of neuronal patterning to existing MEA and patch clamp technologies necessitates the development of a microfabrication-compatible method which will be reliable and easy to implement. This study investigates various microfabrication friendly patterning systems and develops a highly consistent, straightforward and cost effective cell patterning scheme based on two common ingredients: the polymer parylene and horse serum.

The first part of this work describes the new patterning method and highlights its capabilities. Stripes of parylene on silicon thermal oxide (SiO_2) were fabricated in the cleanroom, cleaned and subsequently activated by horse serum in a simple dip and rinse procedure. Glia and neurons from dissociated rat hippocampi were cultured on the patterned substrate and imaged after 7 days *in vitro*. Standard cell culture and immunofluorescent imaging protocols were used. A comparison between experimental and control samples indicate that the protein load in horse serum is able to alter parylene into a cytophilic substrate.

The second part of this project focuses on the optimisation of the parylene based patterning method. Aspects, such as the sustainability of the cell patterns beyond the first week and the effect of glia division on the quality of the patterns are investigated. Furthermore, the reduction of the immersion time of the substrates in the horse serum is explored while a behavioural model for the cells during their first week in culture is proposed. Submersion in an alternative serum is examined while the effects of UV radiation on the parylene are revealed not to be contributing to cell patterning.

In the last part of this study an attempt is made to analyse the parylene and thermal oxide surfaces before and after immersion in the horse serum. An initial theory explaining the preference of cells towards parylene is disproved, while three probable hypotheses are proposed. Evidence from XPS analysis and electrophoresis gels suggests that the amount and conformation of proteins on the parylene and thermal oxide substrates might be responsible for inducing glial and neuronal patterning.

Declaration of originality

I hereby declare that the research recorded in this thesis and the thesis itself was composed and originated entirely by myself in the School of Engineering and Electronics at The University of Edinburgh unless otherwise specified.

Evangelos Delivopoulos

Acknowledgements

First, I would like to thank my supervisors Professor Alan Murray, for his constant support and guidance during my project and Dr. Tom Stevenson for helping me out in the Scottish Microelectronics Centre by doing all the pattern printing on the stepper and much more.

This project would not have been as successful as it was without Dr. John Curtis' scientific enthusiasm, keen intellect and attention to detail which he would call "covering all the bases". His mentoring and input in all of the biological procedures and protocols is priceless.

A very special thank you to Keith Baldwin who not only showed me the ropes in the Scottish Microelectronics Centre but also assisted far beyond the call of duty even when he had practically finished his Ph.D.

I would also like to thank Andrew Patterson for our long discussions on the proper way of analysing data and for leaving me his computer as well as Dr. Nikki MacLeod for offering me her lab and providing input to the project.

A lot of people at the Scottish Microelectronics Centre assisted me invaluably in my project. I would especially like to thank: Dr. Andy Bunting, for helping me oxidise all those wafers and insisting that I wear protective gear while "'playing"' with dangerous acids, Richard Blair for tirelessly coating my wafers with parylene and Alec Ruthven, for sawing all those wafers for me.

I would also like to thank Dr. Ronald Brown for showing me how to use the XPS machine in the Chemistry department, Linda Wilson for showing me how to use the confocal microscope, Professor Steve Chapman for allowing me to use the facilities in his lab and the transferable skills program for introducing me to LaTeX, a proper editing software.

Lastly, a big thank you to my mother Vasiliki, my father Stelios and my girlfriend Amirah for believing in me and encouraging me during my dark moments. I dedicate this thesis to them.

Contents

List of figures

List of tables

Acronyms

Acronyms

BSA	Bovine Serum Albumin
DIV	Days In Vitro
EBSS	Earle's Balanced Salt Solution
FBS	Foetal Bovine Serum
GFAP	Glial Fibrillary Acidic Protein
HS	Horse Serum
MEA	Multi Electrode Array
MEMS	Micro-Electro-Mechanical-Systems
PAGE	Protein Acrylamide Gel Electrophoresis
PDL	Poly-D-lysine
PDMS	Poly(dimethylsiloxane)
PEG	Poly(ethylene)glycol
SAM	Self Assembled Monolayer
SDS	Sodium Dodecyl Sulfate
SMAP	Selective Molecular Assembly Patterning
TFA	Trifluoroacetic acid
TO	(Silicon) Thermal Oxide
TVEMF	Time Varying ElectroMagnetic Field
UV	Ultraviolet radiation
XPS	X-ray Photo-electron Spectroscopy

Chapter 1

Introduction

1.1 The Brain and the Neuron

Despite the recent plethora of research and advancements in neuroscience the human brain still remains a largely unexplored scientific frontier. Comprehending the *modus operandi* of this sophisticated and complex organ is one of the ultimate challenges in biological sciences. Understanding of the human brain will not only allow us to utilise its design in various electronic equipment or combat some of the lethal diseases associated with it, but it will also permit us to explain how humans think, feel, learn and perceive.

The human brain, like every tissue and organ in the human body, consists of cells. The cells which constitute the brain are divided into two broad categories: *neurons and glia*. Within these two categories there are many types of cells that differ based on their structure, function, chemistry and purpose. The human brain has approximately 100 billion neurons and although this might seem like a large number, glia outnumber the neurons by tenfold. Despite their increased quantity it is not the glia but the neurons that act as protagonists in cognitive processes such as perception, decision making, sensing the environment and responding to stimuli. The role of the glia is thought to be mainly auxiliary, supporting neighbouring neurons by nourishing and insulating them. Perhaps, the simplicity of this popular theory is a good indication of our lack of knowledge on glial function. Nonetheless, the majority of current neuroscientific research focuses on 10% of brain cells, the neurons [1].

The function of isolated neurons has to a large extent been explored thanks to the pioneering work of Hodgkin, Huxley and Katz [2–5] regarding the ionic conduction of membranes. According to the established models the basic information processing currency in the brain is the action potential. The action potential, also referred to as a spiking event, is a sudden depolarisation and repolarisation wave of about 100mV in the resting potential across a neuron's membrane. This lasts approximately 1msec and is transmitted to other neurons via a cell process called the axon (figure 1.1). Axons form connections onto processes of other neurons called

dendrites, which can be seen in figure 1.1 as shorter, branching structures emanating from the cell body. These connections are called synapses and as figure 1.2 illustrates they consist of two parts: the pre-synaptic axon terminal and the post-synaptic dendrite which contain the synaptic vesicles and the receptors respectively. The action potential is thus transmitted from one cell to another, either electrically, via a gap junction, or chemically, via the release of synaptic vesicles to the synaptic cleft and their attachment to the receptors in the post-synaptic dendrite. This results in a post-synaptic potential that travels along the dendrite and is integrated together with further post-synaptic potentials arriving from other synapses (figures 1.3b and 1.3c). Depending on the neurotransmitters present at the synapse, the transmitted action potential either adds to the aggregate of post-synaptic events and is called **Excitatory** Post-Synaptic Potential or EPSP (figure 1.3a), or subtracts from the aggregate and is called **Inhibitory** Post-Synaptic Potential or IPSP. Subsequently, the aggregate of EPSPs and IPSPs travels to the soma of the recipient neuron where it will induce a new action potential if its amplitude is higher than a specific threshold [1].

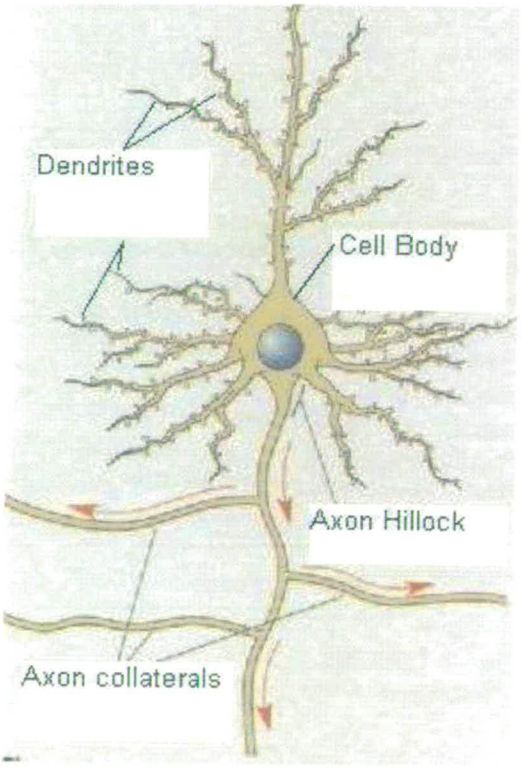

Figure 1.1: *A neuron, its axon (bottom) and its dendrites (top and sides). The action potential travels along the axon and the axon collaterals (arrows) to the dendrites of other neurons. Image taken from [1].*

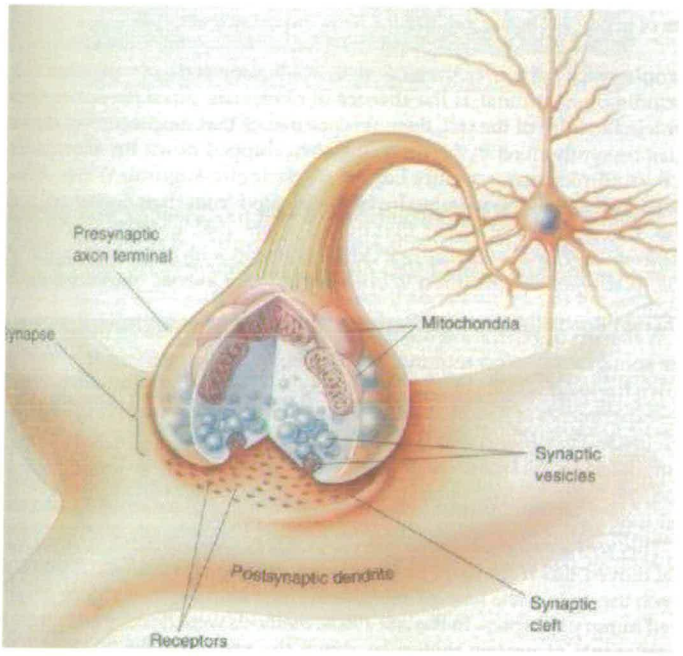

Figure 1.2: *A synapse and its structure: the pre-synaptic axon terminal attaches to the post-synaptic dendrite. Image taken from [1].*

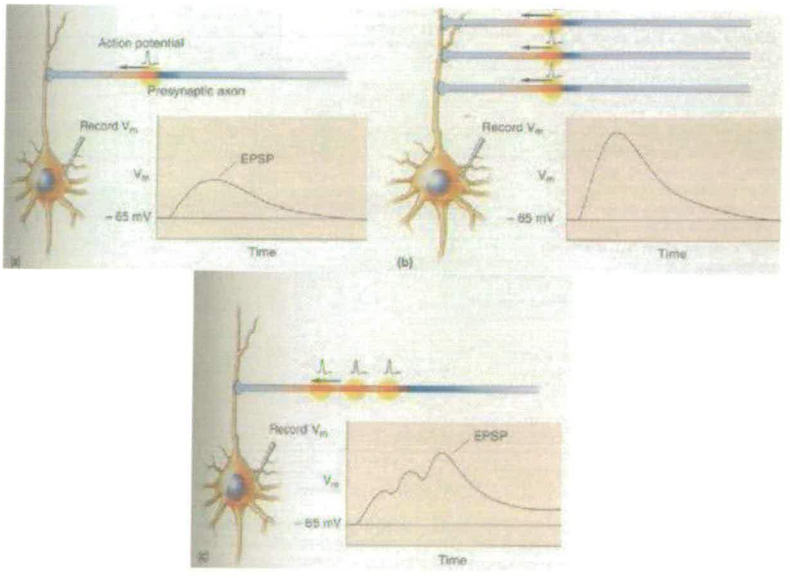

Figure 1.3: *EPSP summation. (a) An Excitatory Post Synaptic Potential. (b) The action potentials arrive at the same time from different axons and thus the individual EPSPs contribute to the depolarisation of the membrane potential. This is called spatial summation. (c) When the same axon transmits a quick succession of action potentials the individual EPSPs are again added together. In this case the summation is temporal. Image taken from [1].*

1.2 Networks of Neurons and the Importance of *in vitro* Cultures

The systematic research and scrutiny of individual neurons has led to the development of a robust model of neuronal operation. Nonetheless, the interaction and function of ensembles of neurons remains largely a *terra incognita*. Little is known about the dynamic behaviour of neural networks or the method by which they process information. The majority of research in this field involves either *in vivo* investigation of specific brain areas [6], *in vitro* experiments using slices taken directly from the brain and studies of primary dissociated neuronal cultures [7]. In these cultures, neuronal tissue is collected and dissociated without damaging the neurons which are subsequently cultured in medium on an appropriate substrate.

Despite the skepticism as to whether the morphology of neurons and the synaptic connections and topology of two-dimensional neural networks *in vitro* will actually be similar to those found in the brain [8], primary cultures of neurons are producing great advancements in our understanding of network behaviour [9, 10]. They are utilised constantly as they are simpler to carry out and sustain compared to brain slices or *in vivo* experiments and constitute imaging experiments easier hence offering the ability to visualise the cells. In addition, they allow gene manipulation, cell growth and cell differentiation experiments to be performed. Cultured neural networks may offer insight not only into the principles of neuronal computation, but also to neuropathogenic disorders such as Alzheimer's disease, epileptogenesis [11] and schizophrenia. In addition, synaptic formation and cell behaviour may be monitored and their effects on network formation studied by manipulating the environmental conditions during culture. Finally, cultured networks may highlight the extent to which the brain is "hard-wired", a recurrent question in the field of neuroscience. Existing research suggests that *plasticity* is prevailing in the brain as synaptic connections become reinforced or deteriorate depending on their use or disuse, a process which is also known as synaptic learning [12].

In order to obtain information regarding the function of individual neurons and subsequently the operation of neural networks, conductive electrodes are utilised to detect and record electrical signals generated in the neurons. The recording method is either intracellular, in which case the electrode gains access to the interior of the neuron (sharp glass micropipettes, patch-clamping) [13] or extracellular, in which case the electrode remains outside the neuron but in close proximity (MEAs) [14]. Both intracellular and extracellular techniques have their distinct advantages and drawbacks. Briefly, extracellular techniques are easier to execute and are less damaging to the cells thus, may be employed for longer time spans. In addition, with the

emergence of Multi Electrode Arrays (see figure 1.4), devices which have typically up to 60 or more electrodes, a significant amount of data can be gathered from multiple neurons, shedding more light onto neural network behaviour (eg. circadian rhythms and differentiating firing patterns in dissociated cell cultures of hippocampal neurons) [15, 16]. On the contrary, intracellular techniques are more complex and damage the neuron substantially, as its membrane gets penetrated. Moreover, intracellular recordings are often limited to a small number of neurons, to this date up to three neurons have been recorded from simultaneously with conventional techniques [17], primarily due to issues involving the dimensions of neurons compared to the dimensions of the apparatus used. Nonetheless, they have two important advantages compared to extracellular recordings. First, the recorded activity can be associated with absolute certainty to the monitored neuron. Second, intracellular recordings can detect not only spiking events, like extracellular techniques, but sub-threshold activity (EPSPs and IPSPs) as well.

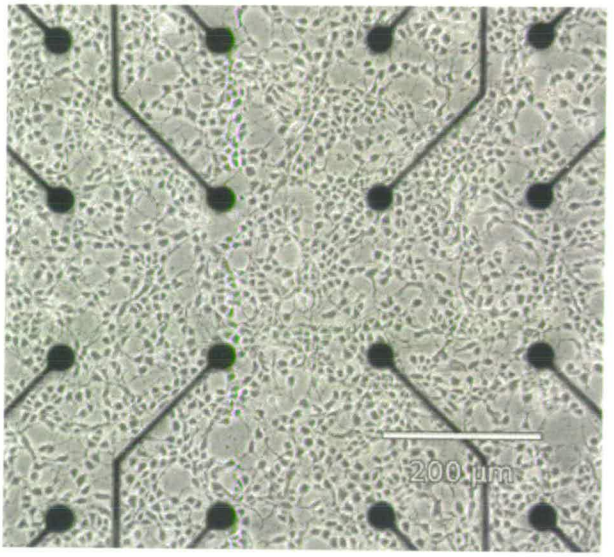

Figure 1.4: *Example of an in vitro culture grown on a Multi Electrode Array. From Wagenaar [14].*

At the University of Edinburgh a project has been undertaken to produce a device which would enable intracellular recordings of multiple neurons, by integrating an intracellular recording technique known as "patch-clamp" on silicon based microchips [18, 19]. As can been seen in figure 1.5 the intention has been to culture a patterned neural network on a planar patch-clamp device with multiple patch-clamp sites and subsequently perform recordings. The current study is part of the greater planar patch-clamp project and one of its aims has been the development of the neural networks that were necessary for the recordings.

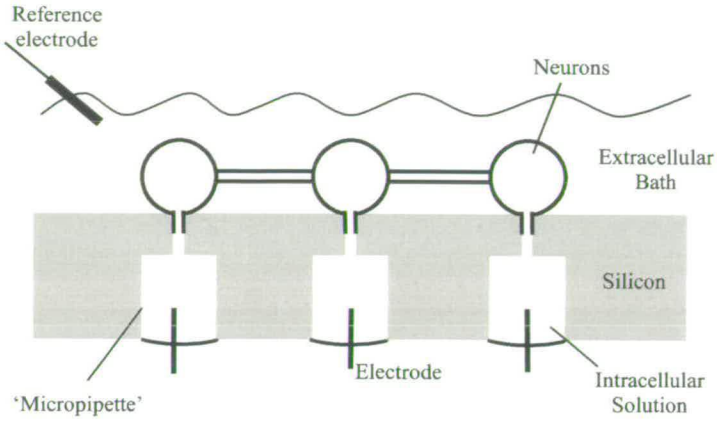

Figure 1.5: *The proposed planar patch clamp setup. From Keith Baldwin, 2006 [19].*

1.3 Cell Patterning and its Contribution

As mentioned previously, cultures of neurons *in vitro* may advance our understanding of neural network behaviour greatly. However, if we are to comprehend systematically how neurons interact in large numbers or how the topology of neural networks affects their operation, the data derived from our recordings needs to be mapped to and associated with individual neurons and even individual synapses. In other words, knowledge of the firing patterns of neurons in two different areas is not as complete or valuable, without the information encoded in the topology or the connections between these neurons, as well as the sub-threshold events occurring at their synapses and dendrites. Cell patterning, a technique of manipulating brain cells and forcing them to grow and connect in specific predetermined schemas, offers an opportunity to shed more light into these areas and improve the application of existing techniques such as the MEA.

Patterned cell cultures offer great insight into cell behaviour. Specifically, neuronal patterning can offer clues into the properties of neurons, their growth and the biological signals they encounter during development. Early work with simply patterned neuron cultures helped illustrate the interactions between neurons and cardiac myocytes by limiting the number of connections between the two cell types [20]. Similarly, patterned neural networks allow for a greater scrutiny of the synapse, due to the limited number of connections between neurons, as well as neuronal activity [21], which in turn assists in a better understanding of memory and learning processes such as Long Term Potentiation. In addition, directed cell growth is often utilised in the research for prosthetic devises and implants such as, retinal prosthesis interfaces [22] or the silicon based neurochip proposed by Fromherz [23, 24].

A variety of different cell patterning methods exist. They will be discussed in detail in chapter 2 where their distinct advantages and shortcomings will also be highlighted. In short, some of the most popular methods include:

- microcontact stamping
- inkjet printing
- photolithographic techniques
- selective molecular assembly patterning (SMAP)
- microfluidics
- physical immobilization
- real-time manipulation

Whereas all of these techniques have strengths and are utilised on different occasions depending on the specific patterning requirements, most of them involve multiple steps some of which are quite complex. Moreover, the majority of protocols involve the substantial use of biological agents, while those that do not, cannot often offer high quality patterning. In addition, it is rather difficult if not impossible to incorporate the patterning techniques currently available into the micro-fabrication processes necessary to build the planar patch-clamp device. Therefore, a new cell patterning technique was required which would ensure the following:

- neuronal patterning should be effective and reliable
- the method should be suitable for mass production
- the patterning method must be simpler than existing techniques while the quality of the patterning should be at least equal to, if not better than the best existing patterning methods
- the patterns should be fully effective even after prolonged periods of storage
- the patterning procedure should be feasible to carry out within a cleanroom facility and be compatible with cleanroom protocols and requirements which would include:

a exclusion of biological and other materials such as gold which are unusable in a standard cleanroom

b any materials used should adhere firmly to silicon

- the technique should be embeddable into any MEMS or chip manufacturing process. It should be feasible to integrate the pattern directly onto a device (MEA, planar patch-clamp etc.) rather than dealing with alignment issues later
- the technique should not have high temperature requirements to avoid damage to underlying structures

Taking the above aims into account and considering the crucial role of proteins into cell behaviour and guidance, this project set out to:

Develop the simplest possible photolithographic technique for patterning neurons and glia, that can be integrated with silicon microchip/MEMs technology, MEAs and planar patch-clamp structures.

The next chapter of this thesis will present the existing cell patterning techniques and describe the current progress in this field.

Chapter 3 describes the development of the novel patterning technique and demonstrates the high quality patterning results.

Chapter 4 discusses the experiments performed to optimise the patterning protocol.

Chapter 5 details the experiments undertaken to investigate the causes of patterning.

Finally, chapter 6 is a summary of the thesis and draws conclusions on the new cell patterning technique. It also suggests further work in this area and on the technique.

1.4 Publication Patents and Exploitation

From the onset, it was clear that this work was likely to generate knowledge that has significant commercial value. This was confirmed by the results in chapters 3-5 and as a result, the work has not yet been submitted for external publication.

Chapter 2

Background

2.1 Introduction

This chapter summarises the various categories of patterning techniques that have and are currently employed by researchers. A brief explanation of the patterning methods within each group is provided, as well as a critical assessment of the advantages and disadvantages of each strategy and the caveats under which it may be employed. At the end of the chapter, our investigation into cell patterning is briefly outlined, while the necessities that compelled us to choose a specific scientific path are explained. Finally, comparisons are drawn between our patterning method and the already established schemes, in order to arrive at a classification of our technique under one of the presented patterning strategies.

2.1.1 Important Characteristics of a Patterning Technique

When critically assessing a patterning method, one usually examines some, or all, of its following aspects:

- the quality of the cell patterning
- the flexibility in changing the fabricated patterns
- the compatibility of the technique with other technologies and processes
- the biocompatibility of the utilised substrates
- the simplicity of the method and the difficulty of the manufacturing process
- the resolution of the pattern
- the cost of the patterning technique
- the ability to reuse the fabricated substrates

- the longevity of the cell patterns
- the potential for mass manufacturing of the substrates

To this date, no single patterning method manages to excel in all of the above qualities forcing researchers to make compromises by prioritising the aspects that are important in their work. Some of the patterning schemes, such as micro-contact stamping, are prevalent mainly due to their simplicity, flexibility and low cost, while other more complicated methods are utilised only under specific circumstances. The most common cell patterning strategies that will be examined are:

- microcontact stamping
- inkjet printing
- physical immobilization
- real time manipulation
- microfluidics
- photolithographic techniques
- selective molecular assembly patterning (smap)

This categorisation follows Franks' review of cell patterning techniques [25].

2.2 Microcontact Stamping

Microcontact stamping is a technique originating in the group of George Whitesides at Harvard University [26]. It entails the use of photoresist to form structures on a silicon substrate called the master pattern. Subsequently, a prepolymer, typically of PDMS, is cast against the master pattern to create an elastomeric stamp with a complementary relief pattern, as illustrated in figure 2.1(a). The stamp is then "inked" either with an alkanethiol or with proteins directly [27]. In the former case, Self Assembled Monolayers (SAMs) can be formed by bringing the stamp into conformal contact with a gold surface [28], to utilise the common gold-thiol reaction:

$$R\text{–}SH + Au(0)_n \rightarrow RS\text{–}Au(I)Au(0)_n + \frac{1}{2}H_2 \text{ [25]}$$

where R is the functional group, such as a methyl group, to which the proteins will adhere (the brackets next to the Au symbol refer to the oxidation state of gold). The gold substrate is then rinsed with a second alkanethiol, R'-SH, which has a protein repellent functional group (R') such as oligo(ethylene glycol) ($(CH_2)_{11}(OCH_2CH_2)_3OH$). This alkanethiol binds to the unbound regions of the gold substrate creating a high contrast protein adhesion pattern as shown in figure 2.1(b). Lopez et. al investigated the adsorption of proteins such as fibronectin and fibrinogen on SAMs and demonstrated that proteins adhered at the methyl groups only [29]. Subsequently, Mrksich showed that bovine capillary endothelial cells adhered only to the adsorbed proteins [28].

As mentioned before, proteins can be stamped directly onto the substrate with the PDMS stamp. In such a case, the quantity of the deposited proteins is similar to that adsorbed in the SAMs however, protein bioactivity can be compromised when outside of solution, which is the case during microcontact stamping.

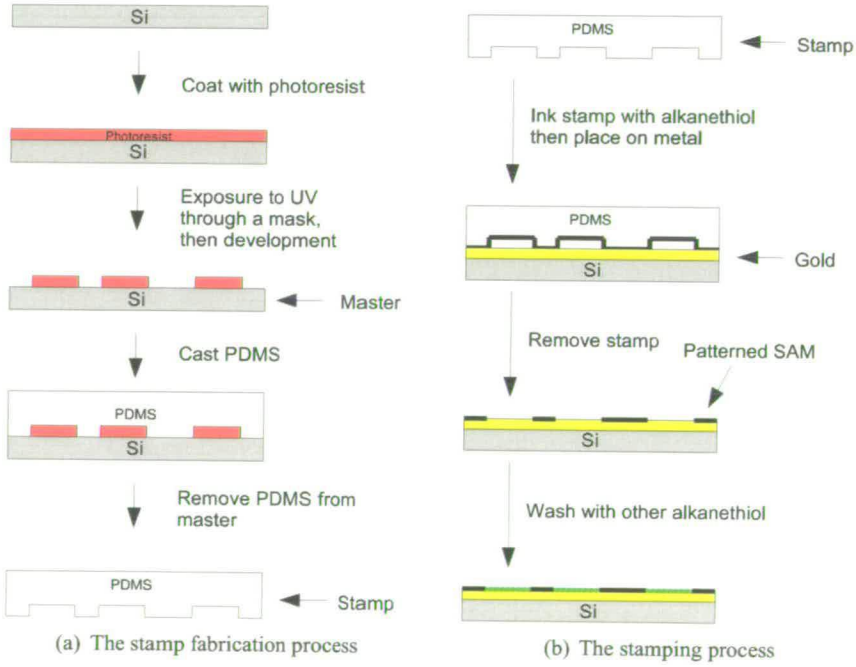

Figure 2.1: *The stamp fabrication process and the stamping procedure during microcontact stamping.*

2.2.1 Advantages and Problems of the Technique

The main advantage of microcontact stamping is its simplicity. Once the stamps are manufactured the technique is very easy to implement without the need for any complicated equipment or a cleanroom facility. In fact, if the size of the features on the stamp is greater than 20μm, a cleanroom is not necessary for the stamp fabrication either, as a high quality laser printer can be utilised to create the mask through which photoresist areas on the substrate are exposed. Moreover, depending on the surface chemistry, good quality patterned cell cultures can last up to 3 weeks [30], while the resolution of the patterns can range from 2 to 500μm [31]. Finally, the technique is inexpensive, as the stamps can be used multiple times without noticeable degradation in their performance [31].

On the other hand this patterning method is not very flexible. Although a researcher can experiment with various SAM molecules, substrates and proteins, once a stamp is created it cannot be modified. An alteration of the pattern geometry requires the stamps to be redesigned. In addition, the possibility of denaturation during protein stamping obliges the researcher to use SAMs, which are more complicated and include additional protein deposition steps. Most importantly however, microcontact stamping is not very compatible with MEAs and cannot be easily incorporated into the patch-clamp device experiments due to the required alignment of the stamps with underlying electrodes and patch-holes. Finally, the potential for market applications and mass manufacturing of microcontact stamping is very limited, as each patterned substrate has to be stamped individually.

2.3 Inkjet Printing

Inkjet printing is a fast and highly flexible method for cell patterning, which entails the modification of a printer cartridge to deposit small quantities of cell adhesive or cell repulsive substances. The desired pattern is stored as software in the computer, which robotically controls the print head in two dimensions. Adhesive and repulsive mediators are dispersed through the orifice of the print head onto the substrate, which lies stationary underneath (see figure 2.2). Sanjana and Fuller successfully employed this technique to deposit a mixture of collagen and PDL (adhesive) onto a poly(ethylene)glycol (PEG) background (repulsive) [32]. Similarly, Turcu printed a solution of laminin and Vinnapas (a co-polymer of vinyl acetate) patterns on glass, silicon, gold and carbon substrates [33].

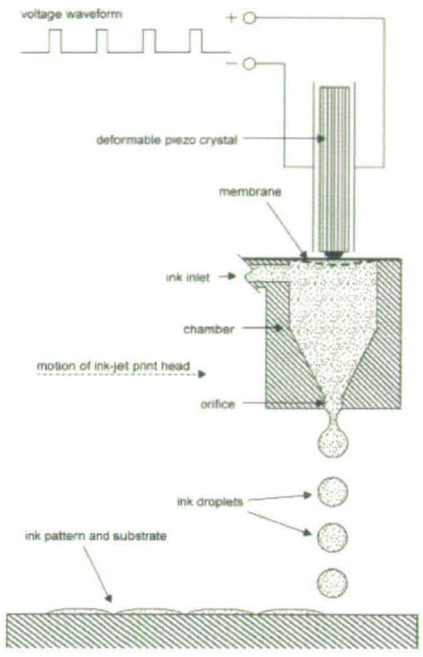

Figure 2.2: *Diagram of the inkjet print head depositing adhesive mediators on the substrate underneath. Figure taken from Sanjana et. al. [32].*

2.3.1 Advantages and Problems of the Technique

The digital format in which the pattern is stored makes this technique highly flexible. Any modifications to pattern geometry are implemented on a software level, while new adhesion mediators and substrates can easily be adopted. Thus, inkjet printing is ideal for conducting research into various pattern geometries and adhesion chemistries. In addition, the process is easily executed once the printer is assembled and yields good quality patterning that lasts up to 25 days when an inhibitory background is used [32]. Finally, the cost of the method is low and can be tailored to the needs of the researcher.

Nevertheless, the pattern resolution of inkjet printing is limited. Although Sanjana and Fuller believe the technique can achieve resolutions up to 30μm, which is the dot size of the best commercially available inkjet printer, they demonstrated patterns of 65μm [32]. However, even if a resolution of 30μm could be achieved it would still be far from the sub-micron resolutions other patterning schemes accomplish. Therefore, fine detail patterning, such as axonic or dendritic guidance, can not be easily performed with inkjet printing. Furthermore, as Sanjana and Fuller point out, the printing speed is relatively slow, since each ink droplet has to be allowed to dry on the surface before the next one is dispensed. Therefore, this technique is not suitable for

complex or repetitive patterns, due to the amount of time it would take to print. Consequently, the potential for commercial exploitation of the technique and mass manufacturing of the patterned substrates is rather limited. Finally, inkjet printing can not be easily integrated into other technologies, such as our patch-device or MEAs, due to additional alignment requirements.

2.4 Physical Immobilisation

Physical Immobilization is a general term used to describe a group of cell patterning techniques that revolve around the manipulation of the culture substrate to induce cell guidance. Patterning schemes in this category range from the fabrication of 3D structures, such as cages and pillars to trap cell bodies, to the modification of surface roughness and topography in order to provide adhesive areas to cells. For example, Maher manipulated individual neurons with glass pipettes into the neurochip wells of figure 2.3(b), made from silicon and silicon nitride. As seen in figure 2.3(a) platinum electrodes were fabricated at the bottom of the wells in order to record and stimulate individual neurons, similarly to MEAs [34]. A cross section and a schematic of the Maher's neurochip are provided in figure 2.4. Likewise, Zeck and Fromherz immobilised *Lymnaea stagnalis* snail neurons with picket fences made from polyimide (see figure 2.5). They achieved a silicon-neuron-neuron-silicon circuit through non invasive capacitive coupling between electrode and cell [24].

The effects of surface topography on neuronal development and behaviour have also been examined. Dowell et. al. cultured hippocampal neurons on PDL coated fields of pillars of varying geometries. It was shown that axonic and dendritic orientation and length were affected by the topographic features, as neuronal processes grew orthogonally on dense pillar fields and randomly on smooth surfaces [35]. Similarly, Britland et. al. examined the effect of grooves and ridges fabricated on silicon substrates, on the growth of nerve cells. They concluded that neurons respond to such features when their dimensions are above 1μm and that surface cues can act in concert with adhesive cues in neuronal guidance [36]. It has also been proposed that surface roughness can induce cell patterning. Fan et. al. demonstrated that when the average surface roughness (Ra) of silicon substrates ranged between 20 and 50 nm, cultured cells had normal morphology and growth, whereas on silicon substrates with Ra less than 10nm or greater than 70nm cells adhered poorly [37].

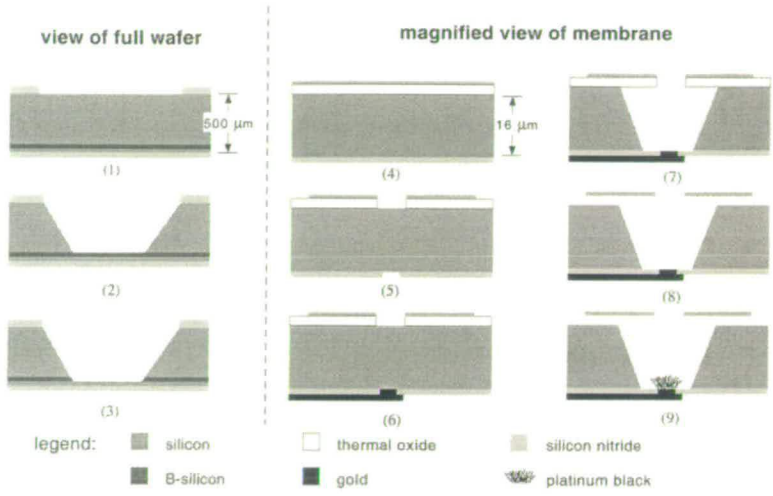

(a) The fabrication steps of the "Neurochip"

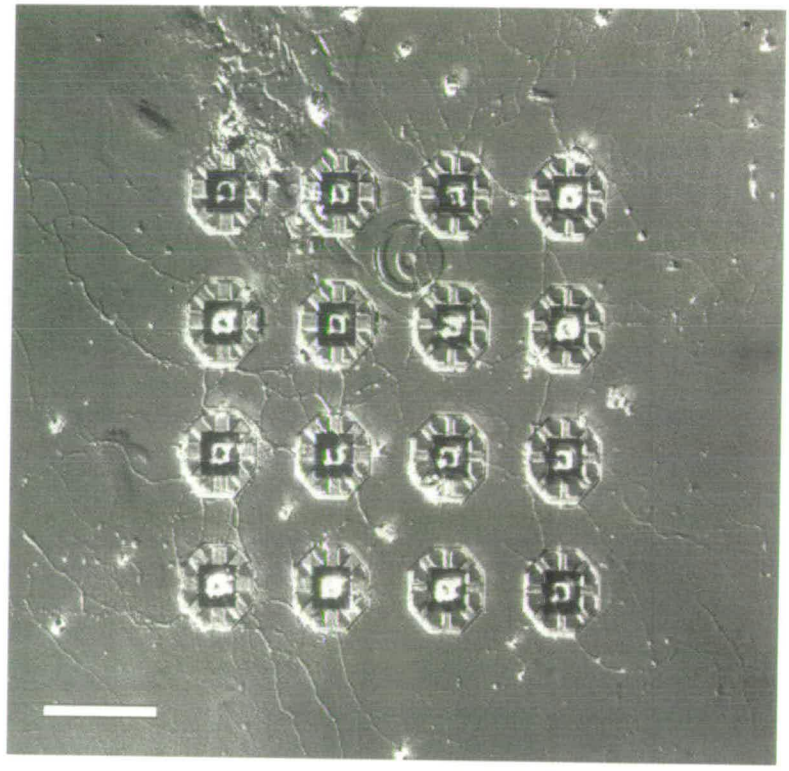

(b) A culture of hippocampal neurons and glia on the "Neurochip"

Figure 2.3: *The "Neurochip". Images taken from [34].*

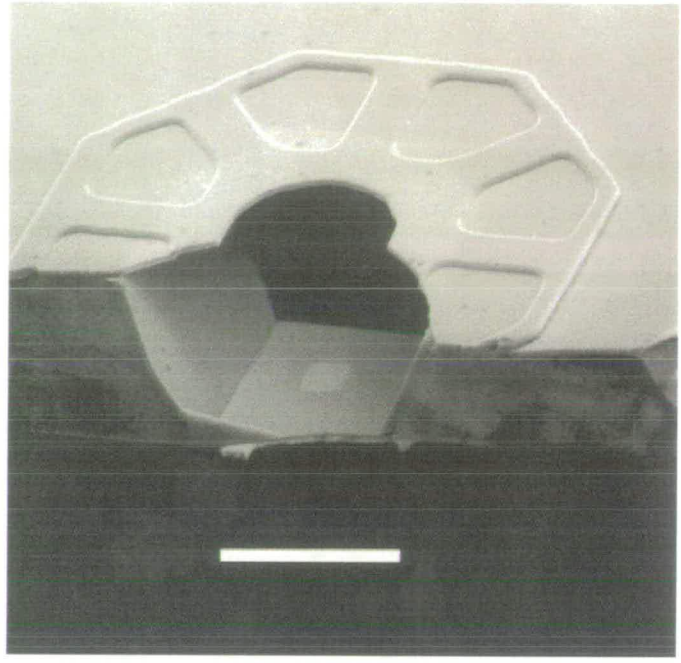

(a) SEM of the cross section of a "Neurochip" well

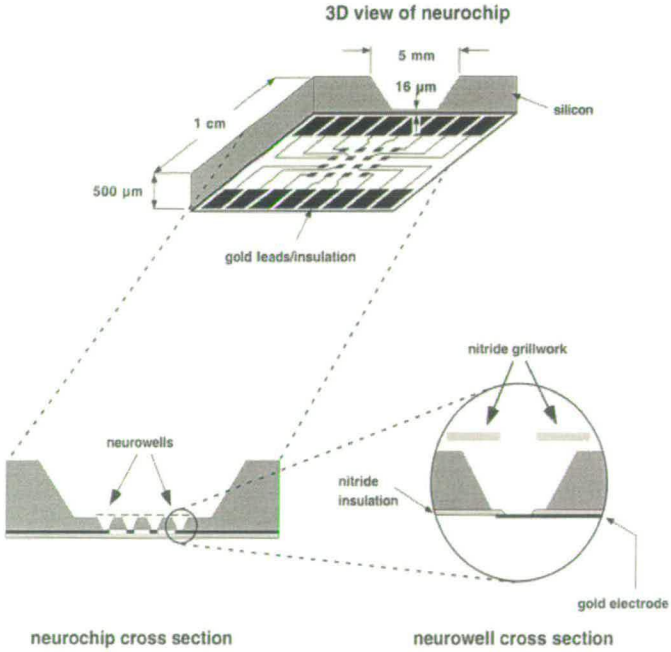

(b) Schematic drawings of the "Neurochip"

Figure 2.4: *The "Neurochip". Images taken from [34].*

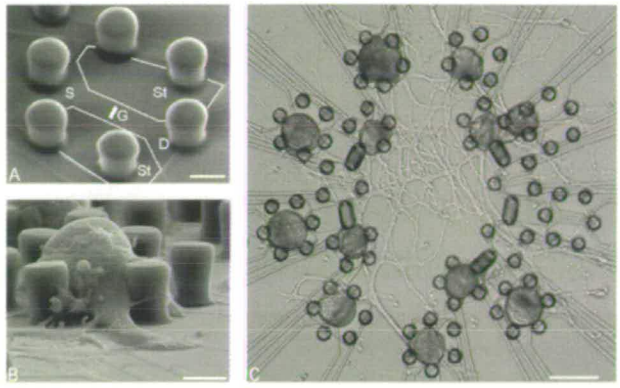

Figure 2.5: *A neuron silicon chip proposed by Zeck and Fromherz. (A) Electronmicrograph of the polyimide picket fence. The source (S), gate (G) and drain (D) of the transistor are marked (scale 20μm), (B) Electronmicrograph at 3 DIV after fixation. A neuron is trapped in the picket fences (scale 20μm), (C) Micrograph at 2 DIV of neuronal cells trapped in picket fences. The dark blobs are the cell bodies while the bright thread are the neurites (scale 100μm). Image taken from [24].*

2.4.1 Advantages and Problems of the Techniques

The main advantage of providing physical cues to pattern cells is the absence of biological agents from the procedure. It is known that chemical cues tend to degrade over time and thus any patterning technique based on their application needs to take this into account. Physical characteristics on the other hand, can remain on the surface indefinitely allowing the same substrate to be used multiple times. Moreover, physical immobilisation guarantees the presence of a specific cell to a specific locale thus, is suitable when single cell analysis is required.

Nevertheless, physical immobilisation techniques can be quite difficult to implement. The fabrication of silicon cages, silicon nitride wells and polyimide fences on the micron scale is not simple or easy. What is more, the physical manipulation that is usually required afterwards, in order to place the cell into the fabricated structure, adds another level of complication to the method. Even though these patterning schemes can be integrated with other technologies to record and stimulate cells (as Maher and Zeck have shown), they often require additional alignment steps during the device manufacturing process. Therefore, their compatibility with MEAs and other similar technologies is poor. Moreover, the resolution of mechanical immobilisation is of the order of several microns, which is considered low, while the flexibility of the technique is minimal, as changes in the pattern geometry require physical alteration of the surface which is often impossible without destroying the substrate altogether. Finally, the cost of assembling

3D structures on silicon can be significant, due to the complicated procedure.

2.5 Real Time Manipulation

Real time manipulation involves the guidance of cellular growth by employing techniques *in situ*. In other words, guidance cues are given to the cells while they are still in culture. In particular, the application of an extracellular dc electric field is a common technique in this area, as neurons have a tendency to grow towards the cathode [38]. Weak extracellular electric fields have also been employed in nerve fiber regeneration studies with very promising results [39]. In addition, the effect of time varying electromagnetic fields (TVEMF) on neural progenitor cell growth has been studied revealing a direct correlation between the presence of TVEMF and cell proliferation rate [40]. Finally, an alternative method utilises multiphoton excitation to alter the 3D topography in dissociated cultures. In this approach, structures such as barriers and growth lanes are fabricated from proteins that adhere locally, due to photon excitation of non cytotoxic photosensitizers [41]. The conditions inherent in the technique do not compromise the short or long term viability of cells.

2.5.1 Advantages and Problems of the Technique

The implementation of electric fields and photon excitation is easily integratable to MEA and other cell recording technologies, as it does not require complicated alignment steps. In addition, the circuitry necessary for the application of such fields can be pre-embedded in an MEA design.

However, real time manipulation techniques have some serious drawbacks. First, they often require sophisticated apparatus and as such are not easy to implement, when electric fields are applied to the culture and the entire substrate. Alternatively, if the circuit generating the fields is microfabricated beneath the substrate, pattern generation becomes complicated and not easily alterable. Additionally, not enough high quality patterning examples exist, to persuade researchers that such methods can achieve cell guidance to a high resolution. Also, unlike chemical cues, real time cues need to be constantly provided to the cells or the desired cell growth will be lost. Data regarding long term pattern stability is not available as this technique is best suited for short term experiments. Finally, the cost of designing and embedding in a device, the circuitry necessary to generate the electric fields which will induce cell patterning is

substantial. Thus, the commercialisation potential of real time manipulation schemes is limited.

2.6 Microfluidics

Microfluidics is a group of patterning methods in which micrometer sized channels are fabricated on a substrate. An elastomer stamp, such as PDMS, or photoresist is usually employed in the creation of the microstructures. The former is usually derived from a casting process similar to that described in section 2.2, to obtain a negative relief pattern of the master. The PDMS structure is then placed onto a substrate to create a 3D channel [42]. Alternatively, photoresist and microfabrication techniques can be used to build structures in silicon [43]. It has also been proposed, that the capillary action of low viscosity polymers can be exploited, to micromould a pattern of parallel or rectangular channels [44].

Once the channels are fabricated, they are flooded either with the adhesion molecules or with a cell suspension. In the first case, once the adhesion mediators are patterned, if elastomer stamps were used they are removed and the cells are cultured normally, over the entirety of the substrate. If microfluidic channels are build in the substrate, cells and culture media can be introduced inside the channels however, cell culturing in such small volumes can be quite challenging and would probably require a specialised culturing protocol.

2.6.1 Advantages and Problems of the Technique

Microfluidic patterning methods usually yield high contrast patterns, if the cells are confined within the channels. Moreover, it has been demonstrated that these techniques can be integrated into MEAs [45], although additional alignment steps are required to do so. Finally, specific kinds of cells, such as the PC12 and yeast cells, can survive up to 3 weeks within the channels, providing the researcher with a high quality, durable cell pattern.

However, microfluidic methods are not easy to implement. First, the fabrication process is rather complicated and requires the execution of multiple precise steps. Second, when cells are cultured inside the channels, in order to obtain high contrast patterns, the cell culturing protocol becomes difficult, since cells need to be provided with nutrients, growth factors and oxygen in a confined space. In addition to their applicational problems, microfluidic methods are not flexible as any change in the pattern geometry necessitates the redesigning and the

fabrication of channels anew. Another concern is that the survivability of neurons within the channels is limited to one week. Finally, the manufacturing cost of microfluidic channels is higher compared to other methods due to the number and complexity of the steps involved.

2.7 Photolithographic Techniques

Photolithographic techniques encompass a broad range of different patterning methods. In the majority of cases a layer of photoresist is spin coated onto a substrate, exposed to UV radiation via a mask and developed in order to create a pattern. Due to the involvement of photolithography, sub-micron pattern resolution is feasible. The patterned substrate is then flooded with either cell repellent molecules, in which case the photoresist acts as a protective layer, or with attachment factors, in which case the photoresist acts as a sacrificial layer in a lift off procedure (see figure 2.6). Inhibiting factors that have been used include alkane chains [46] (alkyl-trichlorosilanes), while adhesive molecules of choice have been collagen (Type IV) [47] and PDL [48].

Alternatively, photoresist can be utilised during an etching process. Wyart et. al. [49] coated glass coverslips with hydrophobic fluorosilane and then selectively etched it away by utilising a photoresist mask. Subsequently, the surfaces were flooded with poly-L-lysine, which adhered only to the etched areas. Finally, the unexposed photoresist was removed. Similarly, both the lift off and the plasma etching methods were used by Sorribas to generate complementary patterns of two different proteins [50].

A novel patterning scheme termed Molecular Assembly Patterning by Lift-off (MAPL) has recently been proposed by Falconnet in Switzerland and promises long term cell patterns of high resolution and contrast. In this technique, a wafer is coated with photoresist and a pattern is printed through a mask via standard photolithography. The wafer is then diced to 1cm x 1cm chips and the samples are then immersed in a solution of functionalised PLL-g-PEG/PEG-X (X = cell adhesive peptide). An organic solvent then strips the remaining photoresist away and the surface is reimmersed in non functionalised PLL-g-PEG, which adheres to the background and prevents cells from attaching to those areas (see figure 2.7) [51].

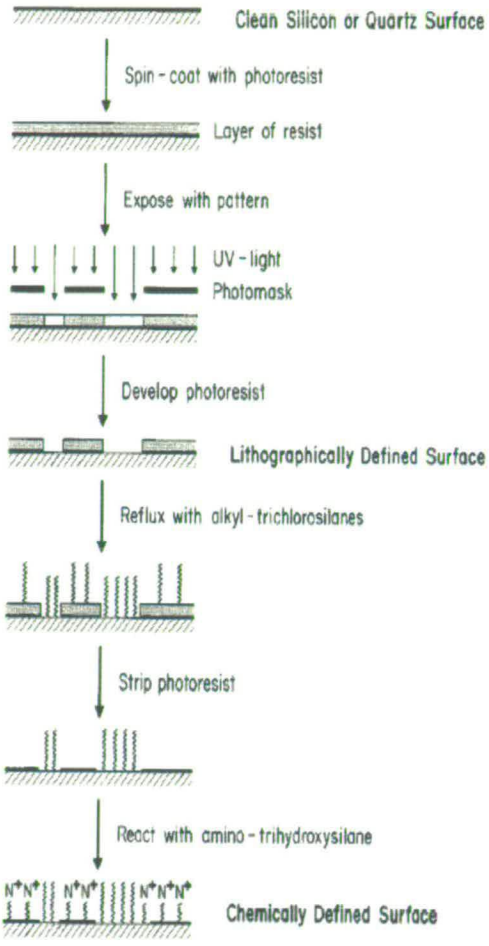

(a) The photoresist acts as a protective layer preventing the area underneath from being coated with cell inhibiting material. Once it is stripped off, the unbound regions are coated with cell adhesive amine derivatives

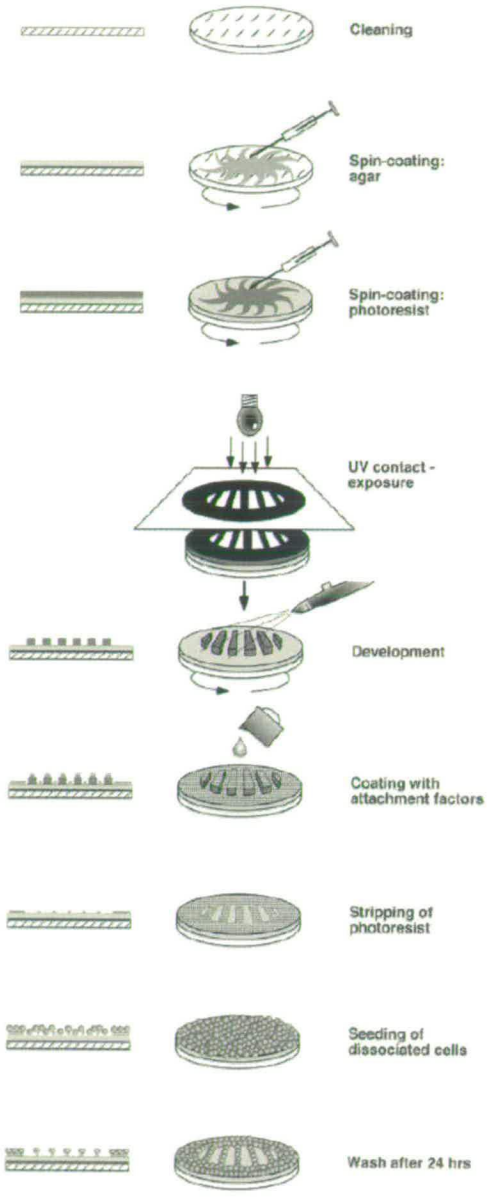

(b) The photoresist acts as a sacrificial layer. The areas underneath the stripped photoresist are not coated with collagen and as such are non permissive to cells

Figure 2.6: *Two different approaches at using photolithography to pattern cells. Images taken from [46] and [47] .*

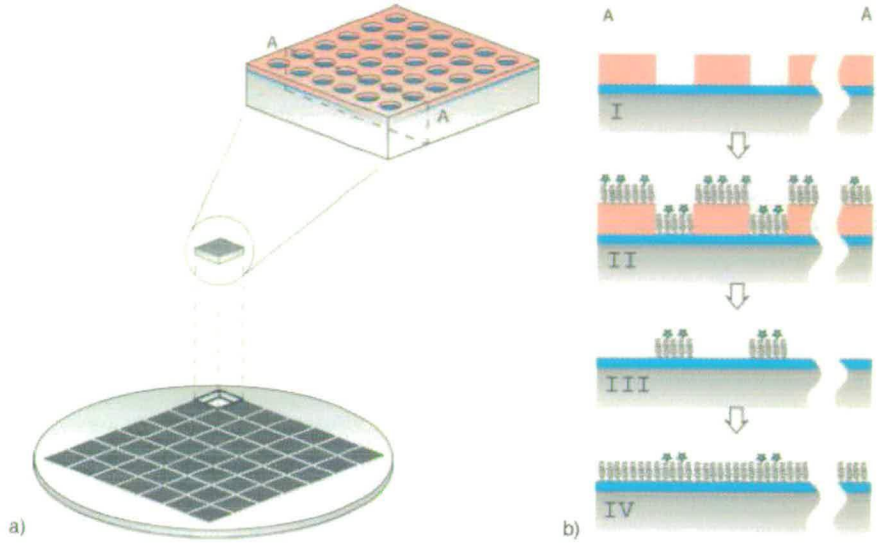

Figure 2.7: *Molecular Assembly Patterning by Lift-off as proposed by Falconnet [51]. In the first step a photoresist coated wafer is patterned via photolithography (a). Subsequently, the adhesion mediator is applied, followed by a photoresist lift-off and the application of the non permissive material on the background (b). Image taken from [51].*

2.7.1 Advantages and Problems of the Technique

High pattern resolution is one of the main advantages of photolithographic techniques. With the miniaturisation of stepping technology, mask patterns can be printed to a sub-micron level, allowing for pattern dimensions that are not feasible in other techniques. Furthermore, these methods are moderately flexible as changes in pattern geometry require only a new mask. The quality of cell patterning is good and it has been shown that neuronal networks remain healthy and maintain a stable pattern for up to 5 weeks [49]. The manufacturing costs of substrates vary depending on the fabrication steps involved. The MAPL technique for example is promoted as highly cost-effective and suitable for industrial applications [52]. Finally, wafer-level lithography and processing allows the fabrication of multiple substrates at once making photolithographic methods ideal for mass manufacturing.

On the other hand, the fabrication process of photolithographic techniques is not lab based. Not only does the coating, exposure and lift-off of photoresist require a cleanroom and high-tech apparatus, but the necessary application of biological materials on the surfaces, between microfabrication steps, comes into conflict with cleanroom procedures. As biological agents

are not allowed inside a cleanroom due to contamination concerns, special arrangements must be made whenever photolithographic schemes are employed. Additionally, these techniques are not very compatible with MEAs and similar technologies unless chip-level lithography is performed. However, if entire wafers are processed, the fabricated MEA or patch-clamp surfaces must be protected from damage during dicing.

2.8 Selective Molecular Assembly Patterning

Selective molecular assembly patterning (SMAP) is a recently developed technique. It combines photolithographic steps to engineer a substrate of two complementary materials and the selective self-adsorption of organic molecules on them. The original scheme proposed by Michel et al. can be seen in figure 2.8 and it involved the fabrication of squares of titanium dioxide (TiO_2) within a thermal oxide matrix (SiO_2), through the use of standard photolithography. The patterned surface was then immersed in a solution of an alkane phosphate, which selectively adheres only to TiO_2, rinsed in ultra pure water and blown dry. Subsequently, the substrate is exposed to a solution of the graft copolymer PLL-g-PEG, which binds only to the SiO_2 and renders the surface resistant to protein adhesion. In contrast, the alkane phosphate coated TiO_2 selectively adsorbed protein, producing patterned growth of human foreskin fibroblasts [53, 54]. The novelty, as well as the success of the technique, relies on the selection of an appropriate chemistry, to ensure the self-assembly of the chosen molecules on the correct substrates and to prevent the disruption of previously assembled molecules.

In a variation of the SMAP process, Franks utilised a system of gold (Au) on thermal oxide (SiO_2) to pattern primary neonatal rat cardiomyocytes and the HL-1 cardiomyocyte cell line. Various gold patterns were fabricated on glass and SiO_2 as seen in figure 2.9 and were functionalised with an amine-terminated SAM. The usual protein repellent graft copolymer PLL-g-PEG was utilised, to inhibit the adsorption of protein onto the SiO_2. This scheme was also integrated into an array of extracellular microelectrodes which was used to record cardiomyocytic activity [55].

2.8.1 Advantages and Problems of the Technique

Once the physical patterning of the substrate has been completed, SMAP is easy to carry out. The functionalisation of the protein permissive and non permissive substrates is easy to imple-

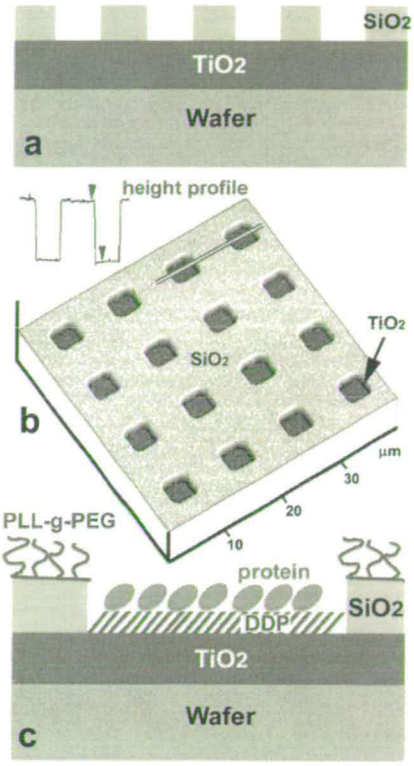

Figure 2.8: *Selective molecular assembly patterning as developed by Michel et al [53]. After the TiO_2/SiO_2 substrate patterning through photolithography, protein adhesive DDP and protein repellent PLL-g-PEG are attached to TiO_2 and SiO_2 respectively in a simple dip-and-rinse process. Image taken from [53].*

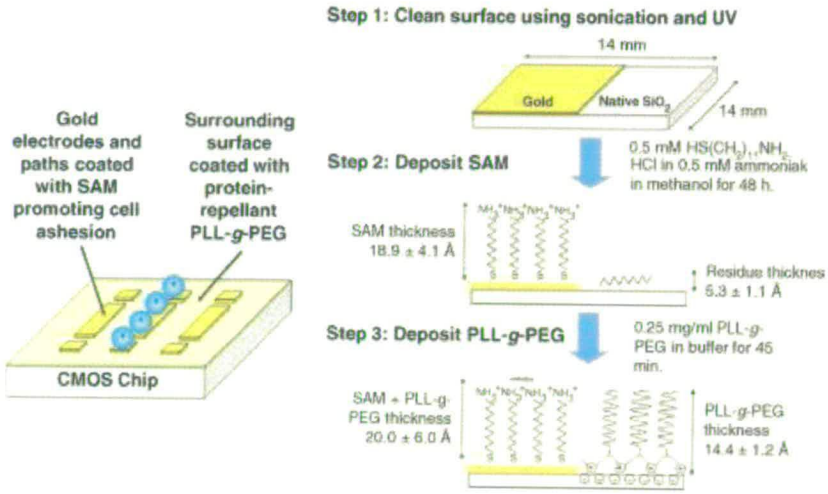

Figure 2.9: *A variation of selective molecular assembly patterning by Franks et al. Gold (Au) and an amine-terminated SAM are utilised instead of TiO_2 and DDP. Image taken from [55].*

ment, as it only involves two simple dip-and-rinse processes. Additionally, the compatibility of the technique with MEAs and other microfabricated recording devices is good [25]. Patterned substrates can be stored and functionalised at a later time, allowing the researcher to work from a prepared stock of patterns. The smallest feature size presented by both Michel and Franks was between 3 and 5μm however, as the method is based on photolithography it is possible that sub-micron resolution can be achieved. Examples of cultures by both Michel (human foreskin fibroblasts) and Frank (rat hippocampal neurons and glia) show that even after 2-3 weeks in culture cells follow the patterns. Finally, the standard photolithographic steps of SMAP are suitable for mass manufacturing of substrates, which can then be supplied to research labs, where patterns will be activated. With an appropriate choice of substrate chemistry to minimise manufacturing costs, selective molecular assembly patterning could potentially be exploited commercially.

Although SMAP is not a highly rigid scheme it is not as flexible as inkjet printing. Alterations to the geometry of the patterns can be implemented through a new mask design and the completion of the microfabrication steps. This is not a serious problem per se, but if variation in pattern geometry is required it has to be factored into the fabrication requirements from the beginning of the manufacturing process. Another minor issue raised by Franks is the possibility that the patterned surfaces might be deleterious to neuronal growth, as he observed that his cultures had a low neuron count despite the plethora of glia [25]. This does bring the biocompatibility of the technique into question. Nevertheless, such a problem, should it be true, can easily be circumvented by a change in substrate chemistry and protein adhesion mediators.

2.9 Investigating Patterning Methods for the Patch-Clamp Device

The long term goal of the patch device project was to build and array of patch-clamp sites in order to perform multiple whole cell recordings on a network of neurons. Multiple schemes were suggested as to how cells would come into close contact with and form seals to the patch holes. One possibility was to culture cells on the devices and allow them to grow towards the patch sites as in cultures on MEAs. Obviously, for this to be implemented a patterning method was necessary to guide the neurons to the desired locations. Such a technique would have to be factored into the fabrication of the patch devices and would have to be compatible with microfabrication procedures and cleanroom protocols and regulations.

Another important aspect of the candidate patterning scheme was its long term stability. To record spontaneous activity, neurons must remain in culture for at least a week. Therefore, if recordings were to be performed, cells would have to remain in their target positions for the entire period. In addition, a method with high patterning resolution was desired to ensure the positioning of neurons would be exact and to prevent problems during seal formation. Finally, a simple and cost effective technique would be preferable for the commercial exploitation of the devices in the future.

Taking into account the above parameters, it is evident that photolithographic techniques would be the best choice. Alignment issues are involved in inkjet printing and microcontact stamping, while pressure from stamps might soil or damage the delicate patch holes. Physical immobilisation by 3D structures is not only a complicated technique but is also difficult to integrate to the patch device fabrication. What is more, the complex manufacturing steps would significantly add to the fabrication cost of the devices.

Real-time manipulation was employed when prototype devices with one patch hole were tested. In particular, neurons were attached to glass pipettes via suction and manipulated over the patch site. However, there are some serious problems with this technique. First, cells tend to get damaged by the suction onto glass pipettes compromising the subsequent seal formations and whole cell recordings. Additionally, it is not practical to apply this method to multiple neurons. Besides, the primary goal of the patch device has always been to circumvent the spatial problems present during multiple patch-clamp recordings with glass pipettes. Perhaps, real time manipulation via the use of DC or AC electric fields might be feasible however, such a scheme would introduce additional complexity to the protocol, while the electric fields may interfere with the accurate measurement of physiological parameters.

Microfluidics were also considered but rejected, as it would be highly challenging, if not impossible, to incorporate microfluidic channels over, underneath or around the patch holes, especially in the presence of a plumbing system beneath the patch-sites.

Photolithographic techniques on the other hand can be integrated into the manufacturing process of the patch device. They only require cleanroom facilities, to which our research group had access and they can produce high resolution patterning. Furthermore, entire wafers of devices can be processed at once, making these schemes cost effective and less time consuming. As biological agents are not allowed in the cleanroom and because it is debated that they might

interfere with seal formation during patch-clamping, we tried to avoid their use. We also aimed to produce a simpler photolithographic technique that would be easily integratable to our existing patch-clamp device fabrication protocol. We experimented with patterns of photoresist, boron doped tracks and parylene, all generated via standard photolithography.

2.10 Conclusions

In this chapter the existing patterning schemes in literature have been presented and critically assessed. Due to the requirements of the previous patch-device projects, photolithographic patterning techniques were initially explored in this study. Experimentation on these techniques and its results are presented in the following chapters, where the course of our investigation is outlined and our proposed patterning method revealed. We will also illustrate the high quality patterning results of our proposed technique and explain the steps taken to optimise it. Finally, we will identify the underlying causes of patterning in our method and propose upon how it may be improved.

Chapter 3

Serum Activated Patterning with Parylene

3.1 Introduction

3.1.1 Neuronal and Glial Guidance

According to Trinkaus, the extrinsic factors that contribute to directional neuronal movement can be classified under the following five groups: steric guidance, chemotaxis, haptotaxis, galvanotaxis (electrical fields) and contacts among cells [56].

"Steric guidance" refers to the physical and topographical cues, present in tissue and organs that direct migrating cells and their processes. These cues include grooves, porous matrices or even aligned tracks of other cells that can serve as pathways in an organism. It has been shown, that neurites in particular react significantly to steric factors in their environment [57]. Due to the crucial role of steric guidance *in vivo*, many researchers have tried to mimic its effects in cell patterning *in vitro* experiments, by utilising substrate topography (see sections 2.4 and 2.6).

Chemotaxis is the guidance of cells via chemical cues. Specific molecules are diffused into the extracellular matrix and create a chemical concentration gradient. Subsequently, cells move either towards or away from the chemical stimulus. Neurons for example, secrete and have on their membranes glycoproteins that play a critical role during interaction with other cells [58]. Chemotaxis is rarely used in *in vitro* cell patterning. The fabrication of a patterned substrate that releases specific biomolecules at precise sites would be a complex endeavour.

In haptotaxis, a gradient of cell-surface adhesiveness is utilised to guide the cells towards more adhesive substrates. Collins [59] and Letourneau [60] for example have shown that neurite outgrowth is mediated by the strength of its attachment to the surface. Haptotaxis is the predominant force behind the majority of *in vitro* cell patterning experiments. Cell attractive and repellent surfaces are frequently used to direct cells to desired locations. Specific proteins, such

as laminin, PDL and glycoproteins are usually adsorbed and form a layer onto a substrate to make it adhesive. Integrin receptors on cell membranes bind to these proteins and form focal contacts. Subsequently, cell reactions and material characteristics modify the protein layer. Vitronectin and fibronectin are two glycoproteins commonly involved in cell-surface adhesion, as they both contain the RGD (Arg-Gly-Asp) amino acid sequence, which is a binding site for integrin receptors [61].

The surface of most cells is charged. In particular, the neuronal membrane potential constantly rests at around -60mV [62]. Based on this, many researchers believe that electrical fields can guide migrating cells *in vivo*, an effect called galvanotaxis. Cooper's investigation in the movement of fish epidermal cells in DC electric fields [63] and Patel's research into the response of the nerve growth cone to focal electric currents [64] provide abundant evidence that cells do react to electric stimuli.

Both DC and time varying electric fields have been used to guide cells *in vitro* (see section 2.5). Alternatively, surface charge may be used to create a contrast in cell adhesiveness, between two substrates. Neurons in particular adhere better on substrates with positive surface charge, due to their negative membrane potential [65]. This has also been tested in our lab by Dworak [18].

The last factor affecting cell migration is contact with other cells. It has already been mentioned that cells can be involved in steric guidance, by offering topographical cues to other cells, or they can provide a substrate of different adhesiveness upon which other cells can grow (haptotaxis). However, cells can also interact with each other, either via specific molecules present on their membranes or via the emission of biological signals regulated by proteins. With regards to neurons and glia, early evidence from Rakic supports his hypothesis that migrating neurons identify and attach to glial fibers via distinct biomolecules on their membranes [66]. In our experiments, we have frequently witnessed such interactions, especially when the adhesiveness of the culture substrate was poor. Glia formed large sheets of cells or coalesced into large clusters, while neurons followed the glia and aggregated into neurospheres [67].

In the glial and neuronal patterning attempts detailed in this work, we utilised haptotaxis to guide the cells to specific areas on the substrate. Our goal has been the fabrication of a high contrast cell attractive surface, on a cell repellent background. Early patterning experiments employed materials of different surface charge, in order to acquire the desired adhesive contrast. Further attempts involved the binding of proteins, present in horse serum, on two different

substrates.

3.1.2 Early Pilot Brain Cell Patterning Experiments

The first brain cell patterning protocol we investigated focused on the contrast between a boron-doped silicon thermal oxide (SiO_2) and a photoresist surface. The intention was for the boron-doped TO to act as the adhesive substrate on a background of photoresist, which was thought at the time to be cell repellent. There were already examples in literature that utilised photoresist to pattern cells [68–70], while evidence showed that boron doping could make the thermal oxide surface more hydrophilic and positively charged thus, attractive to cells [18]. Therefore, grids of boron-doped TO nodes and tracks on a photoresist background were fabricated and tested. Although sporadic indications of patterning existed, the majority of the patterns were either devoid of cells or had been overgrown. In some cases, glia adhered to each other and formed a floating sheet, which was attached to the boron-doped TO via 3 or 4 anchor points. In other instances, neurons coalesced into large neurospheres [67], which adhered to both the cell adhesive and cell inhibiting substrates (unpublished data and [71]). As glia and neurons failed to adhere exclusively to boron-doped TO and photoresist areas were frequently occupied by cells, this patterning approach was categorised as unsuccesful.

In an effort to diverge from the photoresist approach, which seemed unpromising, the cell deterrent surface was changed from photoresist to thermal oxide, as Dworak had already found that TO was a cell inhibiting substrate [18]. Therefore, thermal oxide substrates were created which contained a grid pattern of boron-doped thermal oxide nodes and tracks. The aim was to utilise the difference in hydrophilicity between boron-doped and plain thermal oxide thus, encouraging the cells to adhere to the more hydrophilic regions. Again however, glia and neurons attached to both boron-doped and plain TO. As with photoresist, a few indications of patterning were present in regions of low cell density. In a few occasions, cells were centered either on the node or on the tracks and their processes extended within the confines of the pattern. In most cases however, glia and neurons populated the majority of the grid pattern indiscriminately (unpublished data).

The protocols describing the fabrication of the substrates in the above two approaches are given further in this chapter. It was hypothesised that one of the main reasons of failure in these pilot studies was the lack of adequate contrast between the cell repellent and cell attractive surfaces. In an attempt to increase this contrast it was decided to utilise an extremely hydrophobic

substance, a polymer of xylylene known as Parylene, instead of photoresist or TO Thus, grid patterns of boron-doped TO nodes and tracks on a parylene background were fabricated and tested.

3.1.3 Parylene and its Uses

The term Parylene is used to describe a series of highly crystalline, linear polymers of xylylene. The first member of the series is called poly-para-xylylene or parylene-N and is a primary dielectric. The second polymer, which is the one used in this project, is called parylene-C. It differs from parylene-N only in the substitution of one aromatic hydrogen with a chlorine atom. In parylene-D an additional aromatic hydrogen is substituted with a chlorine atom. The chemical structures of parylene-N,C and D are shown in figure 3.1.

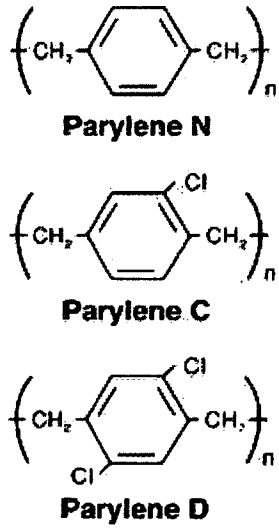

Figure 3.1: *The three types of parylene (N,C,D) and their chemical formulae. Image taken from [72].*

Due to its specifications (refer to appendix A for more details), parylene has numerous applications of a wide variety. Parylene is used by the military and the automobile industry, it is employed as an insulator in electronics and included in many biomedical devices. Its robustness, flexibility and biocompatibility are characteristics intensively sought after in the field of medicine. In addition, its insulating properties make it a perfect candidate for coating microelectrodes [73] and probes [74] especially when those are used in chronic recordings [75, 76]. Recently, parylene was employed to build neuronal cages, or neurocages, which would trap

neurons in specific locations, close to electrodes and thus aid *in vitro* research in synaptic connections, learning and memory. Parylene was chosen because of its reported biocompatibility, non-toxicity, inertness and chemical resistance to moisture and most chemicals [77–79].

In addition to its cell friendly properties, parylene was of particular interest in this project due to its high contact angle. It has been reported that, after testing with drops of water, the contact angle of Parylene-C was close to 90^o [80] while in a similar experiment the contact angle of untreated Parylene-C was found to be as high as 103^o, which translates to a surface energy of approximately $19.66mN/m$ [81]. In contrast, the surface energy of untreated thermal oxide has been previously measured in this lab and was found to be $52mN/m$, while piranha cleaned thermal oxide, which was the surface utilised in our patterning experiments, had a surface energy of $67.23mN/m$ [18]. Therefore, based on these surface energy measurements, we postulated that Parylene-C would act as a better cell-repellent substrate than thermal oxide, since the former is more hydrophobic and thus its contrast with the boron-doped thermal oxide substrate (surface energy of $77.14mN/m$) would be greater.

Early Patterning Experiments with Parylene-C

Although there were some hints of patterning amongst the numerous cultures that were carried out, it was evident that the contrast between parylene and boron-doped thermal oxide on its own was not enough to induce a high quality glia and neuronal pattern. Most importantly however, there was a single powerful result which encouraged us to re-evaluate the way we perceived parylene. The outcome of that result was completely reversed, meaning that the cells had chosen parylene as the adhesive substrate while evading the boron-doped thermal oxide areas. Even though this result was unexpected, and at the time remained unexplained, it altered parylene's role in the patterning project from a cell deterrent to a cell adhesive material and defined the course of the majority of the work described in this thesis. Obviously, a new non-adhesive material had to be found, since parylene was no longer fulfilling that role. Out of the materials available at the time, TO was chosen as the most repellent. Examples of the early patterning experiments with Parylene-C as well as the reversed result attained will be described further in the chapter.

3.1.4 Parylene as the Attractive Substrate

The majority of this chapter focuses on the experiments carried out with Parylene-C as the cell adhesive substrate on a background of unattractive thermal oxide. The compliance of both glia and neurons is investigated and a model of their behaviour during seeding and incubation is presented based on the data gathered.

3.1.5 The Effect of the Schema Utilised in the Outcome of the Patterning

This chapter will also address an important question which emerged just before experimentation with parylene as an attractive substrate commenced:

Do the spatial specifications of the pattern affect in any way the outcome of the experiment?

In other words, does the quality of the cell patterning in this particular technique depend upon the ratio of cell adhesive area to overall area in the patterns? This question emerged due to the recurrent failures to achieve high quality patterning prior to the use of parylene as an attractive surface. It was hypothesised at the time, that one of the main reasons for the bad experimental outcomes was the low percentage of attractive area compared to the overall surface. This created an extremely negative scenario during the random seeding at the start of the culture, since the majority of the cells would land on a cell repellent area and begin drawing even more cells towards them, due to cell-cell attraction forces. As mentioned earlier, cells interact with one another via the secretion and identification of certain molecules present in their membranes. Our concern therefore was that neurons and glia would prefer to attach to each other and ignore a weak attractive-repellent surface contrast.

In order to investigate the above issue, the grid patterns were abandoned in favour of patterns which contained parylene stripes of increasing width. Therefore, by keeping one dimension constant while varying the other we could see whether changes in the total area of the attractive substrate had any effect in the quality of the patterning. The patterns were labeled according to the percentage of the parylene area in the total surface. The five different percentages tested were 10%, 20%, 30%, 40% and 50%.

3.2 Materials and Methods

3.2.1 Stripe Pattern Fabrication

Between 2-8 silicon wafers were thermally oxidized in the furnace. Specifically, thermal oxide of approximately 200nm thickness was grown in a furnace with H_2 (1.88sccm) and O_2 (1.25sccm) at 950°C for 40 minutes as shown in figure 3.2. The thickness of the thermal oxide layer was verified with the Nanospec (Nanometrics NanoSpec/AFT, Microarea gauge) and found to be 250nm, which was considered sufficient. As illustrated in figure 3.2 Parylene-C 100-120nm in thickness was then deposited on the oxidised wafers via a Labcoter 2 Parylene deposition Unit (Model PDS2010) at a rate of 1.298nm per mg of dimer (average amount of dimer used 77mg). The deposition was performed at room temperature [72].

Hexamethyldisilazane (HMDS) was deposited on the parylene coated wafers on an SVG 3 inch photo-resist track. The wafers were then spun at 4000rpm for 30 seconds, while applying positive photo-resist (Rohm & Hass SPR350-1.2) on them for an even plating of the surface (see figure 3.2). The theoretical resulting thickness of the photoresist is 1μm. A soft bake at 90°C for 60 seconds followed. The wafers were then inserted in an Optimentrix 8605 5x reduction stepper together with the previously created mask. The patterns on the glass mask (either stripes or grids) were printed on each wafer. A post exposure bake at 110°C for 60 seconds was performed and subsequently, the wafers were developed in Microchem MF-26A developer which removed the exposed photo-resist (step 5 in figure 3.2). A hard bake was not performed since we did not want to stabilise the photo-resist but remove it at the end of the process.

The wafers were then inserted into the Plasma therm in order to etch away the undesired parylene, which was not protected by photo-resist (step 6 in figure 3.2). The etch was performed at 50mTorr chamber pressure, 50 sccm O_2 and 500 Watts RF power for approximately 90 seconds. This should theoretically remove about 150nm of parylene (etch rate is approximately 100nm/min) and reveal the thermal oxide underneath. The presence of thermal oxide on the etched areas was verified using the Nanospec. The residual photo-resist was removed through the spinning of acetone on the wafers on the photo-resist track (1600rpm for 55 seconds) per the last step of figure 3.2.

The wafers were cut with a DISCO DAD 800 Dicing Saw (spindle speed 30000rpm, feed speed 7mm/sec), rinsed with DI water and blown dry with Nitrogen. The chips were collected with

tweezers from the mounting film and placed in dust free boxes.

Figure 3.2: *A step by step representation of the parylene pattern fabrication procedure.*

3.2.2 Spatial Specifications of Stripe Patterns

Five different stripe patterns were fabricated and tested. These were labeled as 10%, 20%, 30%, 40% and 50% and their dimensions are given on table 3.1 below:

Stripe pattern	Parylene stripe width	TO background width	Stripe length
10%	20	180	2000
20%	40	160	2000
30%	60	140	2000
40%	80	120	2000
50%	100	100	2000

Table 3.1: *Dimensions of parylene stripe patterns (all units are in μm).*

Grids of Boron Doped Thermal Oxide on a Parylene Background

Silicon wafers were oxidized as above and subsequently boron doped for 30 minutes at $1000^{o}C$ in N_2 gas. The protocol described above was carried out afterwards in order to attain grids of boron doped thermal oxide tracks and nodes on a parylene background.

3.2.3 Surface Cleaning and Sterilisation

Glass Coverslips (purchased from R.A.Lamb Ltd.) as well as silicon chips containing stripe or grid patterns were cleaned in the cleanroom with piranha acid. Specifically, 25ml of 30% Hydrogen Peroxide (H_2O_2) were added to 15ml of 98% Sulphuric Acid (H_2SO_4) and left to stand for half a minute in order to cool down. The chips were then immersed in the acid and left for 10 minutes while being stirred and re-submerged constantly. Subsequently, they were rinsed three times in distilled water, blown dry with nitrogen and placed in plastic dust free cases inside a vacuum desiccator.

The surfaces were transferred out of the cleanroom in a vacuum desiccator, placed in 24-well plates and sterilised under ultraviolet light (2x15W light bulbs) for 1 hour in a class 2 hood. The backside of the parylene stripes was also sterilised for an additional hour in order to minimise the number of contaminants, as silicon is opaque.

Glass coverslips were also used in order to assess the overall success of the culture. They were immersed in 0.5ml of poly-D-lysine solution ($50\mu g$/ml concentration) and left in the incubator overnight. For the experiments in which serum proteins were utilised, the silicon chips were immersed in horse serum and left in the incubator overnight in order to activate the patterns. Controls were immersed in sterilised distilled water (H_2O) instead for the same amount of time.

3.2.4 Primary Neuronal Cultures

The protocol outlined in table 3.2 below is an adaptation of the gradient cell isolation protocol presented in previous literature [82, 83]. Prior to the culture six Pasteur glass pipettes and an adequate number of plastic tips were autoclaved. To accelerate the protocol and to ensure that the neurons would not remain idle for long time spans, all necessary media was prepared before the culture commenced. All the media as well as the entirety of the culture was performed under a sterile class 2 fume hood to prevent bacterial and fungal contamination.

Step	Description
1	Purchase 5 to 12 post-natal rats, aged between 1 and 7 days and anaesthetise them individually with halothane inside a glass jar
2	Decapitate the rat and remove the skin and the sculp with scissors to expose the cortex
3	To remove the hippocampus split the cortex by gentle insertion of forceps between the two hemispheres, then open the forceps to pull away the cortex and revel the hipocampus underneath
4	Collect the tissue with tweezers and immediately place on EBSS solution in ice
5	Discard the carcass
6	Slice the isolated tissue in two perpendicular directions using a McIlwain tissue chopper
7	Digest the tissue for 30 to 40 minutes, depending on the amount present, in a 15ml tube containing a 6.25ml pre-heated solution (refer to appendix A for more details) of 30 units of papain, 500 units of DNASE-I and 0.5M EDTA, purchased from *Sigma*©. The tube should be placed inside an incubator at 37°C and 5% CO_2 with a loose lid for the CO_2 gas to diffuse into the solution
8	To agitate the tissue shake the tube once every 10 minutes and place it back in the incubator
9	Fire polish six pasteur glass pipettes to obtain five different bore sizes (wide, medium, small, very small and fine)
10	Upon completion of the enzymatic treatment, triturate the tissue 15 times with each of the following 4 pipettes: wide, medium, small and very small
11	Centrifuge the cell suspension at 1250rpm (300g) for 5 minutes in a 15ml tube
12	Discard the papain and re-suspend the centrifuged tissue in a 3.15ml EBSS solution (see appendix A) containing: 6mg BSA, 6mg ovomucoid and 150μl DNASE-I (300units)
13	Layer the solution on top of a Nycoprep gradient solution which has four gradient layers of increasing density (from top to bottom 15% (F1), 20% (F2), 25% (F3), 35% (F4)), and centrifuge at 1900rpm (800g) for 15 minutes
14	Meanwhile take the glass coverslips and the silicon surfaces of the poly-D-lysine and serum respectively and rinse them twice in distilled sterilised water. Then immerse them individually in 1ml of Neurobasal-A growth media (see appendix A) and leave them in the incubator
15	Depending on the experiment collect either the F3 fraction (rich in neurons) or the F2 fraction (rich in glia) and place it in a new 15 ml tube
16	Centrifuge the fraction for 5 minutes at 1250rpm (300g) and discard the supernatant
17	Re-suspend the remaining pellet of cells in 500μl of Neurobasal-A growth medium
18	To get an approximate cell density place 20μl of the solution in an eppendorf together with 20μl of Trypan Blue to stain all fragments and non-viable cells. Obtain cell counts per mm^2 using a hemocytometer cavity and a glass coverslip
19	If there are visible cell aggregates, re-triturate fraction F3, to break down remaining clumps of tissue
20	Dilute the suspension down to 5ml
21	Depending on the desired plating density (low: 50-100 cells per mm^2, normal: 100-150 cells per mm^2, high: 150 or more cells per mm^2) pipette 10-200μl of cell suspension into the wells containing the surfaces in Neurobasal-A growth media
22	Place cultures in the incubator for 3 hours to allow the cells to settle and adhere to the surface
23	Rinse unattached cells and debris by shaking the wells, removing the Neurobasal-A growth media and replacing it immediately with 1ml of the same media. Cells that have already stuck to the surface of the chips by the end of the 3 hours will remain unaffected (see also [46])
24	After 3 days of incubation shake the wells and exchange the entirety of the media with 1ml of fresh Neurobasal-A growth media
25	Fix and stain the cultures after 7 days *in vitro*

Table 3.2: *A variant gradient cell isolation protocol.*

3.2.5 Immunofluorescence Staining and Confocal Microscopy

Assessment of the cultures, as well as the degree to which the cells followed the pattern, was performed via fixation and immunofluorescence staining of the neural networks, followed by imaging with a confocal microscope. Immunofluorescence is a histological method in which antibodies conjugated with fluorescent markers adhere to specific sites of proteins that are expressed in certain areas or certain types of cells. Confocal microscopy was preferred over standard optical microscopy due to the advantages it offers with regards to the sharpness of the images and control of the depth of field. More details on immunofluorescence and confocal microscopy maybe found in recent literature [84, 85].

The following antibodies (purchased from Molecular Probes© and $Sigma$©) were used in the immunofluorescence staining:

- mouse anti-β-tubulin [86] at 1:500 dilution for neuronal specific labelling
- goat anti-GFAP [87] at 1:50 dilution for glia (astrocyte) specific labelling
- donkey anti-mouse 594 Alexa Fluor^{TM} at 1:500 dilution (red colour)
- donkey anti-goat 488 Alexa Fluor^{TM} at 1:50 dilution (green colour)
- TOPRO-3 [88] at 1:5000 dilution for nuclear labelling

The immunofluorescence protocol is described in table 3.3 below.

For general imaging a Leica Confocal Microscope was used. The specifications of its various compartments can be seen in table 3.4.

The lenses used were Leica Germany HC PL FLUOTAR and the area covered by each one can be seen in table 3.5.

During imaging the chip containing the pattern was positioned on the microscope's base and aligned so that the stripes were running from top to bottom (this was mostly done for consistency purposes and does not bare any scientific significance). An image of the entire stripe pattern was taken with the x5 lens where priority was given to the excitation wavelength maxima of 590nm and 495nm (emission wavelength maxima 617nm and 519nm or colours red and green for neurons and glia respectively). Subsequently, an image of the central area of

Step	Description
1	After the incubation period, discard the Neurobasal-A growth media and rinse the cultures once with a Tris(hydroxymethyl)aminomethane buffered saline solution (refer to appendix A for more details) (Tris) for 5 minutes
2	Fix the cultures in a 4% para-formaldehyde solution for 30 minutes and wash them once in fresh Tris solution for 5 minutes
3	Immerse the surfaces in 0.2% Triton-X100 solution for 15 minutes to permeate the cell membranes (refer to appendix A for more details)
4	Block against non specific binding for 1 hour in donkey serum solution made in 0.2% Triton-X100 (refer to appendix A for more details)
5	Meanwhile cover the base of petri-dishes with Whatman filter paper and soak them in distilled water. Place a strip of paraffin film on each petri-dish on top of the filter paper. Place the coverslips and the chips on top of the film and apply the primary antibody solution (refer to appendix A for more details), made in blocking solution, for one hour at room temperature[1] (alternatively the antibody can be applied overnight at 4°C). With the lid closed, the atmosphere within the petri-dish will remain humid and thus the dilution of the antibody solution does not change
6	Rinse the surfaces twice in 0.2% Triton-X100 solution for 5 minutes
7	Apply the secondary antibody solution (refer to appendix A for more details), also made in blocking solution, for 1 hour
8	Rinse the cultures twice in Tris solution for 5 minutes
9	Apply the TO-PRO 3 antibody solution (refer to appendix A for more details), made in Tris-solution, for 20 minutes
10	Rinse the surfaces once in Tris solution and once in distilled water
11	Mount the chips and coverslips on glass slides with Mowoil mounting agent (refer to appendix A for more details)

Table 3.3: *The immunofluorescence staining protocol.*

Unit	Description
Laser	Leica Lasertechnik Gmbh, Type TCS NT
Scan Unit	Leica DMRE, Leica TCS NT, Type:020-525.756
UV lamp	Ebq 100 isolated-L/131-26B, Prof. class IP 20

Table 3.4: *Specifications of the various confocal microscope units.*

Lens	Area covered
x5	2000μm x 2000μm
x10	1000μm x 1000μm (rarely used)
x20	500μm x 500μm

Table 3.5: *Area covered by the lenses used.*

the pattern was taken with the x20 lens where priority was given to the excitation wavelength maximum of 642nm (emission wavelength maximum 661 or blue colour for cell nuclei). The reflection of each chip was also imaged at both the x5 and x20 magnifications, in order to distinguish the underlying pattern. In a few cases, the reflection exhibited an artifactual fringe effect, which did not affect the results. In figure 3.3 we can see an imaging example of a glia and neuronal culture taken with the confocal microscope at a x40 magnification. All three different channels, red (neurons), green (glia) and blue (nuclei) have been gathered via separate wavelenght excitations of the fluorescent dyes and combined to create one image.

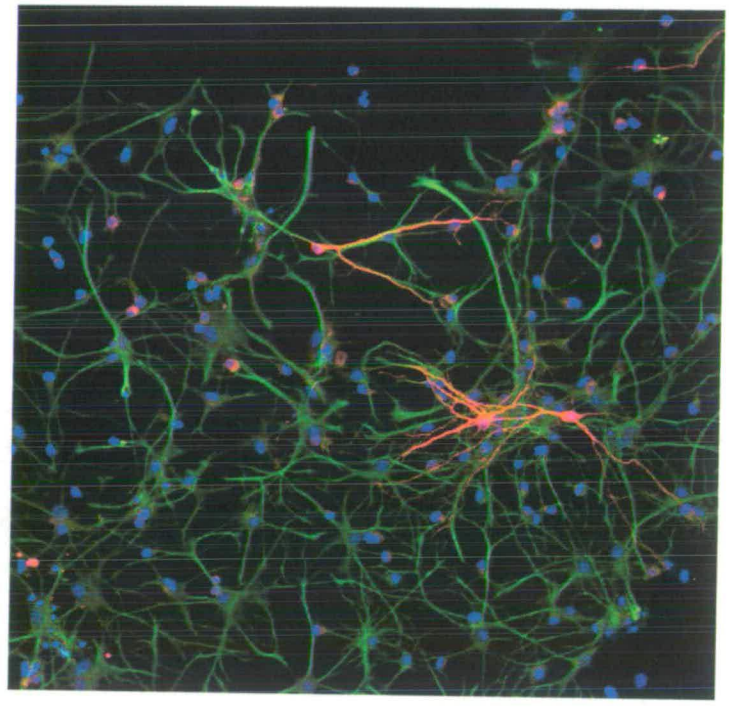

Figure 3.3: *Typical neurons and glia and their nuclei in culture, as envisioned through the three different channels. The red stained cells are neurons while the green are glia. Their respective processes are also stained. The circular blue spots are the cell nuclei (culture at x40 magnification, square area 250μm x 250μm).*

3.2.6 Statistical Analysis

Two different techniques were employed in order to assess the degree in which cells followed the parylene stripes. The first involved the scoring and averaging of glial and neuronal nuclei on the parylene stripes and the TO background, in order to produce a **nuclear density ratio**. The second entailed the quantification and averaging of the green, red and black pixel intensity of

the parylene stripes and TO background, so as to calculate a **green, red** and **black pixel density ratio** respectively (also referred to as green, red, black or colour ratios). Each patterning index highlighted a different aspect of cell conformity to the pattern and contributed in the critical evaluation of our patterning method. Both techniques are described below.

Nuclear Density Ratio

With the use of the software ImageJ, the cell nuclei (stained with the TOPRO-3) that resided on the parylene stripes were counted and contrasted to the cell nuclei that were on the thermal oxide (an example of nuclear scoring can be seen in figure 3.4). This nuclear scoring offers a straightforward indication of whether the cell somata are following the pattern and a good measure of the degree to which they do. Nuclei which lay on the borders of the stripes were counted separately. The area covered in this technique and depicted by figure 3.4 was restricted to a 500x500μm square at the center of the pattern and included 3 parylene stripes (light red in figure 3.4) and 2 TO backgrounds (dark red in figure 3.4). This was necessary as the x20 lens had to be utilised, in order to distinguish the cell nuclei and because in larger areas the number of cell nuclei would make the scoring very difficult. The number of nuclei on the parylene stripes was averaged (once including nuclei laying on the edge of the parylene and once excluding them) and then compared to the average number of nuclei on the TO background. Both averages (parylene and thermal oxide) were subsequently normalised with regards to surface area, to obtain one average nuclear density for parylene and one for thermal oxide. The average parylene density was divided by the average thermal oxide density to produce the **nuclear density ratio**. Two way ANOVA and correlation tests were performed on nuclear density ratios taken from different images.

Green, Red and Black Pixel Density Ratios

Since the first technique focused on approximately 1/16 of the total area and did not take into account glial and neuronal processes or their orientation, an additional technique was needed, which would summarise and describe the entirety of the cells and the majority of the pattern on the image. In order to accomplish this, we used the Leica Lite Confocal Software to individually select each parylene stripe and thermal oxide background and calculate the histograms of the pixel intensity for both green (glia) and red (neurons) channels. In figure 3.5 we can see the selection of the parylene stripes and the thermal oxide backgrounds. Only the central parylene

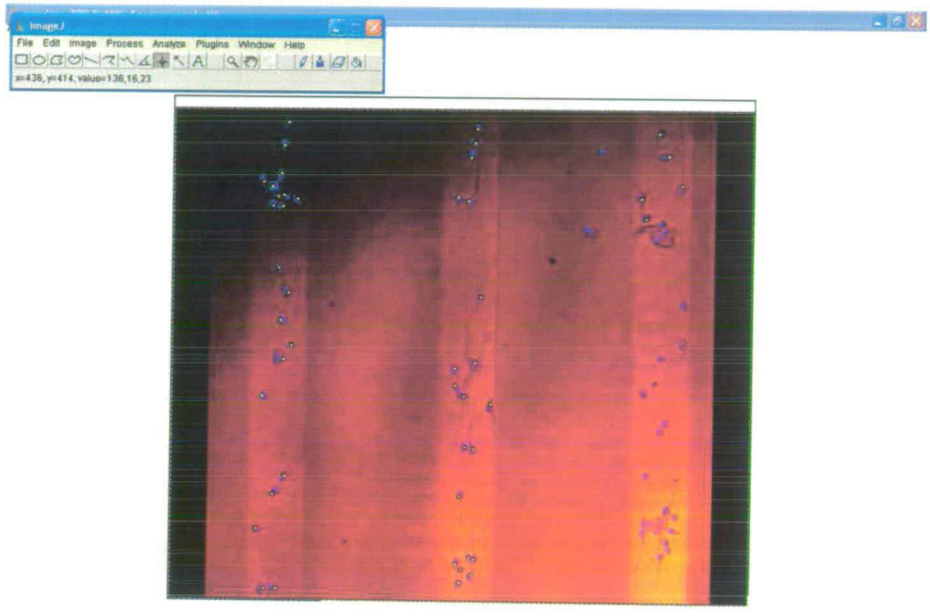

Figure 3.4: *The nuclear scoring process: 3 parylene stripes (light red) can be seen in this pattern. The nuclei (blue spots) residing on the parylene stripes are chosen individually (yellow dots) and counted. Subsequently, the same procedure is carried out for the nuclei residing on the 2 TO background areas (dark red) (30% parylene stripes at x20 magnification).*

stripes are selected, while the two at the far left and far right are omitted in order to avoid contamination of the data by border effects. Figure 3.6 depicts the histograms of a parylene stripe and a neighbouring thermal oxide background in the green channel (glia).

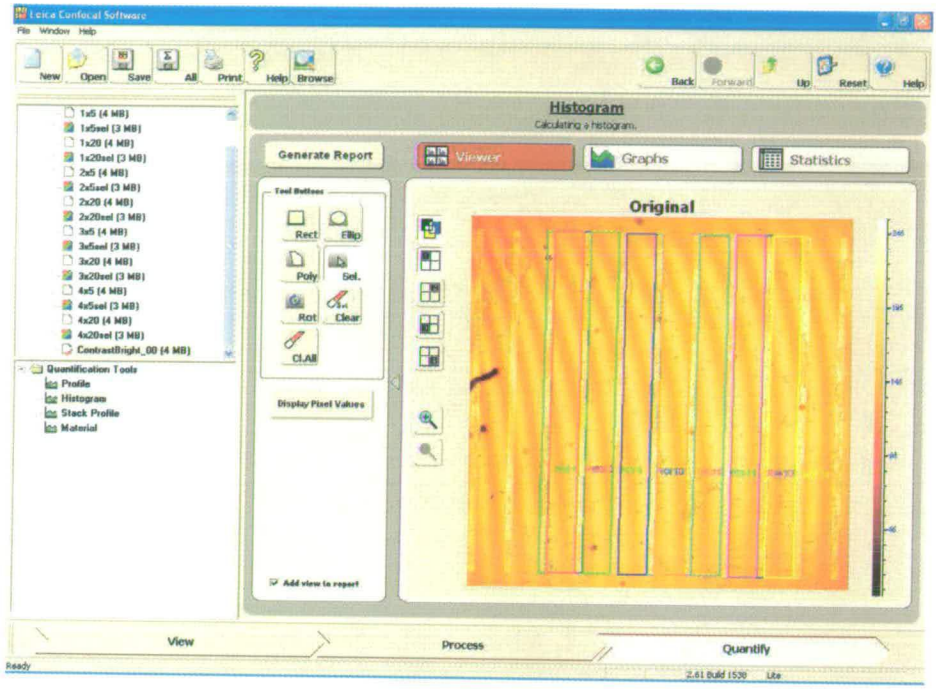

Figure 3.5: *Selection and assessment of individual parylene stripes and SiO_2 regions with the Leica Lite Confocal Software. The two parylene stripes at the far left and the far right of the pattern were omitted in order to avoid contamination of the data by border effects.*

By thresholding the corresponding photograph, a cutoff value was assigned to all the histograms calculated. As we can see in figure 3.7 this is a subjective procedure, in which the aim is to include as much biological data possible (axons, dendrites and cell somata) without adding artifactual noise. The area of the histogram above the cutoff value was considered as the amount of "green" (glia) or "red" (neurons) pixels present, while the area below was taken as the amount of "black" or void space (see figure 3.6).

On each area, parylene and thermal oxide, the quantity of green pixels was expressed as a percentage of the total pixels, by dividing the number of green pixels by the sum of green and black pixels. The same was done for the red colour and the black.

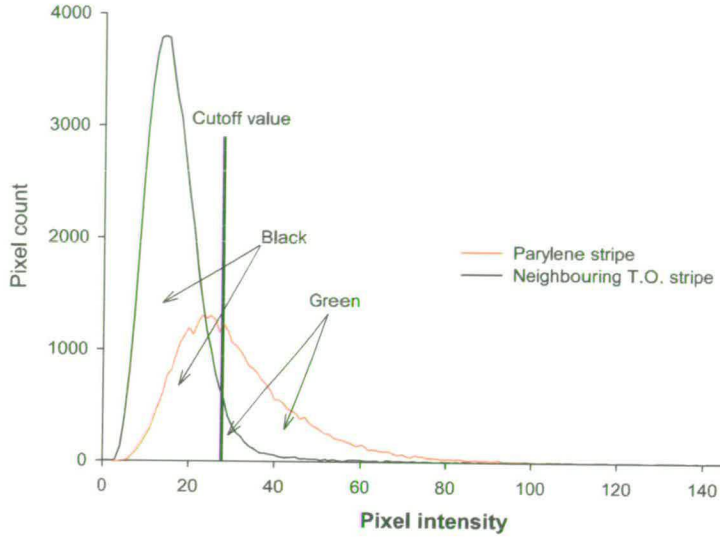

Figure 3.6: *Histograms of one parylene and one TO region seen in figure 3.5 for the green (glia) channel. The total area underneath the curves left of the cutoff value denotes the amount of black pixels, while the total area right of the cutoff values signifies the amount of green pixels. Leica Lite Confocal Software and Sigmaplot were used.*

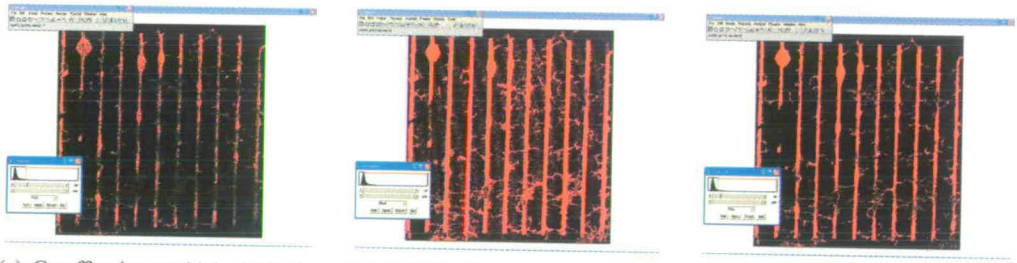

(a) Cutoff point too high: biological data will be lost

(b) Cutoff point too low: artifacts and noise are introduced

(c) Cutoff point at correct value

Figure 3.7: *Choosing the right cutoff point while thresholding an image.*

$$\%green = \frac{Green}{Green + Black_g}$$

After acquiring one "green", one "red" and two "black" percentages for each parylene stripe and thermal oxide background, the parylene percentages for each colour and the blacks were averaged. The same was done for the thermal oxide background percentages.

$$< \%green_{Parylene} >= \frac{\sum_{pstr=1}^{n} \%green_{pstr}}{n}$$

where the symbols <> denote an average while "pstr" stands for "parylene stripe".

Subsequently, the average "green" percentage of all the parylene stripes was divided by the average "green" percentage of all the thermal oxide backgrounds to attain a measure of overall glia conformity to the pattern. This was called the **green pixel density ratio**. Similarly, the measure of neuronal conformity to the pattern was termed **red pixel density ratio**. Two **black** or **void pixel density ratios**, one corresponding to green (glia) and one to red (neurons) were also calculated. The **black pixel density ratios** indicate the overall amount of glia and neurons respectively, that are present on the patterns.

$$Green\_Ratio = \frac{< \%green_{Parylene} >}{< \%green_{ThermalOxide} >}$$

The values of **green** and **red pixel density ratios** ranged from 1 (random culture) to ∞ (perfectly patterned culture), while the values of **black pixel density ratios** ranged from 1 (random culture) to 0 (perfectly patterned culture). Theoretically, in cases of inverse patterning (i.e. should neurons and glia adhere to the TO substrate and not the parylene), the **green** and **red ratios** would range from 1 (random culture) to 0 (perfectly reversely patterned culture), while the **black ratios** would range from 1 (random culture) to ∞ (perfectly reversely patterned culture).

Two way ANOVA and correlation tests were performed on pixel density ratios drawn from different images.

Polar plots In order to acquire a better contrast between experimental and control samples, each image Im_i of a patterned culture was plotted as a data point i in a polar coordinate system.

The green ratio $Green\_Ratio_i$ of each image Im_i indicated the radial coordinate ρ_i of the data point i. Therefore, data points further from the center signified images with high glia conformity to the parylene stripes.

Likewise, the black ratio $Black\_Ratio_i$ corresponding to the $Green\_Ratio_i$ signified the azimuthian angle θ of each data point i. The black ratio was expressed in degrees via the following transformation:

$$\theta_i = \frac{360 \times asin(Black\_Ratio_i)}{\pi}$$

As $Black\_Ratio_i$ values range from 0 to 1, θ_i values range from 0^o to 180^o degrees. Therefore, data points with large polar angles indicate images with low number of glia.

In a few instances where the black ratio ranged from 1 to ∞ the following transformation was adopted:

$$\theta_i = 360 - \frac{360 \times asin(\frac{1}{Black\_Ratio_i})}{\pi}$$

The same procedure was carried out for the red ratios and their corresponding black ratios for each image. This second polar scatter plot illustrated the contrast between experimental and control samples in neuronal conformity to the pattern and the amount of neuronal tissue.

Critical Assessment of the Patterning Indexes

The two statistical techniques used to analyse the data are complementary. The first patterning index focuses only on a small area at the center of the pattern. Also, it fails to account for the behaviour of the neuronal and glia processes like dendrites and axons, since the analysis summarises the cell in its nucleus. Additionally, glial and neuronal conformity to the parylene stripes can not be determined from nuclear density ratios alone, as both glial and neuronal nuclei are stained blue and can not be differentiated. On the other hand, the green and red ratios take into account the entire pattern and are not vulnerable to bias from low cell numbers. The colour or pixel ratios also incorporate dendritic and axonal behaviour as well as cell outgrowth, something which nuclear scoring fails to do. Nonetheless, green and red ratios do not examine how the cells respond to the edge between parylene and TO and rely heavily upon the quality of

the image taken with the confocal microscope and proper thresholding. In this aspect, nuclear density ratios, derived from nuclear scoring, is superior because it is more objective and offers more insight into cell reaction towards the parylene-TO border.

3.3 Results

3.3.1 Early Patterning Experiments with Parylene-C

As mentioned earlier Parylene-C was utilised at first as a non-adhesive background. Two examples of grid patterns cultured with neurons and glia can be seen in figures 3.8 through 3.10 below.

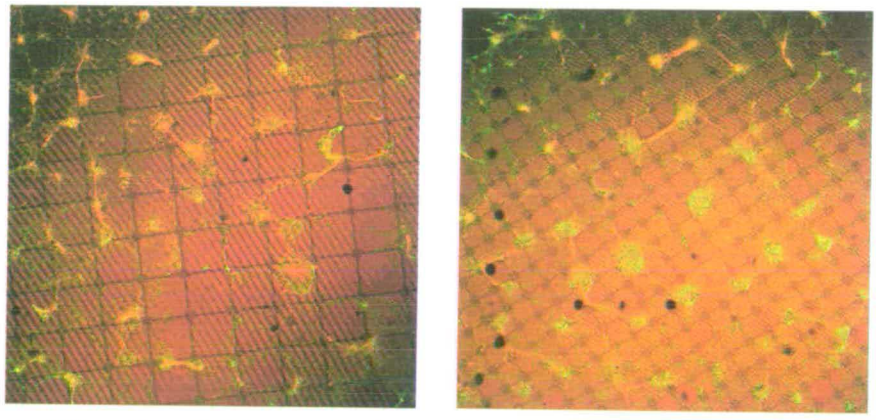

(a) Grid pattern sample 1 (x5 magnification) (b) Grid pattern sample 2 (x5 magnification)

Figure 3.8: *Parylene as the cell repellent substrate. The adhesive substrate is boron doped TO (black nodes and tracks), while the non-adhesive surface is parylene (orange background between nodes and tracks). All channels (neurons, glia and pattern) are visible. This patterning attempt has failed. Square area 2000μm x 2000μm.*

Figures 3.8 through 3.10 were classified as failed patterning attempts. It is clear that neither glia nor neurons are following the grid patterns (the black nodes and tracks is the boron doped TO while the orange background is the parylene). The neurons have coalesced into large clusters (neurospheres) that are connected through fascicled processes[2]. On the other hand, the glia have formed a large sheet of tissue which spans the entire grid pattern and provide the neurons a surface to adhere to. In both cases, there are small areas in which glia seem to be avoiding the parylene background and conforming to the nodes and tracks. However, both patterns are

[2] fascicle=bundle

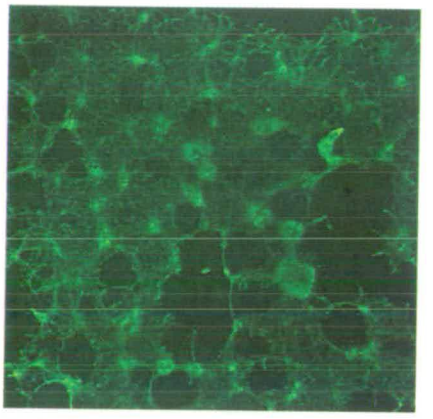

(a) Grid pattern sample 1 (x5 magnification), glia only visible

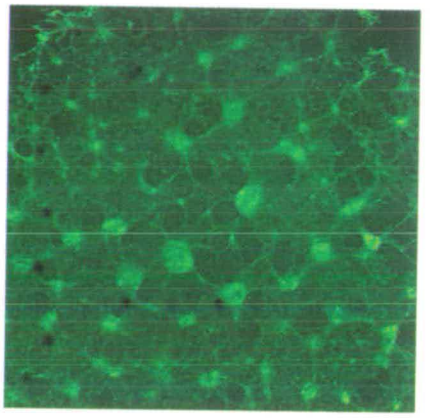

(b) Grid pattern sample 2 (x5 magnification), glia only visible

Figure 3.9: *Parylene as the cell repellent substrate. Green channel only of images 3.8(a) and 3.8(b). The patterns are overgrown with glia.*

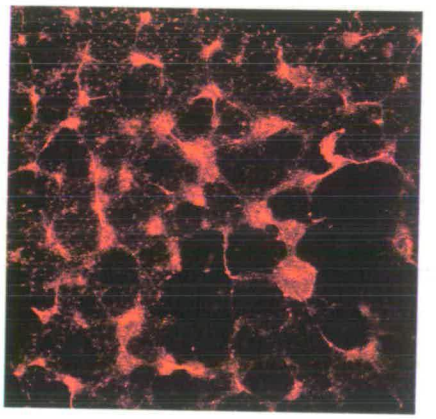

(a) Grid pattern sample 1 (x5 magnification), neurons only visible

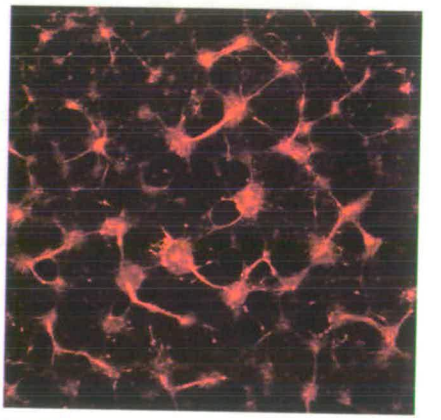

(b) Grid pattern sample 2 (x5 magnification), neurons only visible

Figure 3.10: *Parylene as the cell repellent substrate. Red channel only of images 3.8(a) and 3.8(b). Neurons have aggregated into neurospheres.*

extensively overgrown with cells that are attached to both substrates.

Further experimentation with boron doped TO and parylene yielded an inverse result, where cells avoided the former and instead adhered to the latter. This can be seen in figures 3.11(a) through 3.13

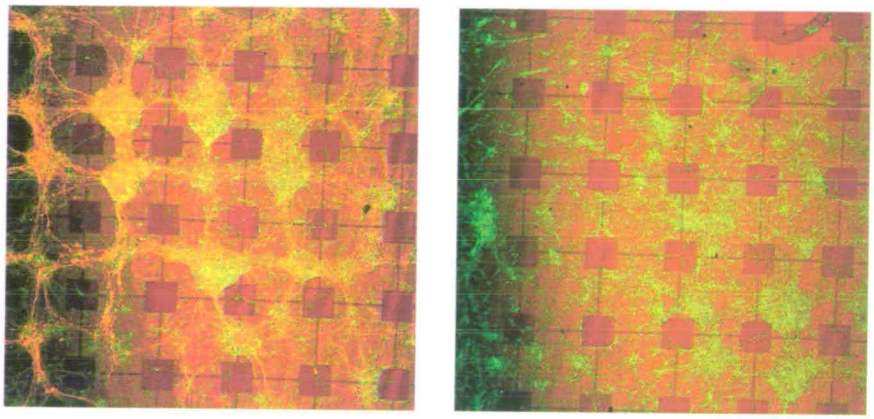

(a) Area a, all channels

(b) Area b, all channels

Figure 3.11: *The above images are from two different areas on the same pattern. Neurons (dark red) and glia (green) are adhering to parylene (light orange background), while avoiding the boron doped TO (black nodes and tracks). Notice how the nodes are empty of cells (x10 magnification, square area 1000μm x 1000μm). This result was classified as inverse patterning.*

Figures 3.11 through 3.13 illustrate a very interesting result. The majority of glia avoided the boron-doped TO and adhered to parylene instead. A number of the boron-doped TO nodes in image 3.12(b) are completely empty of cells, while the rest have only minor glia growth. The same is true in image 3.11(b). Similarly, neurons are following the glia and remain outside the grid nodes. Very few single, visible, neural processes cross a node in figure 3.12(a). This behaviour is not limited to one specific area but extends nearly over the entirety of the grid pattern in figure 3.13.

3.3.2 Parylene as the Attractive Substrate

Due to the failure of parylene as a cell repellent substrate and based on the inverse patterning result presented above, we decided to utilise parylene as a cell adhesive substrate. The patterns were also altered from grids to stripes, in order to investigate possible correlations between the spatial specifications of our patterns and the quality of patterning (see section 3.1.5). Plain TO

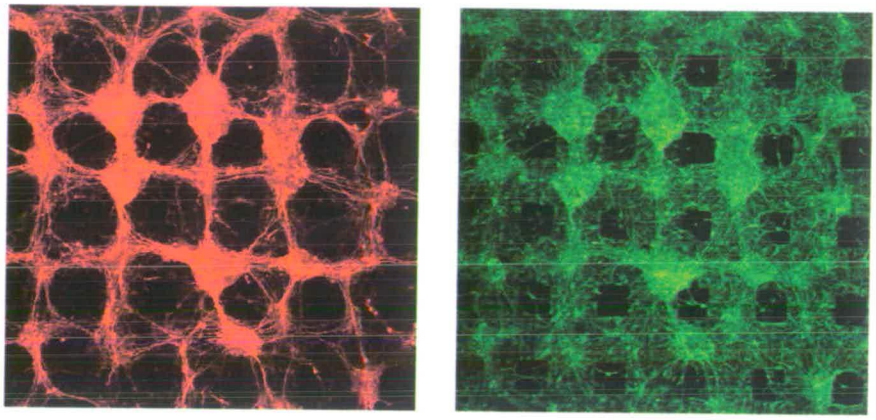

(a) Area a, neurons only

(b) Area a, glia only

Figure 3.12: *Red (neurons) and green (glia) channels of image 3.11(a). Some of the black nodes (boron doped TO) are empty, while glia are adopting peculiar conformations in order to avoid them. Neurons are following the glia. (x10 magnification)*

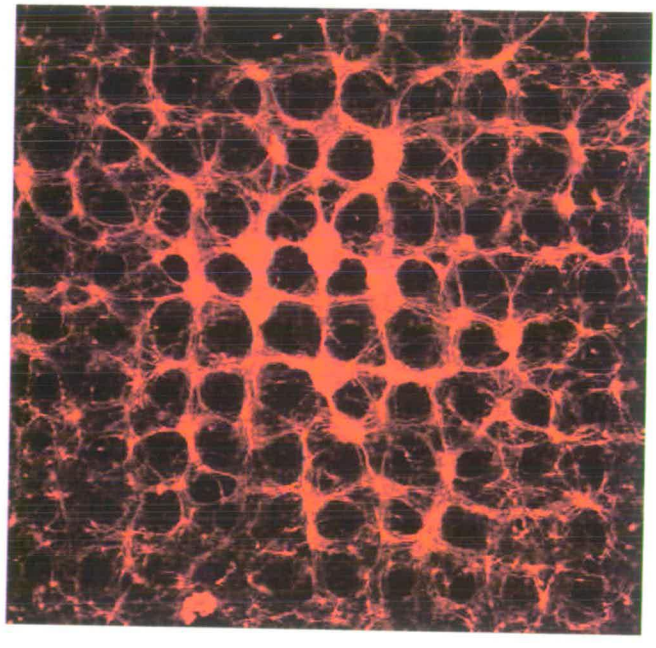

Figure 3.13: *Neurons only on a wider area (x5 magnification).*

was chosen as a new cell repellent background, based on Dworak's glial and neuronal culturing results [18]. A culture example from the early attempts is presented in figure 3.14.

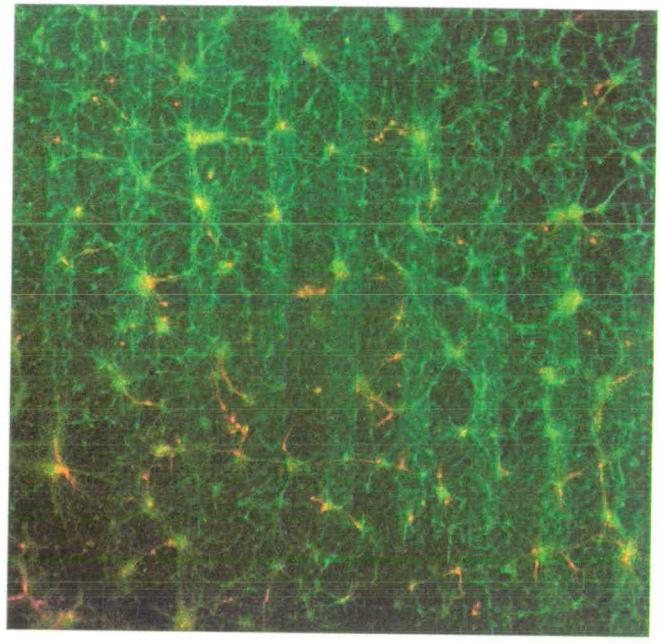

Figure 3.14: *Glia (green) and neurons (red) on a parylene stripe pattern. The black background is the TO, while the stripes can be seen faintly as rectangles running from top to bottom.*

Like in previous attempts, figure 3.14 illustrates that the contrast between parylene and TO was not enough to induce cell guidance. Glia and neurons grew over the stripes and on the TO background, disregarding the pattern. Occasionally, there were hints of patterning. In figure 3.14 for example, we can distinguish that the majority of glial clusters is located on the parylene stripes. However, the abundant growth of glia processes and the neurons residing on the TO background constitute this result suboptimal.

In order to improve these results and increase the patterning capability of parylene, we decided to utilise serum, a technique commonly used by other researchers [46, 89, 90]. The experiments and the results are described below.

3.3.3 Patterning with Horse Serum Activated Parylene

Silicon chips with parylene stripes on SiO_2 background were immersed in horse serum and left overnight in the incubator. It was hypothesized that in 24 hours the proteins in the horse

serum would adhere to either parylene or SiO_2. Control chips, which were not immersed in horse serum but in sterilised distilled water instead, were also included. Four separate experiments were performed and the plating densities for the cells ranged from $70 cells/mm^2$ to $215 cells/mm^2$ with an average of $150 cells/mm^2$.

Nuclear Densities

Figure 3.15 shows the scatter plot of the nuclear density ratios for both controls and horse serum treated samples.

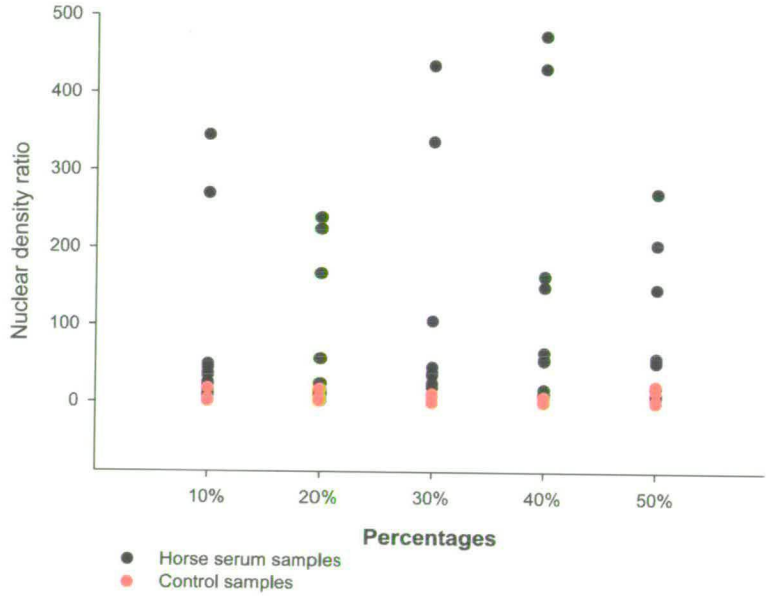

Figure 3.15: *Scatter plots of the nuclear density ratios when border nuclei were counted as being on the parylene. Red data points correspond to control samples, while black data points to horse serum samples.*

Nuclear density ratios from 4 different experiments were processed together in a two way ANOVA [3]. The first factor was Control vs Horse Serum, while the different percentages of the parylene stripes (10%-50%) was the second. The test revealed that there is no statistically significant difference ($P = 0.962$) between the mean values of different percentages: (40.792 $\pm$ 27.544, n=17) for the 10% group, (45.340 $\pm$ 28.862, n=14) for the 20% group, (56.076 $\pm$ 26.721, n=16) for the 30% group, (74.044 $\pm$ 27.910, n=16) for the 40% group and (39.474 $\pm$

[3]The data was transformed through a logarithmic operator in order to pass the normality test

25.873, n=18) for the 50% group. On the other hand, the difference between the mean value of the controls (5.533 $\pm$ 19.996, n=27) and the mean value of the horse serum treated samples (96.758 $\pm$ 14.170, n=54) is statistically significant ($P \leq 0.001$). This can be clearly be seen in figure 3.15 where the red data points (controls) are located close to the x-axis in contrast to the black data points (horse serum), which have higher y-values. In addition, there is no statistically significant interaction between the two factors ($P = 0.413$). Finally, two Pearson Correlation tests amongst the different percentages of parylene for both control and horse serum treated samples, revealed that there are no significant relationships between any pair of percentages ($P > 0.05$).

Figure 3.16 illustrates the scatter plot of the nuclear density ratios, when the cells residing on the border of parylene and SiO_2 were excluded from the calculations.

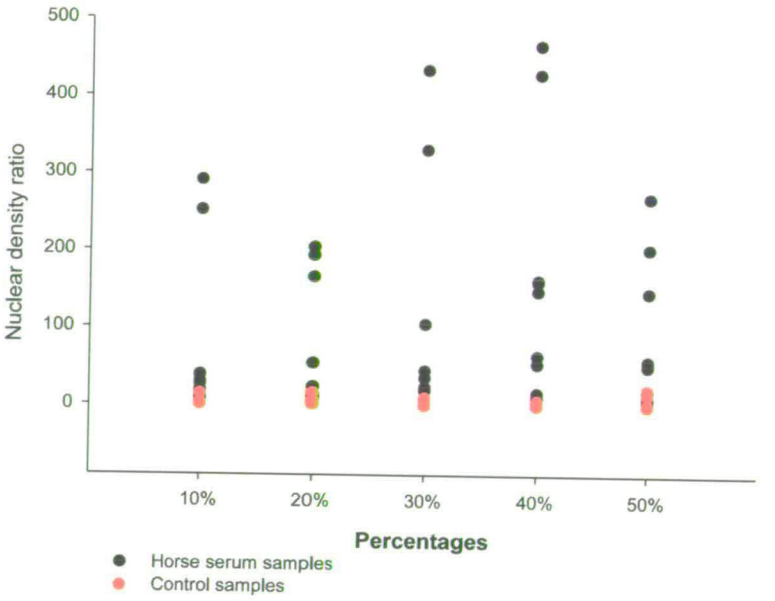

Figure 3.16: *Scatter plots of the nuclear density ratios when border nuclei were excluded. Red data points correspond to control samples, while black data points to horse serum samples.*

The same statistical tests were performed after the exclusion of the nuclei residing on the border. The results were practically the same as no statistically significant difference was found ($P = 0.965$) between the mean values across different parylene percentages: (34.374 $\pm$ 26.517, n=17) for the 10% group, (40.788 $\pm$ 27.787, n=14) for the 20% group, (54.926 $\pm$ 25.725, n=16)

for the 30% group, (72.902 $\pm$ 26.869, n=16) for the 40% group and (39.079 $\pm$ 24.909, n=18) for the 50% group. As before, the difference in mean values between horse serum treated samples (92.035 $\pm$ 13.642, n=54) and controls (4.792 $\pm$ 19.251, n=27) was statistically significant ($P \leq 0.001$). Again, there was no statistically significant interaction between the two factors ($P = 0.464$) and the Pearson correlation test showed no statistical relationships between any pair of percentages ($P > 0.05$).

Figure 3.17 is a bar graph illustrating the difference in nuclear density ratios between horse serum treated and control samples.

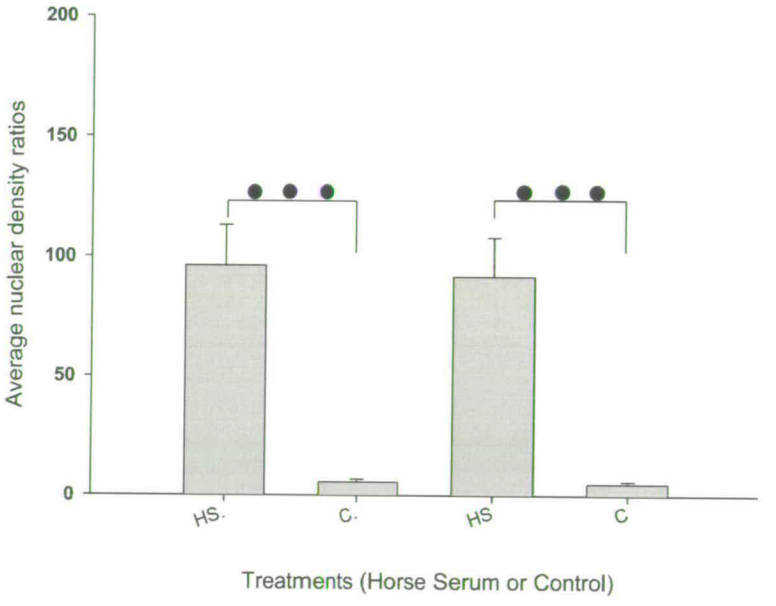

Figure 3.17: *Average nuclear density ratios for horse serum and control samples. In the two bars on the left border nuclei have been included while in the two bars on the right border nuclei were excluded from the analysis. Error bars represent the Standard Error of the Means (SEM). Three dots represent statistical significance of* $P < 0.001$.

Green, Red and Black Pixel Density Ratios

A second analysis was performed on the x5 magnification images, as described in section 3.2.6. Figure 3.18 is the scatter plot of the green pixel density ratios across different percentages for both control and horse serum samples. Similarly, figure 3.19 is the same scatter plot but for the red pixel density ratios.

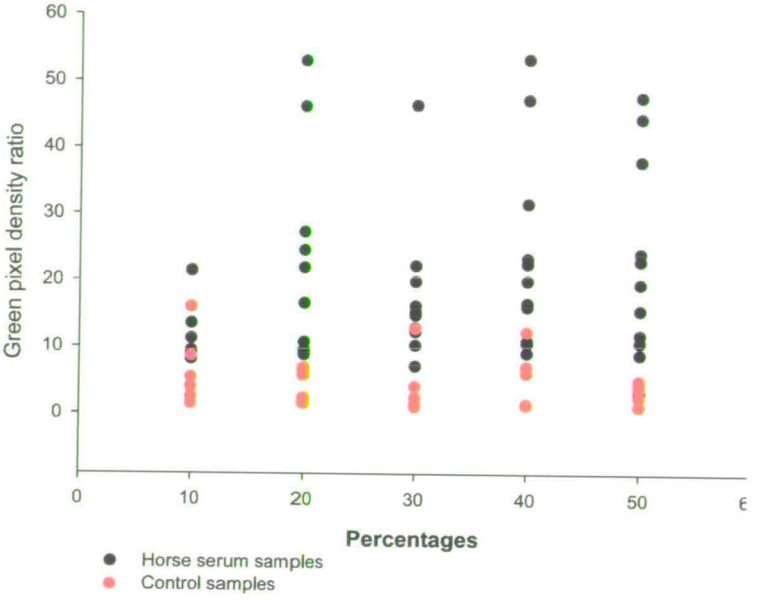

Figure 3.18: *Scatter plots of the green pixel density ratios. Red data points correspond to control samples, while black data points to horse serum samples.*

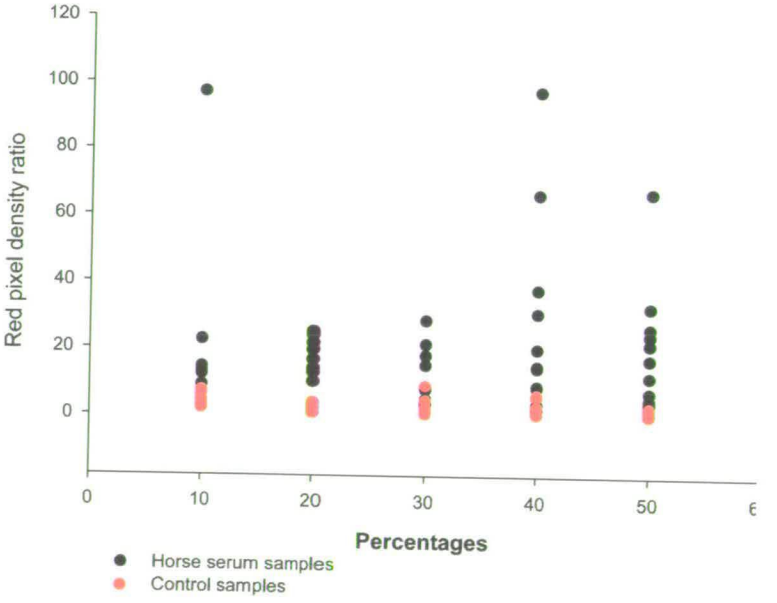

Figure 3.19: *Scatter plots of the red pixel density ratios. Red data points correspond to control samples, while black data points to horse serum samples.*

	Slope	r^2	y-axis crossing
Horse serum (green channel)	4.23×10^{-2}	5.28×10^{-3}	14.70
Horse serum (red channel)	-3.00×10^{-4}	4.00×10^{-8}	20.20
Control (green channel)	-4.35×10^{-2}	2.80×10^{-2}	6.04
Control (red channel)	-4.70×10^{-2}	9.77×10^{-2}	4.63

Table 3.6: *Linear regression statistics for horse serum and control in both channels.*

A two way ANOVA test, similar to the one described in section 3.3.3 on page 52 was performed. The first factor was treatment, horse serum or control, and the second the different parylene percentages. The green ratios were transformed through a (natural) logarithmic operator in order to pass the normality test ($P > 0.200$). The equal variance test was also passed (P=0.209). A statistically significant difference was found between the means of the horse serum treated (20.128 $\pm$ 1.569, n=50) and control (4.780 $\pm$ 2.045, n=29) samples ($P \leq 0.001$). The difference between the mean values among the different percentages ((10.101 $\pm$ 2.966, n=14) for the 10% group, (14.258 $\pm$ 2.895, n=15) for the 20% group, (10.824 $\pm$ 2.836, n=16) for the 30% group, (14.754 $\pm$ 2.962, n=16) for the 40% group, (12.335 $\pm$ 2.746, n=18) for the 50% group), both in horse serum and control samples, was not found to be statistically significant (P=0.650). There was also no statistically significant interaction between the two factors (P=0.548). Similarly, in the red colour two way ANOVA test (normality test passed $P > 0.200$ and equal variance test passed P=0.026 after a logarithmical transformation of the data) there was a statistically significant difference between the means of the horse serum (20.229 $\pm$ 2.423, n=50) and control (3.246 $\pm$ 3.158, n=29) samples ($P \leq 0.001$) while no statistically significant difference was found amongst the mean values of different percentages (P=0.234) ((14.116 $\pm$ 4.580, n=14) for the 10% group, (10.959 $\pm$ 4.470, n=15) for the 20% group, (7.679 $\pm$ 4.379, n=16) for the 30% group, (15.677 $\pm$ 4.574, n=16) for the 40% group, (10.256 $\pm$ 4.240, n=18) for the 50% group). There was also no statistically significant interaction between the two factors (P=0.883).

Linear regression lines were drawn through the four different data groups of the two scatter plots in order to examine whether a correlation existed between the different percentages. Their slopes, the r^2 values and the y-axis crossings are summarised in table 3.6.

The small r^2 values indicate the absence of any correlation between the different parylene stripe percentages and the green or red pixel density ratios. This is true for both control and horse serum samples and confirms the lack of statistical significance between the differences in the mean pixel density ratio values of various percentages found earlier, by the two way ANOVA.

The ratios of the black or "void" pixels were also calculated for each colour. These were used as a measure of the quantity of cells on the surface and the degree to which their processes had spread. Two polar plots, one for the green and one for the red colour were calculated, as explained in section 3.2.6 and are illustrated in figures 3.20 and 3.21 respectively.

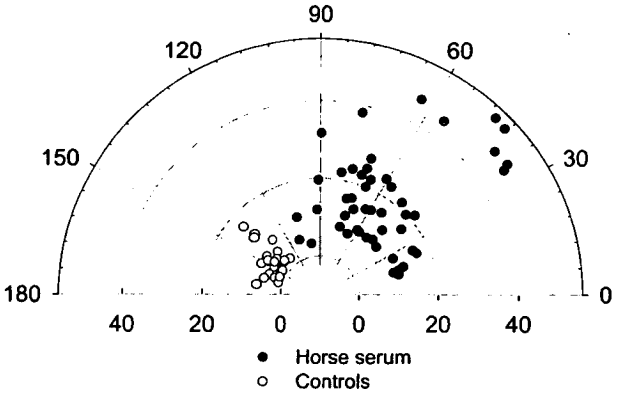

Figure 3.20: *Polar scatter plot of green ratios ρ (distance from the center) versus the corresponding black ratios (black$_g$) θ (angle from positive x-axis). The black ratios corresponding to the green colour denote the number of glia on the surface.*

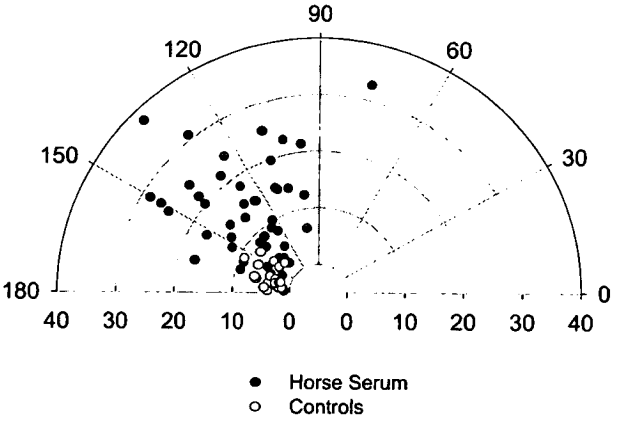

Figure 3.21: *Polar scatter plot of red ratios ρ (distance from the center) versus the corresponding black ratios (black$_r$) θ (angle from positive x-axis). The black ratios corresponding to the red colour denote the number of neurons on the surface.*

Two culture examples on each parylene percentage are given in figures 3.22 through 3.26. The first image of every set (figures 3.22(a), 3.23(a) etc.) depicts a horse serum treated sample, while the second (figures 3.22(b), 3.23(b), etc) shows a control sample.

Glia and neuronal patterning is evident on the parylene stripe patterns that were immersed in

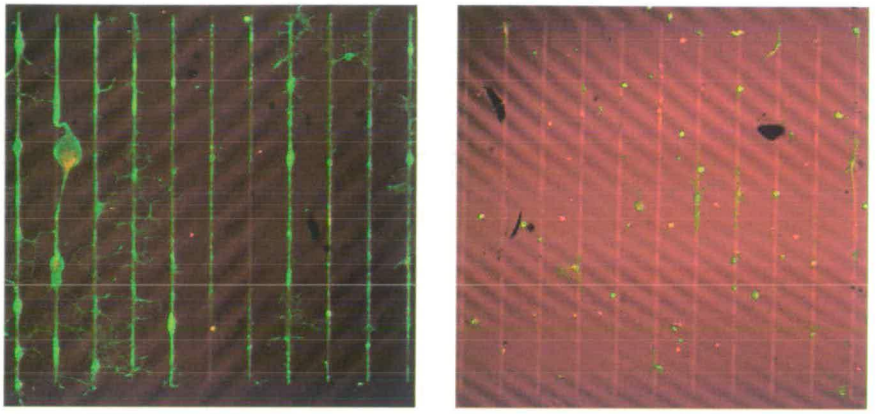

(a) Horse serum treated sample (b) Control sample

Figure 3.22: *Culture examples of 10% stripes. Glia and neurons on the horse serum treated sample have spread on the parylene, covering the entirety of the stripes and avoiding the TO background. In a few instances glia processes extend to neighbouring stripes. In contrast, cells on the control sample have formed clumps and neurospheres and are residing on both substrates (x5 magnification). The fringe effect present on the images is an artifact of reflection.*

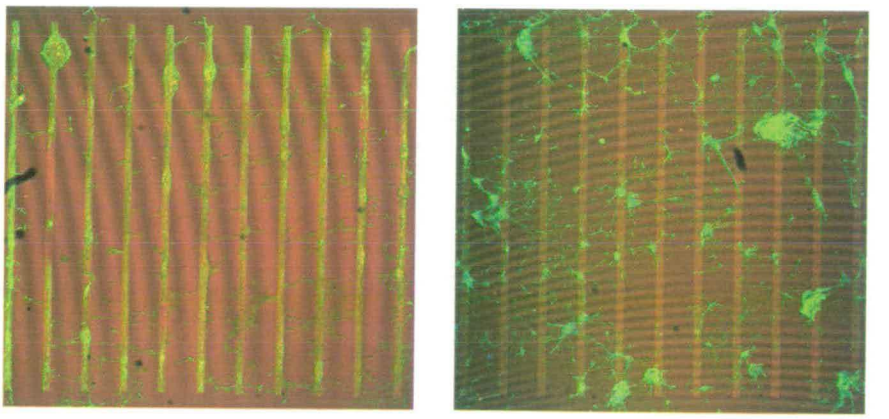

(a) Horse serum treated sample (b) Control sample

Figure 3.23: *Culture examples of 20% stripes. Glia and neurons on the horse serum treated sample have spread on the parylene, covering the entirety of the stripes and avoiding the TO background. In contrast, cells on the control sample have formed networks spanning several parylene stripes and TO background areas. Two large clusters of glia can be distinguished at the far right of the control image (x5 magnification). The fringe effect present on the images is an artifact of reflection.*

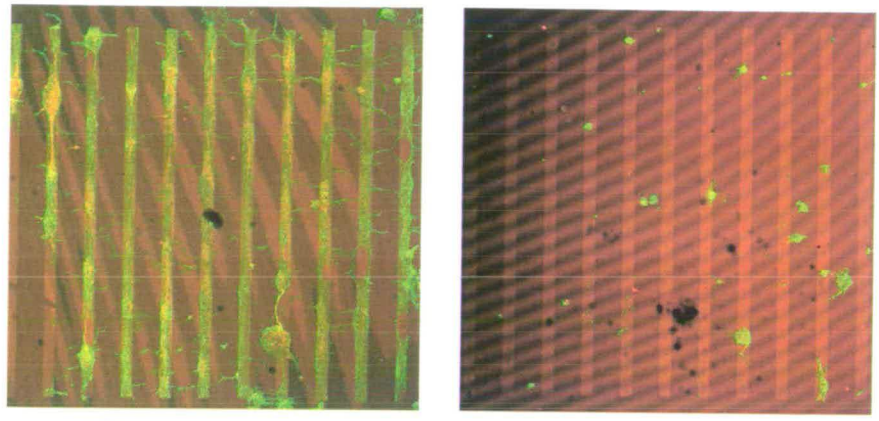

(a) Horse serum treated sample (b) Control sample

Figure 3.24: *Culture examples of 30% stripes. Glia and neurons on the horse serum treated sample have spread on the parylene, covering the entirety of the stripes and avoiding the TO background. In contrast, cells on the control sample have formed clusters and neurospheres and are residing on both substrates (x5 magnification). The fringe effect present on the images is an artifact of reflection.*

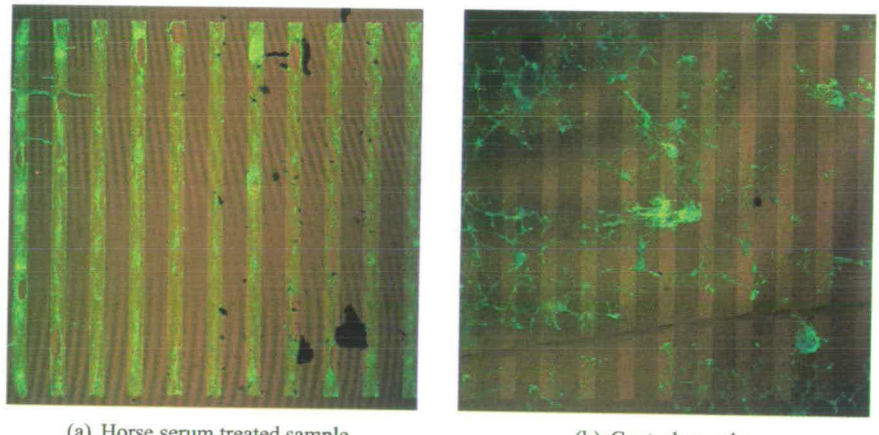

(a) Horse serum treated sample (b) Control sample

Figure 3.25: *Culture examples of 40% stripes. Glia and neurons on the horse serum treated sample have spread on the parylene, covering the entirety of the stripes and avoiding the TO background. In contrast, cells on the control sample have spread across the entire pattern, adhering to both substrates indiscriminately. A large glial cluster is located at the center of the control pattern (x5 magnification). The fringe effect present on the images is an artifact of reflection.*

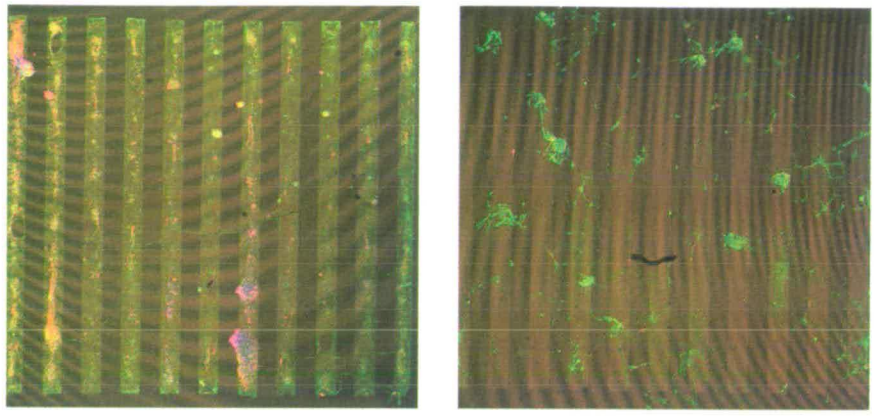

(a) Horse serum treated sample (b) Control sample

Figure 3.26: *Culture examples of 50% stripes. Glia and neurons on the horse serum treated sample have spread on the parylene, covering the entirety of the stripes and avoiding the TO background. In contrast, cells on the control sample have formed clusters covering both parylene stripes and the TO background (x5 magnification). The fringe effect present on the images is an artifact of reflection.*

horse serum overnight. In figures 3.22(a) through 3.26(a) both neurons and glia remained within the parylene stripes. Predominantly, cells have formed connections within their parylene stripes although there are cases in which glia processes have extended to other glia in neighbouring stripes. This mainly occurs on the finer stripes (10%, 20% and 30%) and distracts some neurons from following the parylene (see figure 3.24(a)). Overall however, the structure of the cell culture follows the parylene pattern.

In contrast, control patterns have failed to induce either glia or neuronal patterning. Cells coalesced into clusters and adhered to both parylene and TO (figures 3.22(b) and 3.24(b)). Alternatively, glia grew and multiplied on both substrates indiscriminately (figures 3.23(b), 3.25(b) and 3.26(b)). There are some minor hints of glial patterning in figure 3.22(b) however, cell patterning in the horse serum treated samples is far superior.

Figures 3.27(a) and 3.28(a) are high magnification culture images that illustrate the typical behaviour of glial and neuronal processes in horse serum treated surfaces.

As before, glia have covered the majority of the 3 parylene stripes. Their processes have primarily remained on the parylene, although there are a few instances in which they have extended into the TO background. At the bottom and top of the middle and right parylene stripes respectively, two glia processes are extending in the direction of the stripes and seem to be following

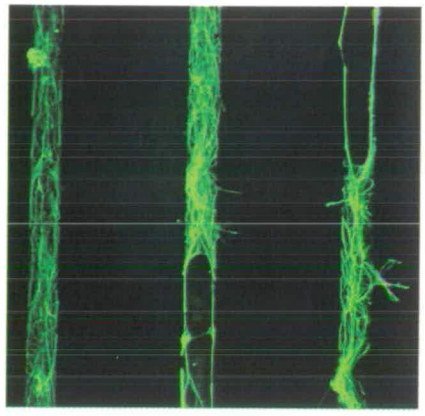

(a) Green channel only, the glia processes remain within the parylene stripes

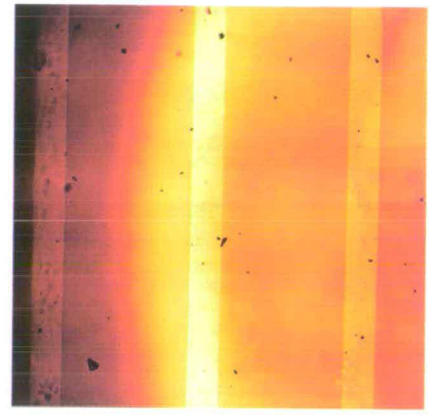

(b) Reflection only, the thinner stripes are the parylene

Figure 3.27: *Glia processes on three 20% parylene stripes (x20 magnification, square area 500μm x 500μm).*

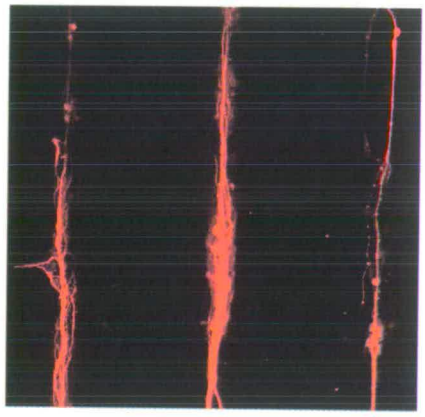

(a) Red channel only, the neuronal processes remain within the parylene stripes

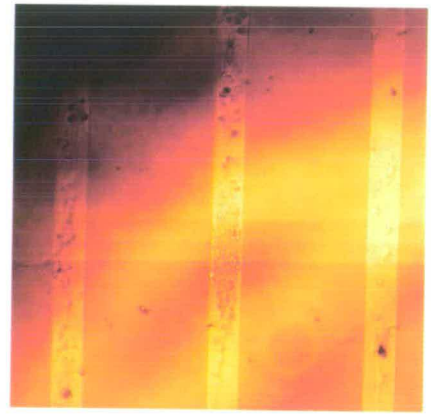

(b) Reflection only, the thinner stripes are the parylene

Figure 3.28: *Neuronal processes on three 20% parylene stripes (x20 magnification).*

the parylene-TO border (figure 3.27(a)). Neurons and their processes on the other hand are centered in the parylene stripes. On the right stripe a neuronal process is following the glia on the edge between parylene and TO (3.28(a)).

3.4 Discussion

3.4.1 Early Patterning Experiments with Parylene-C

It is evident from figures 3.8 through 3.10 that neither glia nor neurons are following the grid patterns. In figure 3.8(b) the cells have aggregated into large masses that reside on the parylene (orange background) rather than the boron-doped thermal oxide. Figure 3.8(a) can be decieving since some of the cell clumps seem located on the boron-doped nodes, while the cell processes seem to follow the tracks. However, the parylene background is still overgrown both with glia and neurons as figures 3.9(a) and 3.10(a) reveal. These cell patterns seem very poor when contrasted to the ones achieved later on when parylene was treated as the attractive surface and horse serum was utilised.

One of the obvious implications of this failure is that the contrast between the surface energies of the boron-doped thermal oxide and parylene-c is inadequate to induce cell patterning. Although prior experiments by Dworak [18] revealed different reactions of neurons and glia towards substrates of different surface energies, it is possible that these preferences on their own are not significant enough to force cells to leave a substrate they dislike for a more favorable one. This is especially true since neurons and especially glia would rather adhere to each other than choose between a surface they dislike and a surface they moderately like. This behaviour can be clearly seen in figure 3.9(b) where the glia have attached to each other forming a layer which spans the entire grid.

Of particular interest are figures 3.11, 3.12 and 3.13 where one can see the cells preferring the parylene while avoiding the boron-doped thermal oxide. This becomes apparent by focusing on the empty black nodes in figure 3.12. The cells surrounding them have adopted unusual conformations in an attempt to stay outside of those areas. This unique result has to this day remained unexplained. In light of the recent experiments with horse serum, it is possible that proteins from the culture media, or even from the cells, attached to the parylene and attracted the cells as is the case with the parylene stripe patterns. This explanation however, does not account for the other samples and does not explain why parylene in those cases did not attract

the cells similarly. In addition, the background in the later experiments of the parylene stripes was thermal oxide, not boron-doped thermal oxide.

Even though the unique sample of attractive parylene remains unexplained, it offers an additional reason as to why patterning with parylene as a repellent surface failed. Parylene despite its strong hydrophobic nature is for some reason attractive to cells, perhaps even more so than boron-doped thermal oxide. In the experiments that followed, parylene was adopted as the adhesive substrate in an attempt to investigate whether that unique result could be repeated and amplified.

3.4.2 Parylene as the Attractive Substrate

The Effect of Horse Serum

It is evident from the statistical analysis of the nuclear counts and the pixel density ratios that horse serum treatment has a significant effect in the outcome of the culture. Even when considering only nuclei that are fully residing on the parylene stripes, on average the nuclear density on the parylene is approximately 90 times higher than the nuclear density on the thermal oxide background when the chip has been immersed and incubated in horse serum. On the other hand, in the controls, the nuclear density on the parylene is only 5 times larger than the nuclear density on the thermal oxide background (see figure 3.17). Moreover, the polar scatter plots in figures 3.20 and 3.21 illustrate a clear distinction between horse serum and control data points in the green and red colour channels respectively. In figure 3.20 we can see the black data points (horse serum) are further away from the center (greater ρ values) than the white data points (controls), which signifies that the glia in the horse serum treated samples follow the parylene pattern to a greater extent than the glia in the controls. In addition, the black data points have smaller black pixel density ratios than the white (smaller θ values) which indicates that the number of glia in horse serum treated samples is greater than the number of glia in the controls. The same is true for the neurons, despite the fact that their number, both in horse serum treated and control samples, is significantly smaller than the glia . This can be seen clearly in figure 3.21 where the black data points are further away from the center than the white.

Serum has been used before to presoak surfaces [89] and also as an ingredient of the culture media [46]. Based on the literature, we hypothesised that the serum's patterning enhancing effect was due to proteins that were being deposited on the parylene, during the horse serum

treatment. Evidence for this hypothesis as well as an in depth analysis of the effects of the serum treatment are provided in section 5.4.1.

The Effect of the Parylene Stripe Width

Both the nuclear counts and the pixel density ratios reveal that differences among various percentages of parylene are not statistically significant. This offers a good indication that the factor of the parylene stripe width does not influence the outcome of the culture, that is whether there is patterning or not, as well the degree or quality of patterning. The Pearson correlations of the nuclear counts ($P>0.05$) and the linear regressions of the colour ratios provide further evidence of this. Not only are the slopes presented in table 3.6 minimal, but each respective r^2 (Pearson product-moment correlation coefficient) is also very close to zero (0) suggesting no correlation between parylene stripe width (percentage) and degree of patterning (green and red ratios).

This is a very important finding since it determines how the data will be grouped and categorised when doing the statistical analysis. Since the different percentages of parylene do not influence the final ratios then data from different percentages may be pooled together to acquire larger N numbers. In addition, it answers a fundamental question which has been present since the first patterning experiments. Are the dimensions of the pattern affecting in any way the degree to which the cells follow it? Ideally, we would like the quality and degree of the cell patterning to be independent of the spatial specifications of the pattern, since this offers greater flexibility and more choices during implementation. These experiments strongly suggest that parylene stripes ranging from 20μm to 100μm, on a silicon thermal oxide (SiO_2) background are able to attract cells equally, regardless of the stripe width.

This result disagrees with Corey's finding of a correlation between neuronal compliance to grid patterns and node diameter [91]. Moreover, Lauer et al. support the suggestion that not only node size but also gap size between nodes has an important effect in the performance of their patterns. In the same study they also illustrate a correlation between cell clustering and the width of the lines in their stripe patterns [92]. Nevertheless, both Corey's and Lauer's patterning chemistries differ from ours. Corey utilises aminosilanes as adhesive and glass or alkyl/phenylsilanes as repellent substrates. Lauer on the other hand uses micro-contact stamping to print laminin. In addition, grid geometries are dissimilar to stripe patterns, as in the former cells can grow in two dimensions. It is also possible that Corey's and Lauer's patterning techniques exhibit an optimum, due to the lack of a strong cell guiding signal in their methods.

This is also implied by Britland et al., where variations in cell alignment among different track widths were present when patterning was induced with chemical cues only (aminosilane), but disappeared when topographical cues were introduced and used in combination with chemical ones [93]. In other words, if the contrast between cell adhesive and repulsive substrates is strong enough, it can overcome the cell-cell attraction forces in patterns of various dimensions, regardless of spatial characteristics such as track width, length or distance.

Number of Glia and Neurons

As mentioned earlier in section 3.4.2 glia far outnumber the neurons in most of the cultures. There are many reasons for this. First, the starting concentrations of glia and neurons during seeding depend heavily upon the individual culture preparation. Minor changes in the culturing protocol (see section 3.2.4 in page 36), such as triturating more or less than the appropriate amount, collecting cells from other bands besides F3 or digesting the tissue for longer periods, usually result in significant variations in the final yield, quantity and types of cells. Therefore, the ratio of glia to neurons during seeding may differ considerably from one culture to the next. Most importantly however, glia divide during the culturing period of a week. Hence, even though one may begin with approximately equal quantities of glia and neurons at culture day 1, by the end of the week when the culture is stained, the glia will have the neurons far outnumbered. More information with regards to glia multiplication and its consequences in patterning are discussed in section 4.3.5.

The tenacity and ability of glia to endure a variety of environments could be another explanation for their greater quantity. It is known that glia not only are more resilient but also adhere to different substrates more quickly and firmly than neurons [94]. This could explain the consistently lower amount of neurons on the chip as some of them might be dying during culture or falling of the surface due to weak adhesion. However, despite their low number, neurons that remain on the chip tend to pattern equally well with, if not better than glia.

Interpreting the Two Patterning Indexes: Nuclear Densities and Pixel Density Ratios

The nuclear counts in figures 3.15 and 3.16 illustrate that glia and neuronal nuclei follow the parylene stripes, especially after horse serum treatment of the surfaces. This result is not affected by nuclei residing on the border between parylene and thermal oxide as the statistical

analysis reveals (see page 53). In addition, patterning of the nuclei can not be explained exclusively by the presence of edges at the parylene stripes as there is a massive difference in nuclear densities between horse serum samples and controls, which is of course statistically significant (see page 52). In other words, cell nuclei do not just follow the edges of the parylene stripes but instead actively seek the adhesive parylene background, particularly when it has been treated with horse serum. Besides, Britland et al. have showed that cells respond to topographical cues when their dimensions are in the range of 500nm-1μm or greater [93]. In our patterns, the height of the parylene stripes is limited to approximately 100nm.

On the other hand, pixel density ratios reveal not only that cells adhere to the parylene but their processes follow and stay in the parylene stripes as well. Combining the pixel density ratios and the nuclear densities we can arrive at the following model of neuronal and glia behaviour in this horse serum and parylene based patterning method:

Following seeding and during the early phases of the incubation, recently dissociated glia and neurons seek and adhere to the protein loaded parylene stripes. As the incubation period (week) progresses, the cells divide while extending processes which also follow the parylene substrate.

Provided the above model is accurate, patterning in this technique is due to a persistent effect which lasts throughout the incubation period of one week. Further to the statistical analysis of the pixel density ratios and the nuclear densities, figures 3.27(a) and 3.28(a) illustrate how the majority of cell processes remain within the parylene area while their orientation matches the orientation of the stripes. Additional, evidence which support this model of cell behaviour are provided in section 4.4.2 on page 102.

3.5 Conclusions

Various patterning techniques based on photolithography were tested. Parylene-C, a polymer of xylylene, was examined as a cell repellent background however preliminary experiments revealed it would be more suitable as a cell adhesive substrate. Following the trend in literature, we used horse serum in an attempt to coat our surfaces with proteins and amplify their patterning capacity. Results indicate that when patterns of parylene on a TO background are immersed in horse serum, they become strongly attractive to neurons and glia and can induce cell patterning for a period of at least one week. What is more, the quality of the glial and neuronal patterns is not dependant on the geometry of the parylene stripes but is consistently

good across different stripe widths, ranging from 20μm to 100μm. This cell patterning method is not relying on the topographical features of the parylene patterns, but is an effect of the horse serum in combination with parylene and TO.

Chapter 4

Optimising the Technique

4.1 Introduction

This chapter focuses on the experiments carried out to optimise and better understand the parylene patterning protocol. Besides the obvious benefit of improving the technique, optimisation experiments would allow us to modify the patterning method in order to better suit the needs of the planar patch-clamp project. Moreover, there were many unknown factors surrounding the protocol which had to be examined. For example, at the time we were not aware whether parylene patterns were storable or whether their quality would degrade over time. In addition, the immersion period of the surfaces in the horse serum was time consuming, while the incubation period of one week was not long enough to allow one to investigate the presence of activity in the neural network.

The issues that were investigated in this project with regards to the parylene patterning method are the following:

- the possibility of decreasing the immersion time of the surfaces in the horse serum to a few hours instead of a day
- the possibility of using alternative serum to coat the surfaces (foetal bovine instead of horse serum for example)
- the sustainability of the patterning beyond the first week
- the effect of glia behaviour and multiplication on the method
- the behavioural model of the cells (the presence of cell migration)
- the effect of various parameters (such as UV exposure and horse serum batch) on the outcome of the experiment

- the durability and longevity of the parylene patterns

There were some minor concerns on the effect of fixation on the final results. The investigation of this issue is also covered in this chapter.

4.2 Materials and Methods

In general the materials and methods employed in optimisation experiments are similar to the materials and methods of section 3.2. The parylene stripe pattern fabrication procedure was altered and stripes of new widths were chosen as explained below. However, the surface cleaning and sterilisation, the primary neuronal cultures, the staining and imaging and the statistical analysis were similar to those in sections 3.2.3, 3.2.4, 3.2.5, and 3.2.6 respectively. Minor alterations are described below.

4.2.1 Stripe Pattern Fabrication

The protocols utilised to create the parylene stripe patterns are similar to those of section 3.2.1. There was however a deviation in the widths of the parylene stripes used. With the exception of the experiments concerning the longevity of the parylene patterns and the serum immersion time, in which the initial 10%-50% stripes were used, 5%, 10% and 20% parylene stripes were generally employed. The patterns were also embedded onto a single rather than separate chips. The layout of the chip and the patterns can be seen in figure 4.1

4.2.2 Surface Cleaning and Sterilisation

Piranha acid was utilised similarly to section 3.2.3 in order to clean and activate the surfaces. For sterilisation the surfaces were exposed to UV light for 1 hour in a class 2 hood as in section 3.2.3. In the experiments where the effects of UV radiation on the surfaces were examined, an alternative sterilisation method was used, while UV sterilisation was applied only to the controls. The patterned surfaces and the glass coverslips were instead immersed in penicillin/streptomycin for 1 hour.

As usual the glass was immersed in poly-D-lysine, while experimental samples were immersed in horse serum overnight. In the experiments examining the immersion period, some parylene

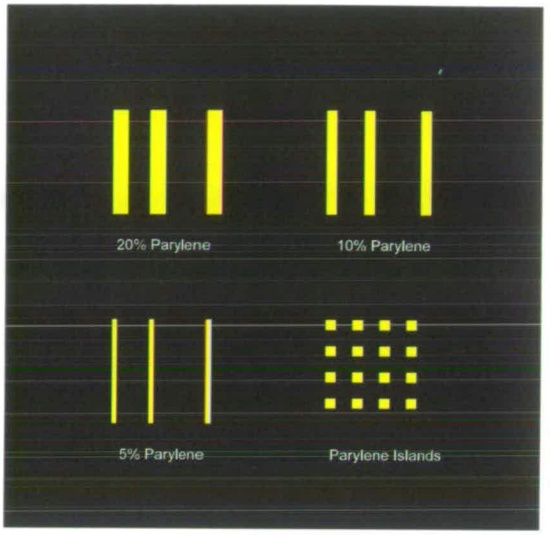

Figure 4.1: *A schematic of the new chip with the 3 parylene(yellow) stripe patterns embedded. The black background is the thermal oxide.*

patterns were immersed only for 3 hours instead of the usual 24.

Foetal bovine serum was also used and contrasted to horse serum. As in horse serum, surfaces were immersed and incubated overnight.

4.2.3 Primary Neuronal Cultures

The dissociation and culture protocols of section 3.2.4 were followed. In experiments testing the longevity of the patterned cultures the incubation times were extended up to 3 weeks. Additionally, in experiments investigating the effect of glial multiplication, various seeding cell densities were tested. Finally, in experiments examining cell behaviour and cell migration, the well shaking steps at 3 hours and 3 days after seeding were omitted in the experimental samples and were applied only to the controls.

4.2.4 Immunofluorescence Staining and Confocal Microscopy

The immunofluorescence staining protocol of section 3.2.5 was followed in all the experiments.

To evaluate the effects of the fixative solution (4% para-formaldehyde), an alternative staining procedure was employed in conjunction with optical microscopy. The technique utilised Green

fluorescent fluorescein diacetate (CellTracker Green CMFDA, C-2925 and C-7025) [88] which is a stain that operates on living cells. The CellTracker Green was added to the growth media while the cells were still alive, to a final concentration of 10μM. Cultured cells were incubated for 60 minutes at 37^{o}C and were then viewed with an optical Olympus BX50WI microscope and imaged with a Hamamatsu ORCA-ER C4742-95 digital camera. Finally, they were fixed and mounted as described in section 3.2.5.

4.2.5 Statistical Analysis

The data from these experiments have undergone the statistical analysis described in section 3.2.6

4.3 Results

4.3.1 Aged Surfaces

Ten parylene stripe patterns were cleaned, left in storage for 2 months and then cultured as per the protocol in section 3.2.4. Ten more patterns were cleaned one day prior to the culture and acted as controls. The plating density of the culture was 60 cells/mm^2. Serum was not used in the experimental or control samples of this experiment.

A one way ANOVA test was conducted on the green pixel density ratios collected. Both normality and equal variance tests passed (P=0.176 and P=0.473 respectively). The difference in the means of the green pixel density ratios between the aged (3.573 $\pm$ 0.472, n=10) and the control samples (4.104 $\pm$ 0.389, n=10) was not statistically significant (P=0.397). A similar one way ANOVA test was carried out on the red pixel density ratios (normality and equal variance tests passed with P>0.2 and P=0.452 respectively). There was no statistically significant difference (P=0.186) between the means of the red pixel density ratios of the aged (2.534 $\pm$ 0.318, n=10) and control samples (3.217 $\pm$ 0.382, n=10).

One way ANOVA tests were performed on the nuclear density ratios as well. When considering all nuclei (normality and equal variance tests passed with P=0.039 and P=0.315 respectively), differences detected between the means of nuclear density ratios of aged (2.559 $\pm$ 0.674, n=10) and control samples (4.160 $\pm$ 0.973, n=10) were insignificant (P=0.193). When nuclei residing on the border between parylene and thermal oxide were excluded differences in the means

of aged (2.241 $\pm$ 0.603, n=10) and control samples (3.112 $\pm$ 0.705, n=10) were again not statistically significant (P=0.360).

The bargraphs of figures 4.2 and 4.3 summarise the above results.

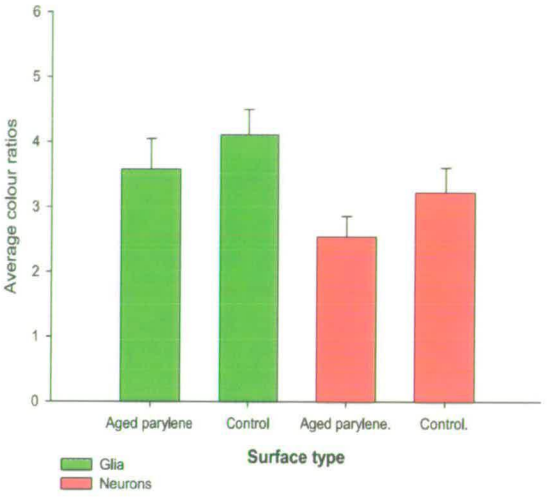

Figure 4.2: *Pixel density ratios in aged surfaces vs recently cleaned surfaces (controls). Horse serum was not used in either group. No statistically significant differences detected. Error bars represent the Standard Error of the Means (SEM). One dot represents statistical significance of* $P < 0.05$*, two dots represent statistical significance of* $P < 0.01$*, three dots represent statistical significance of* $P < 0.001$.

4.3.2 Application of Horse Serum for 3 Hours vs Overnight

Ten surfaces, 2 from each parylene stripe percentage (10%-50%) were immersed in horse serum for 3 hours, while ten more were immersed and left in the incubator overnight. Finally, ten surfaces were also immersed in sterilised distilled water and left overnight as controls, while glass coverslips treated with poly-D-lysine were also included to access the success of the culture. The plating density of the culture was approximately 150 cells/mm^2.

Figures 4.4 and 4.5 are two representative examples of the two treatments, while figure 4.6 is a control.

We can see that little, if any, differences exist between images 4.4 and 4.5. With only minor exceptions, glia (green) and neurons (red) adhered to the parylene stripes and avoided the TO background (brown). In figure 4.4 a cluster of glia is located on the TO background, while

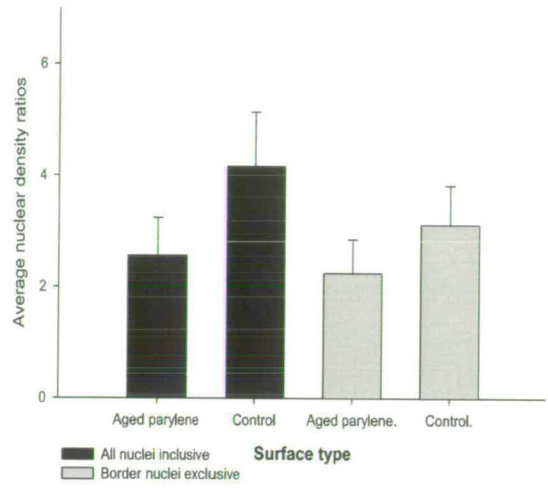

Figure 4.3: *Nuclear density ratios in aged surfaces vs recently cleaned ones (controls). Horse serum was not used in either group. No statistically significant differences detected. Error bars represent SEMs.*

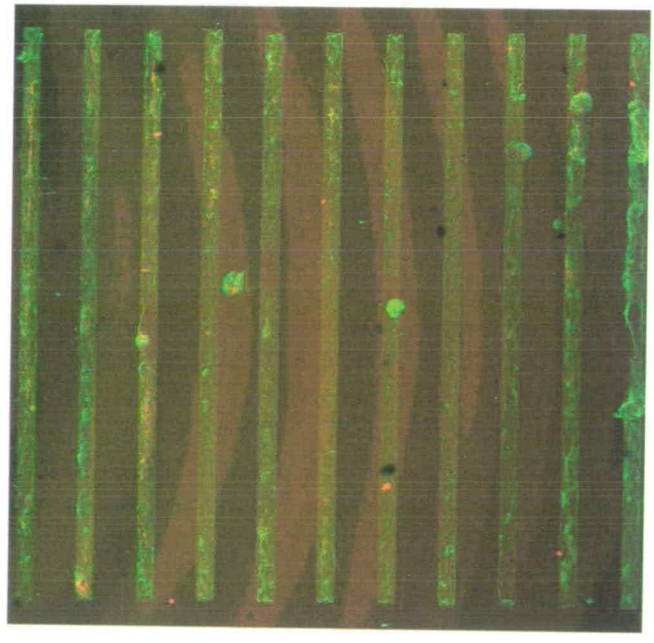

Figure 4.4: *Immersed in horse serum overnight (30% stripes, x5 magnification).*

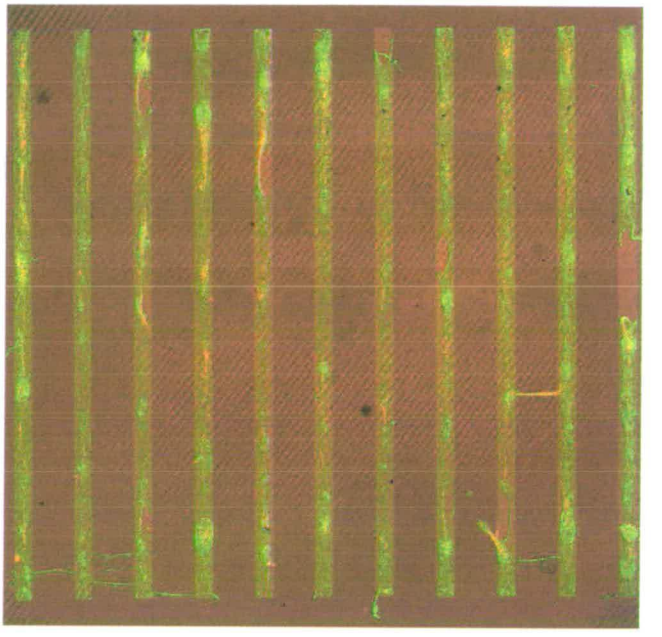

Figure 4.5: *Immersed in horse serum for 3 hours (30% stripes, x5 magnification).*

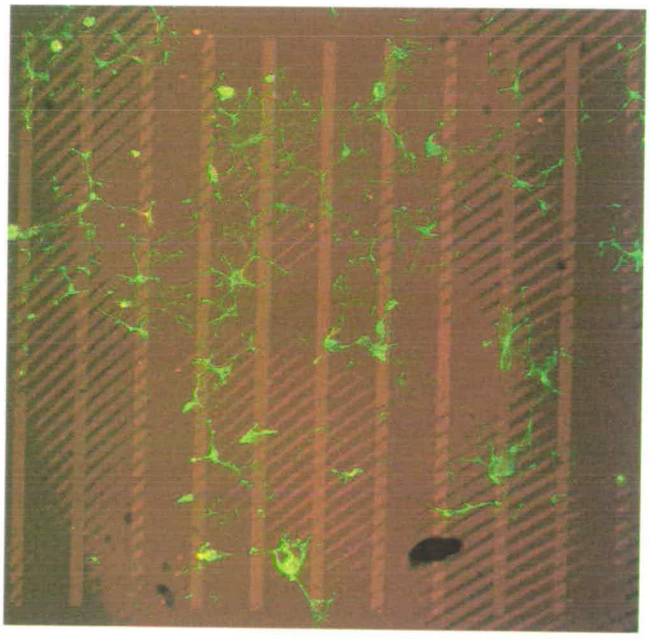

Figure 4.6: *Immersed in distilled water overnight (x5 magnification).*

in figure 4.5 a few glial and neuronal processes have extended to neighbouring stripes. These incidents however are limited and are expected even in good cell patterning examples. In contrast, the control pattern (figure 4.6) is overgrown with glia, which appear to adhere both to the parylene stripes and to the TO background. Additionally, there are distinctly less neurons in this culture than the previous two. The statistical analysis performed on the pixel and nuclear density ratios confirms these findings.

A two way ANOVA test was performed on the green pixel density ratios representing the glia. The first factor was the treatment and consisted of three choices, overnight immersion in horse serum, 3 hour immersion in horse serum and overnight immersion in sterilised distilled water which was the control. The second factor was the different parylene percentages from 10% to 50%. Both normality and equal variance tests passed (P=0.118 and P=0.101 respectively). No statistically significant difference was found between overnight (38.061 $\pm$ 4.762, n=10) and 3 hour (41.865 $\pm$ 12.223, n=10) immersion in horse serum (P=0.982). There was also no statistically significant difference (P=0.479) between the means of different percentages ((35.935 $\pm$ 13.87, n=6) for the 20% group, (26.914 $\pm$ 12.81, n=5) for the 30% group, (21.78 $\pm$ 10.168, n=5) for the 40% group, (23.191 $\pm$ 6.524, n=8) for the 50% group), while the two factors (treatment and percentage of parylene area) did not interact in a statistically significant way (P=0.512). However, as expected, a statistically significant difference was found ($P \leq 0.001$) between overnight immersion in horse serum and control (1.7 $\pm$ 0.173, n=10) and 3 hour immersion and control ($P \leq 0.001$).

The results for the red pixel density ratios (neurons) were similar. Equal variance and normality tests passed with P=0.022 and P=0.111 respectively. Differences in the mean values of the various treatments and differences between the mean values of various percentages ((15.118 $\pm$ 5.467, n=6) for the 20% group, (11.396 $\pm$ 5.827, n=5) for the 30% group, (24.648 $\pm$ 18.601, n=5) for the 40% group, (28.338 $\pm$ 11.271, n=8) for the 50% group) were not found statistically significant (P=0.427 and P=0.948 respectively). Finally, no statistically significant interactions existed between the treatment and parylene percentage factors (P=0.921), while red ratio means in the controls (1.852 $\pm$ 0.37, n=10) were significantly different from those of the overnight (27.933 $\pm$ 9.779, n=10) and 3 hour (34.1 $\pm$ 11.063, n=10) horse serum immersion treatments ($P \leq 0.001$ for both).

Figures 4.7 and 4.8 depict the scatter plots of the green and red pixel density ratios respectively while figure 4.9 is a bar graph which summarises the differences between the green and red

pixel density ratio means of various treatments.

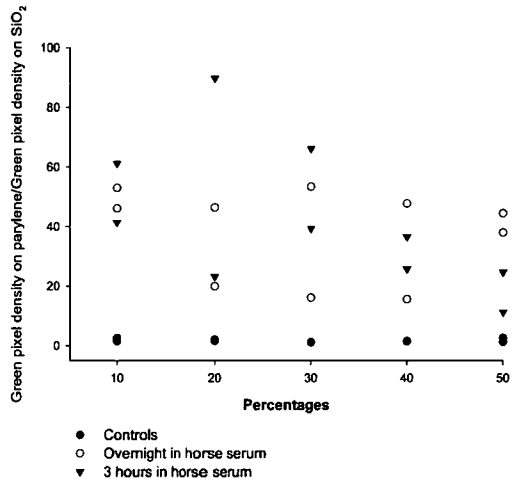

Figure 4.7: *Scatter plots of the green pixel density ratios. The majority of the control data points are close to the x-axis and below the data points corresponding to the 2 horse serum treatments. The data points from the 2 horse serum treatments are entwined*

Similar statistical tests were carried out on the nuclear density ratios. In particular, a two way ANOVA test (normality test passed $P>0.2$, equal variance test passed $P=0.106$) revealed that no statistically significant difference existed between the nuclear density ratio means of various treatments ($P=0.857$). Similarly, no statistical differences existed ($P=0.724$) between the means of various percentages ((104.984 $\pm$ 54.87, n=6) for the 20% group, (74.001 $\pm$ 53.39, n=6) for the 30% group, (142.163 $\pm$ 81.801, n=5) for the 40% group, (128.163 $\pm$ 46.997, n=8) for the 50% group), while there was no statistically significant interaction between treatments and percentages ($P=0.4$). Finally, a statistically significant difference did exist ($P\leq0.001$) between controls (1.872 $\pm$ 0.355, n=10) and 3 hours (138.878 $\pm$ 46.391, n=10) in horse serum ($P\leq0.001$) and controls and overnight (155.728 $\pm$ 46.4, n=12) immersion in horse serum.

When taking into account only nuclei residing fully on the stripe (nuclei residing on the border were excluded) the results remained similar. No statistically significant differences were found ($P=0.835$) between 3 hours (136.901 $\pm$ 46.25, n=10) and overnight (152.345 $\pm$ 45.691, n=12) or various percentages ($P=0.7$) ((104.786 $\pm$ 54.943, n=6) for the 20% group, (73.958 $\pm$ 53.401, n=6) for the 30% group, (142.096 $\pm$ 81.83, n=5) for the 40% group, (128.088 $\pm$ 47.026, n=8) for the 50% group). Treatments and percentages were not found to interact in a statistically

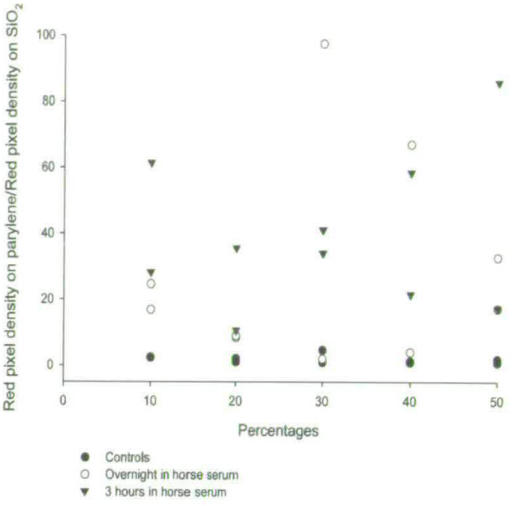

Figure 4.8: *Scatter plots of the red pixel density ratios. The majority of the control data points are close to the x-axis and below the data points corresponding to the 2 horse serum treatments. The data points from the 2 horse serum treatments are entwined.*

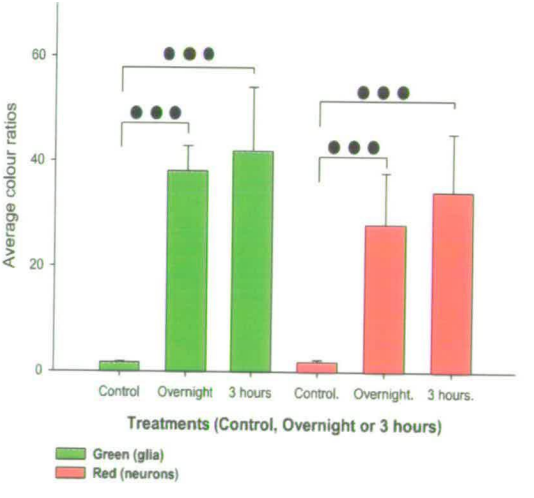

Figure 4.9: *Overnight treatment, 3 hour treatment and control. The 3 bars on the left represent the green ratio means while the 3 bars on the right the red. Error bars represent SEMs.*

significant way (P=0.392). Finally, the differences between controls (1.362 ± 0.22, n=10) and overnight or 3 hours treatment were statistically significant (P≤0.001). Both normality and equal variance tests passed (P>0.2 and P=0.108 respectively).

Figures 4.10 and 4.11 are the scatter plots of the nuclear density ratios with and without border nuclei respectively.

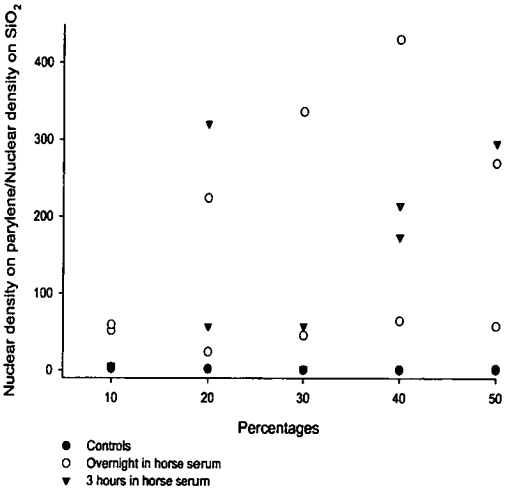

Figure 4.10: *Scatter plots of the nuclear density ratios of the 2 treatments and control across the percentages. Control data points are located close to the x-axis while overnight and 3 hour treatment data points lie entwined, away from the controls. Border nuclei were included in the calculations.*

Figure 4.12 is a bar graph which summarises the differences between the nuclear density ratio means of various treatments.

4.3.3 Detachment of Cells from the Surfaces

Twelve surfaces, 4 from each percentage (5%, 10% and 20%), were immersed in horse serum overnight and cultured with brain cells the following day. Three hours after plating, the wells in which half of the surfaces (2 from each percentage) resided were shaken in order to rinse of cell debris and cells that were not well attached (this technique is also employed by other researchers [46], for more details see the end of the protocol in section 3.2.4). The other six wells were left in the incubator. Similarly, 3 days later, the same wells were shaken again and their media was changed while on the rest, the media change occurred without the usual

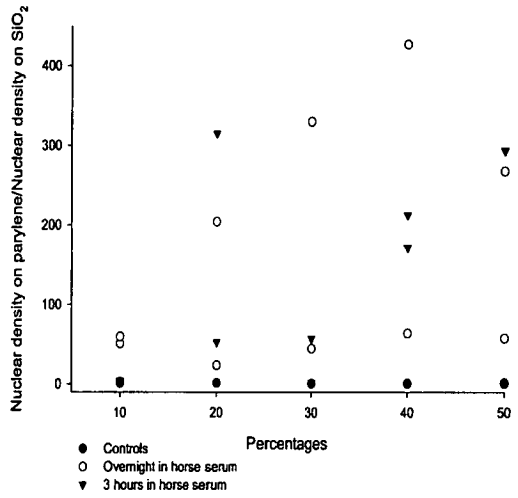

Figure 4.11: *Scatter plots of the nuclear density ratios of the 2 treatments and control across the percentages. Control data points are located close to the x-axis while overnight and 3 hour treatment data points lie entwined, away from the controls. Border nuclei are omitted from the calculations, no significant change in the results.*

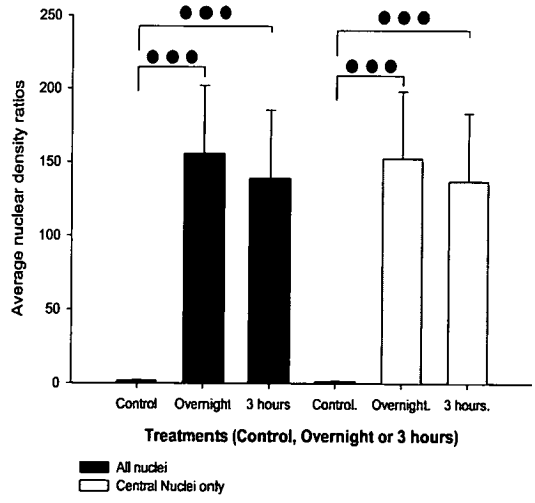

Figure 4.12: *Overnight treatment, 3 hour treatment and control. On the 3 bars on the left all the nuclei were taken into account while on the 3 bars on the right border nuclei have been excluded. Error bars represent SEMs.*

shaking. The first group of surfaces were called "shaken" while the other "non shaken". Twelve surfaces that were not immersed in the horse serum but in distilled water instead were also included as controls. The plating density for all the surfaces was approximately 80 cells/mm^2.

Figures 4.13 and 4.14 are two examples of the shaken and non shaken cultures respectively.

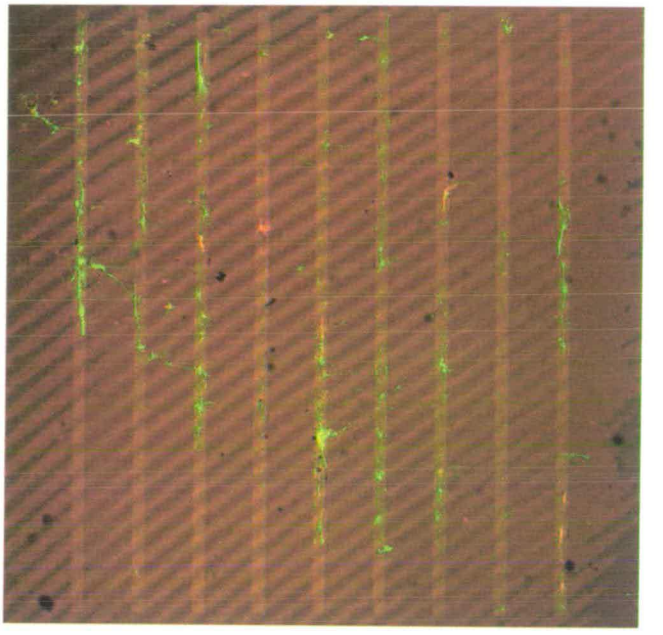

Figure 4.13: *Shaken culture (20% stripes, x5 magnification).*

Despite the apparent difference in amount of cells between the two examples, in both cultures cells have conformed to the pattern equally well. A close inspection of the images reveals that more glia and neurons are present in culture 4.14, as green pixels exist in the full length of all parylene stripes, while red pixels are also more predominant compared to culture 4.13. On the other hand, a number of parylene stripes in image 4.13 are half empty, whereas neurons are more sparse. Nonetheless, glia and neurons have followed the parylene stripes and have avoided the TO background in both cases. This empirical description is supported by the statistical analysis on the pixel and nuclear density ratios.

A two way ANOVA test was performed on the green pixel density ratios. The two factors were "shaken" or "non shaken" and horse serum or control. Both equal variance and normality tests passed (P=0.246 and P>0.2 respectively). The mean value of the "shaken" samples (14.149 $\pm$ 2.170, n=11) was not found to be significantly different (P=0.348) from the mean value of the "non shaken" samples (11.090 $\pm$ 2.313, n=10). Yet again, the difference between the means

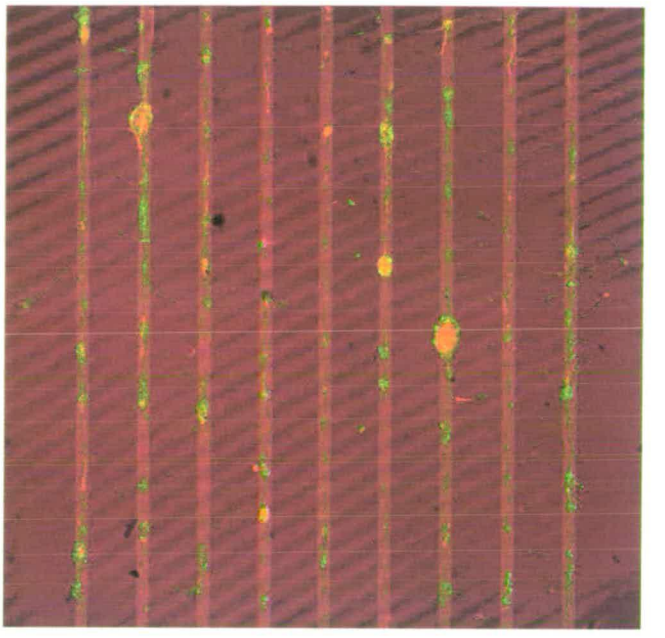

Figure 4.14: *Non shaken culture (20% stripes, x5 magnification).*

of horse serum treated samples (21.054 ± 5.128, n=5) and controls (7.248 ± 1.198, n=6) was found to be statistically significant when taking into account the "shaking" factor (P=0.018). However, there were no statistically significant interactions between the two factors (P=0.099) therefore, the effect of shaking does not depend on whether the surfaces have been immersed in horse serum or not.

A second two way ANOVA test was performed in which the horse serum treatment factor was replaced with the percentage of parylene area (5%, 10% and 20%) factor. Again no statistically significant difference was found between the shaken (13.399 ± 2.794, n=11) and non shaken (10.930 ± 3.061, n=10) samples (P=0.560) as well as between samples of different percentages (P=0.687) ((10.403 ± 4.191, n=5) for the 5% group, (14.610 ± 3.246, n=8) for the 10% group, (11.480 ± 3.246, n=8) for the 20% group). Finally, no statistically significant interaction existed between the factors of shaking and parylene percentage (P = 0.621).

With regards to the red pixel density ratios the results were as follows. The two way ANOVA test passed both equal variance and normality tests with P=0.189 and P>0.2 respectively. As expected there was a statistically significant difference (P=0.002) between the means of horse serum treated samples (8.864 ± 1.596, n=5 for shaken or 10.553 ± 2.067, n=6 for non shaken) and controls (2.885 ± 0.865, n=6 for shaken or 4.4 ± 1.72, n=4 for non shaken). There was no

statistically significant difference (P=0.346) between the means of "shaken" (5.874 ± 1.131, n=11) and "non shaken" (7.478 ± 1.206, n=10) samples. There was also no statistically significant interaction (P=0.959) between the factor of horse serum treatment and the shaking factor.

On the second two way ANOVA test (equal variance and normality tests passed with P=0.822 and P>0.2 respectively) no statistically significant difference was found (P=0.961) in the means of the various stripe percentages ((7.362 ± 2.403, n=5) for the 5% group, (6.851 ± 1.862, n=8) for the 10% group, (6.508 ± 1.862, n=8) for the 20% group). The difference between the means of "shaken" (5.655 ± 1.602, n=11) and "non shaken" (8.159 ± 1.755, n=10) samples was again not significant (P=0.309). No statistically significant interactions exist between the percentage and shaking factor (P=0.877).

Bar graphs 4.15 and 4.16 below summarise the statistical results for the green and red pixel density ratios respectively.

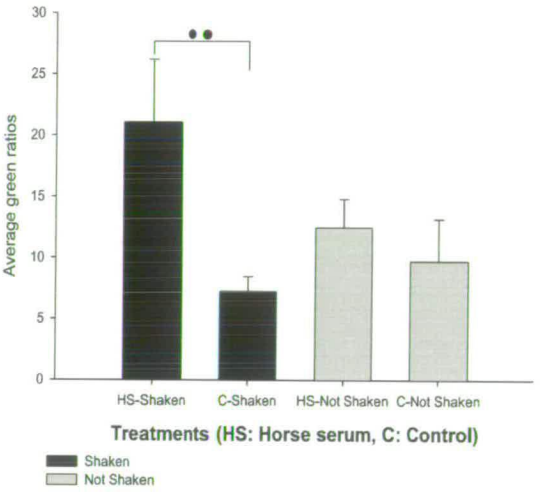

Figure 4.15: *Shaken or not in the green colour (glia). The two bars on the left represent shaken samples while the two bars on the right non shaken ones. Error bars represent SEMs.*

Two way ANOVA tests were also performed on the black pixel density ratios corresponding to the green and red pixels. For the black pixel density ratio corresponding to the green colour (normality and equal variance tests passed with P>0.2 and P=0.011 respectively), statistically significant differences were found (P<0.001 in both cases) between horse serum (131.332^o ± 9.668^o, n=6 for shaken or 64.133^o ± 5.129^o, n=6 for non shaken) and control (158.388^o ±

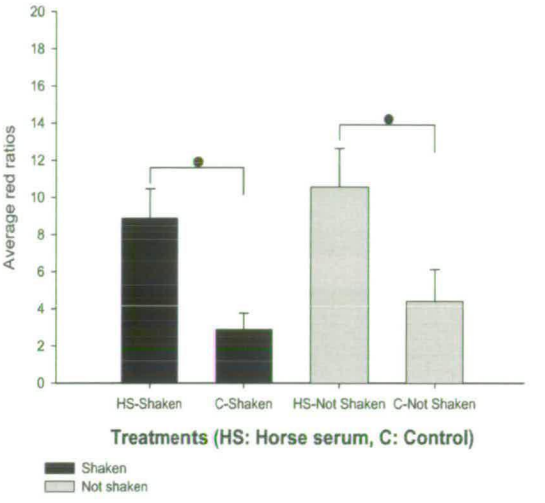

Figure 4.16: *Shaken or not in the red colour (neurons). The two bars on the left represent shaken samples while the two bars on the right non shaken ones. Error bars represent SEMs.*

1.856^o, n=6 for shaken or $146.468^o \pm 7.314^o$, n=4 for non shaken) samples as well as "shaken" and "non shaken" samples. A statistically significant interaction was also detected between the horse serum treatment factor and the shaking factor ($P<0.001$). The results were identical for the black pixel density ratio corresponding to the red colour (normality and equal variance tests passed with $P>0.2$ and $P=0.023$ respectively). A statistically significant difference was found between horse serum ($158.515^o \pm 1.665^o$, n=6 for shaken or $113.405^o \pm 6.559^o$, n=6 for non shaken) and control samples ($173.818^o \pm 2.856^o$, n=6 for shaken or $162.22^o \pm 4.841^o$, n=4 for non shaken) as well as "shaken" and "non shaken" samples ($P<0.001$ in both cases). A statistically significant interaction was also detected between the horse serum treatment factor and the shaking factor ($P<0.001$).

The bargraphs of figures 4.17(a) and 4.17(b) summarise the above results.

With regards to the nuclear densities two additional two way ANOVA tests were performed. In the first all nuclei were included, even those residing on the border between parylene and thermal oxide. The equal variance and normality tests passed ($P=0.299$ and $P>0.2$ respectively) after a logarithmic (natural) transformation of the data. No statistically significant differences were found either between the means of shaken (15.338 ± 3.865, n=4) and non shaken (18.279 ± 4.913, n=11) samples ($P=0.320$), or between the means of the different percent-

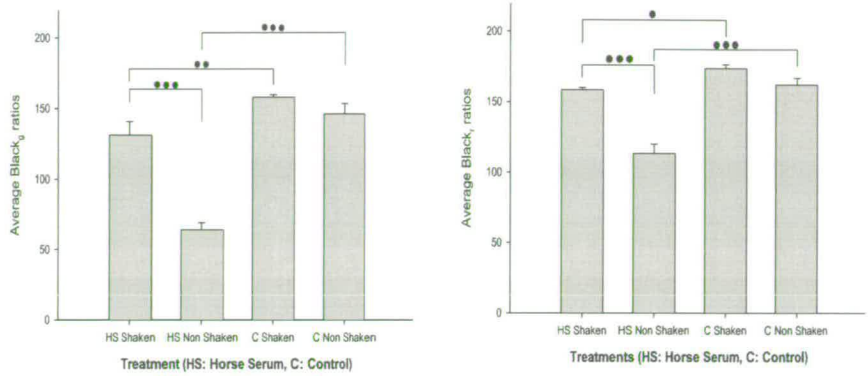

(a) Black ratios (max value is 180^o) corresponding to the green colour (glia).

(b) Black ratios (max value is 180^o) corresponding to the red colour (neurons).

Figure 4.17: *Bargraphs of black ratios representing the number of cells (glia or neurons) on the surfaces. Smaller bars indicate a larger number of corresponding cells (units are in degrees). Error bars represent SEMs.*

ages (P=0.528) ((15.022 ± 19.063, n=5) for the 5% group, (21.509 ± 23.348, n=5) for the 10% group, (59.605 ± 18.085, n=5) for the 20% group). Moreover, no statistically significant interactions between the two factors existed (P=0.476). When taking into account only nuclei centered on the parylene stripes results were similar. Following a logarithmic (natural) transformation of the data, equal variance and normality tests passed with P=0.743 and P>0.2 respectively, while no statistically significant differences were found between the means of shaken (38.039 ± 17.269, n=5) and non shaken (13.067 ± 11.147, n=11) samples (P=0.226), or in the means of different percentages (P=0.402) ((8.639 ± 16.721, n=5) for the 5% group, (14.256 ± 20.479, n=5) for the 10% group, (53.765 ± 15.863, n=5) for the 20% group). No statistically significant interactions existed between the two factors (P=0.421).

A two way ANOVA (equal variance and normality tests passed with P=0.572 and P>0.2 respectively) between horse serum (23.165 ± 4.555, n=10) and controls (6.154 ± 1.178, n=5) (taking into account the different percentages) revealed a statistically significant difference between the two treatments (P=0.011), while reaffirming the lack of any statistically significant differences (P=0.674) between the various percentages ((11.881 ± 25.751, n=5) for the 5% group, (16.753 ± 21.025, n=5) for the 10% group, (35.951 ± 19.946, n=5) for the 20% group). No statistically significant interactions existed between the percentages and treatment factors (P=0.8). The results were similar when border nuclei were excluded (equal variance and normality tests passed with P=0.372 and P>0.2 respectively). The difference between the means of the nu-

clear density ratios of the horse serum treated (30.396 ± 14.15, n=10) and control (4.992 ± 0.619, n=5) samples were statistically significant (P=0.033). Difference between the means of nuclear density ratios among different percentages were not statistically significant (P=0.492) ((7.450 ± 22.738, n=5) for the 5% group, (11.866 ± 18.565, n=5) for the 10% group, (32.351 ± 17.613, n=5) for the 20% group). Again no significant interactions existed between the two factors (P=0.468).

The bar graph of figure 4.18 summarises the above results.

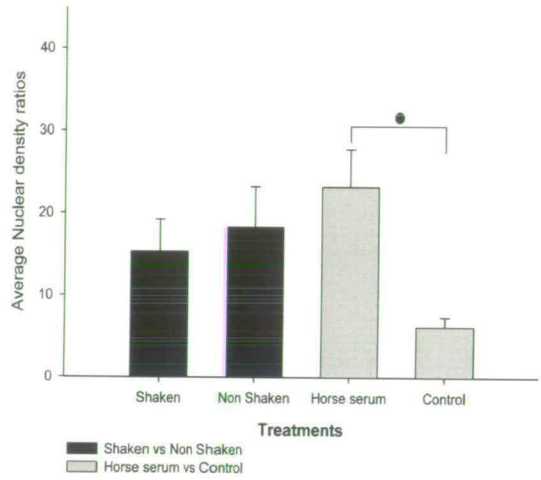

Figure 4.18: *Average nuclear density ratios for various treatments. All nuclei have been included. Error bars represent SEMs.*

4.3.4 Sustainability of the Patterned Networks

Twenty seven patterns, nine for each parylene percentage (5%, 10% and 20%) were immersed in horse serum overnight and cultured normally the following day as per the protocol in section 3.2.4. Nine patterns, three from each parylene percentage, were fixed and stained one week after plating, nine more were fixed and stained two weeks after plating, while the last nine were fixed and stained at three weeks after plating. The average plating density was approximately 125 cells/mm^2.

Images of the cultures at the end of weeks 1, 2 and 3 can be seen in figures 4.19, 4.20 and 4.21 respectively.

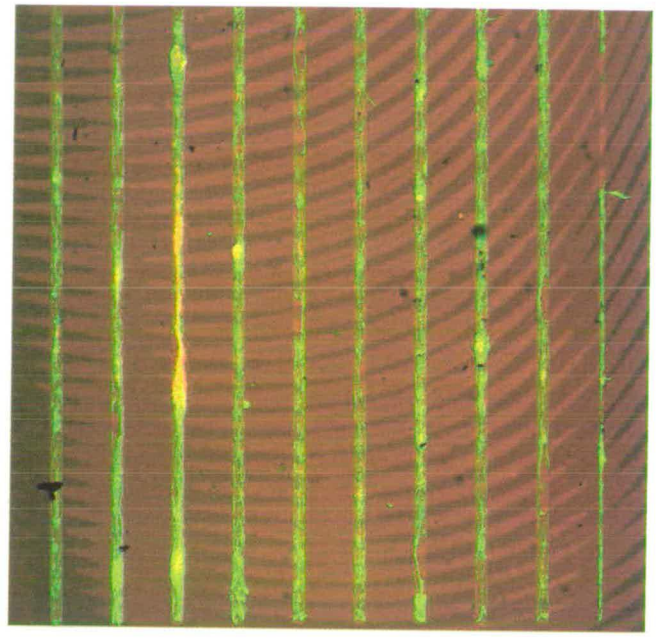

Figure 4.19: *A glial and neuronal culture at the end of the first week (x5 magnification).*

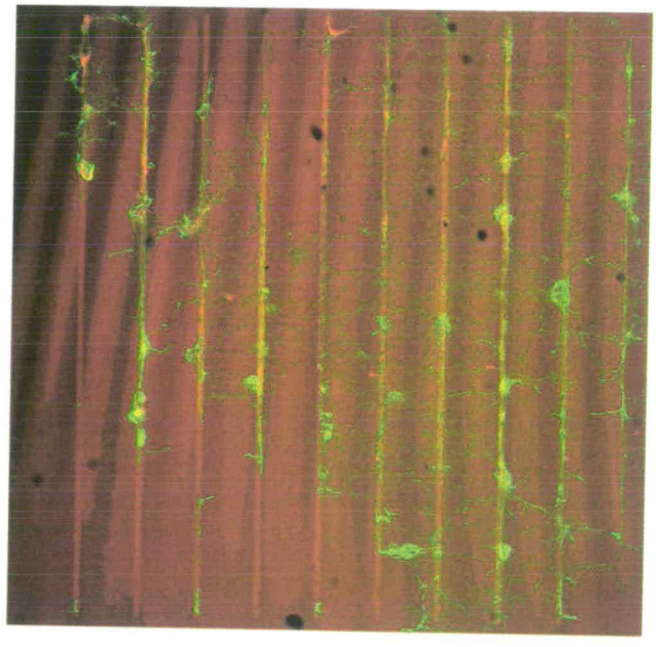

Figure 4.20: *A glial and neuronal culture at the end of the second week (x5 magnification).*

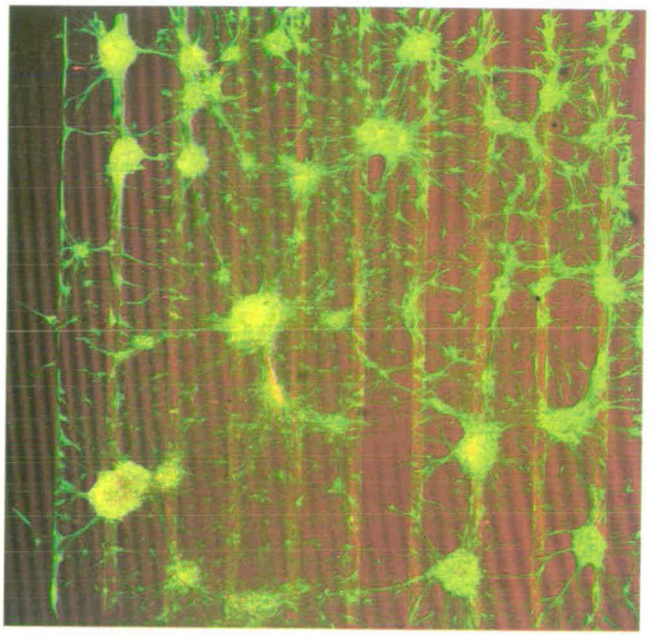

Figure 4.21: *A glial and neuronal culture at the end of the third week (x5 magnification).*

In the sequence of figures 4.19 through 4.21 we can observe the gradual deterioration of the cell patterns over the course of 3 weeks. At the end of the first week (figure 4.19), both glia and neurons conformed to the parylene stripes as in previous patterning experiments. Their somata and their processes remained on the parylene and avoided the TO. By the end of the second week (figure 4.20) however, glia had already spread their processes across the TO background, although most of them were still located on the parylene stripes. The neurons did not follow the glia at this stage and were still adhering to the pattern. At the end of the third week (figure 4.21), the majority of glia had formed large clusters, which abandoned the parylene stripes and attached to the TO background. Neurons, followed the glial clusters and aggregated into neurospheres, which can be seen at the center, bottom left and bottom right of figure 4.21. This decline in the quality of cell patterns over time is expressed by the statistical analysis below.

A two way ANOVA test on the nuclear density ratios[1] (equal variance and normality tests passed with $P=0.466$ and $P>0.2$ respectively) with culturing time as one factor and the different percentages as the other revealed that culturing time has a statistically significant effect on the nuclear density ratio of the culture ($P\leq0.001$) ($(239.219 \pm 50.962, n=9)$ for week 1, $(8.406 \pm 2.69, n=6)$ for week 2, $(2.656 \pm 4.61, n=6)$ for week 3). In contrast, no statistically signif-

[1] data was logarithmically (natural) transformed

icant differences were found across the various percentages of parylene (P=0.994) ((67.714 ± 55.046, n=8) for the 5% group, (133.888 ± 69.003, n=6) for the 10% group, (48.680 ± 58.846, n=7) for the 20% group). In addition, no statistically significant interactions existed between the culture time and percentage factors (P=0.773). As usual the results were the same when nuclei residing on the border between parylene and thermal oxide were excluded from the calculations. Briefly, after a logarithmic (natural) transformation of the data, the equal variance and normality tests both passed with P=0.443 and P>0.2 respectively, while the nuclear density ratio means of different weeks were found to be statistically significant (P≤0.001), ((206.398 ± 45.883, n=9) for week 1, (5.464 ± , n=6) for week 2, (1.593 ± , n=6) for week 3). No statistically significant differences were found between the means of different percentages (P=0.647) ((48.575 ± 49.559, n=8) for the 5% group, (117.022 ± 62.126, n=6) for the 10% group, (47.858 ± 32.153, n=7) for the 20% group) and no statistically significant interactions existed between the two factors (P=0.584).

The bar graphs of figure 4.22 represent these results.

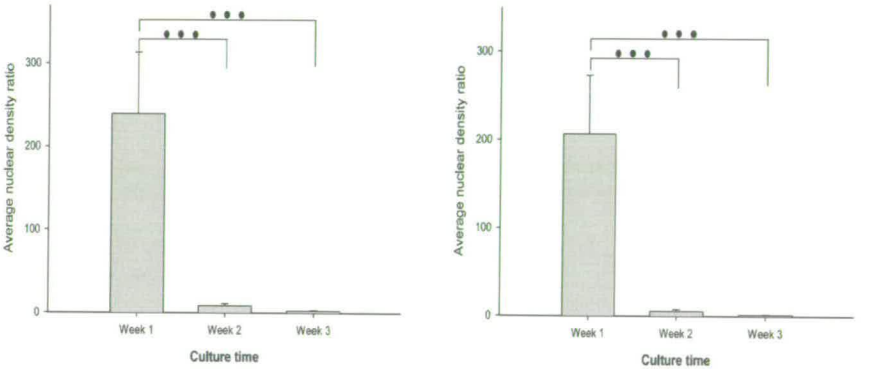

(a) Border nuclei have been included.

(b) Border nuclei have been excluded.

Figure 4.22: *Average nuclear density ratios over the period of 3 weeks. Error bars represent SEMs.*

Two way ANOVA tests were performed on the green and red pixel density ratios as well. The equal variance and normality tests for the green pixel density ratio two way ANOVA passed at P=0.378 and P>0.2 respectively, after a reciprocal transformation of the data. The difference in means of green pixel density ratios across different percentages was not statistically significant (P=0.126) ((21.088 ± 15.435, n=8) for the 5% group, (41.571 ± 18.245, n=7) for the 10% group, (18.073 ± 14.752, n=9) for the 20% group). However, the differences in means of green

pixel density ratios between weeks 1 (68.119 ± 13.987, n=10), 2 (3.88 ± 0.649, n=5) and 3 (1.704 ± 0.1965, n=9) were statistically significant ($P \leq 0.001$). In particular, the difference between weeks 1 and 2 was statistically significant (P=0.005) as was the difference between weeks 2 and 3 (P=0.001) and the difference between weeks 1 and 3 ($P \leq 0.001$).

In the case of the red pixel density ratios, the equal variance and normality tests passed with P=0.041 and P=0.160 respectively after a logarithmic (natural) transformation of the data. Statistically significant differences were detected between the means of red pixel density ratios of various weeks ($P \leq 0.001$), ((64.766 ± 14.386, n=10) for week 1, (5.054 ± 0.605, n=5) for week 2, (1.684 ± 0.18, n=9) for week 3). Differences in the means of red pixel density ratios between percentages were insignificant (P=0.803) ((17.430 ± 15.875, n=8) for the 5% group, (40.314 ± 18.765, n=7) for the 10% group, (21.142 ± 15.172, n=9) for the 20% group). Specifically, differences between the first week and second and third weeks were statistically significant ($P \leq 0.001$ for both) while the second week was also significantly different from the third (P=0.034).

The bar graph of figure 4.23 illustrates these results.

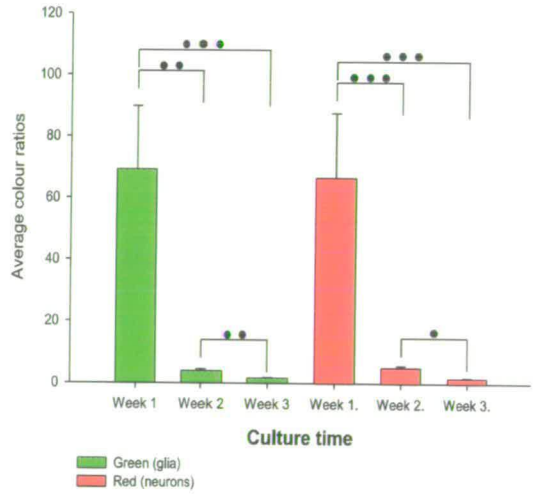

Figure 4.23: *The effects of prolonged culturing over a period of three weeks on patterning quality (the three green bars on the left represent the glia while the three red bars on the right the neurons). Error bars represent SEMs.*

4.3.5 Glia Division

In order to investigate the effect of glia division on the quality of the cell patterning, 24 different patterns were immersed in horse serum overnight and cultured with the glia-rich fraction F2 the following day, as per the protocol in section 3.2.4. The patterns were divided into 3 groups of plating densities, low, medium and high, during seeding. The plating densities in the low cell density group ranged from 12 to 47.5 cells/mm^2, while in the medium cell density group from 48 to 95 cells/mm^2. In the high density group the lowest cell density was 118 cells/mm^2 while the highest 140 cells/mm^2. All cultures were fixed and stained after 7 DIV.

A two way ANOVA test was performed on the pixel density ratio data gathered from the images taken. The first factor was the plating density while the second was the percentage of parylene coverage of the total area. In the green pixels, which represented the glia, both the normality and equal variance tests passed ($P>0.2$ and $P=0.495$ respectively) after a logarithmic (natural) transformation of the data. Differences in green pixel density ratio means between plating densities were statistically significant ($P\leq0.001$). In particular, the low plating density (25.72 $\pm$ 5.146, n=10) was significantly different from the medium (2.236 $\pm$ 0.731, n=7) and high (2.735 $\pm$ 0.973, n=6) plating densities ($P\leq0.001$ and $P=0.001$). The medium and high plating densities did not exhibit any statistically significant differences ($P=0.990$). There were also no statistically significant differences between the means of various percentages of parylene coverage ($P=0.839$) ((9.522 $\pm$ 3.706, n=7) for the 5% group, (13.315 $\pm$ 3.073, n=10) for the 10% group, (18.874 $\pm$ 4.346, n=6) for the 20% group) neither were any statistically significant interactions between the two factors ($P=0.744$).

The same two way ANOVA test was performed in the red pixel data (neurons). Both normality and equal variance tests passed ($P>0.2$ and $P=0.178$ respectively). As previously, statistically significant differences were found in the means of red pixel density ratios among different plating densities ($P=0.003$). Specifically, the low plating density (8.712 $\pm$ 1.732, n=10) was statistically different from the medium (1.877 $\pm$ 0.606, n=7) and high (2.98 $\pm$ 1.004, n=6) plating densities ($P=0.004$ and $P=0.014$). The medium and high plating densities did not exhibit any statistically significant differences ($P=0.882$). No statistically significant differences were detected among the parylene percentages ($P=0.353$) ((4.060 $\pm$ 1.464, n=7) for the 5% group, (3.837 $\pm$ 1.289, n=10) for the 10% group, (6.671 $\pm$ 1.553, n=6) for the 20% group). In addition, no statistically significant interactions between the two factors were found ($P=0.319$).

The bar graph of figure 4.24 illustrates the above results.

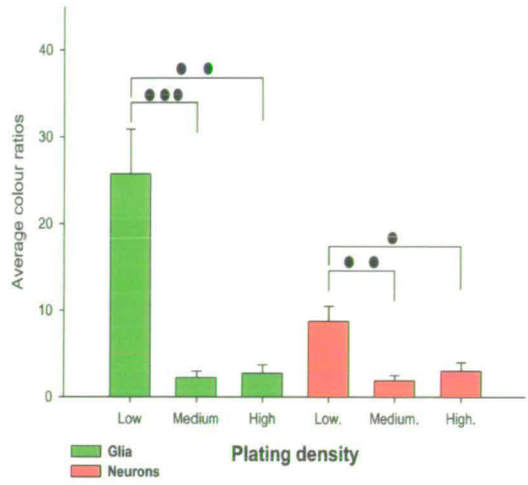

Figure 4.24: *The effects on glia plating density on the quality of the pattern. The three green bars on the left represent the glia while the three red bars on the right the neurons (in cells/mm^2 low:18-48, medium:70-95 and high:118-140). Error bars represent SEMs.*

Similar two way ANOVA tests were performed on the nuclear density ratios. When considering all nuclei (the data were transformed through a logarithmic operator to pass normality and equal variance test (P=0.128 and P=0.682 respectively)), a statistically significant difference was found between the means of the low plating density group (47.501 $\pm$ 26.795, n=8) and the groups of medium (3.142 $\pm$ 0.91, n=5) and high (1.27 $\pm$ 0.511, n=3) plating densities (P=0.045 and P=0.024 respectively). In contrast, the difference in means between the medium and high plating density groups were insignificant (P=0.724). The parylene percentage factor was also insignificant (P=0.171) ((44.328 $\pm$ 36.79, n=6) for the 5% group, (19.868 $\pm$ 10.757, n=6) for the 10% group, (3.586 $\pm$ 1.882, n=4) for the 20% group), while no statistically significant interaction existed between the plating density and the parylene percentage factors (P=1.000). When border nuclei were excluded from the calculations, the statistically significant differences between the means of the low plating density (32.374 $\pm$ 16.648, n=8) with the medium (1.676 $\pm$ 0.528, n=5) and high (0.703 $\pm$ 0.201, n=3) plating densities remained (P=0.048 and P=0.036 respectively), while differences between the medium and high plating densities were still insignificant (P=0.851). As usual the parylene percentage factor was did not create significant differences (P=0.403) ((26.135 $\pm$ 22.658, n=6) for the 5% group, (16.703 $\pm$ 9.45, n=6) for the 10% group, (3.113 $\pm$ 1.688, n=4) for the 20% group), while the two factors remained

independent of each other (P=0.999).

These results are summarised in the bar graph of figure 4.25.

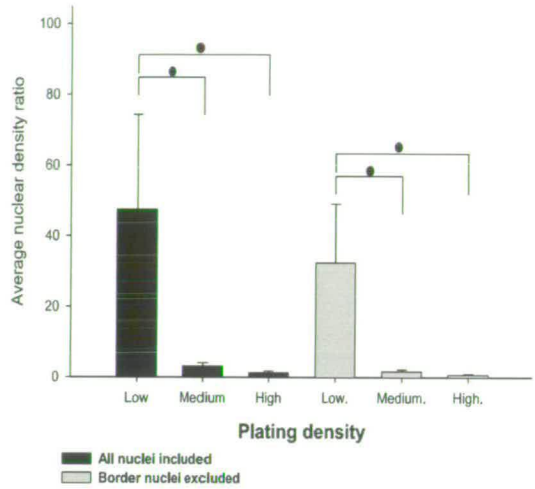

Figure 4.25: *Average nuclear density ratios for various plating densities (in cells/mm^2 low:18-48, medium:70-95 and high:118-140). In the three bars on the left all nuclei were included in the calculations, while in the three on the right nuclei residing on the border between parylene and thermal oxide were excluded. Error bars represent SEMs.*

4.3.6 Exposure of Surfaces to UV

In order to assess the effect of UV radiation on the parylene surfaces the following experiment was performed. Twelve parylene stripe patterns (4 for each percentage) were cleaned and sterilised for 1 hour under UV radiation as per the protocol in section 3.2.3. Twelve more were exposed to UV radiation for 1 hour and then immersed in Penicillin/Streptomycin for an additional hour. Finally, twelve surfaces were sterilised just via 1 hour immersion in Penicillin/Streptomycin. The first two groups acted as controls while the last group would be used to gauge the effects of the UV sterilisation step in the overall protocol. The plating cell density was 73 cells/mm^2.

Figures 4.26(a) through 4.26(d) are examples of cultures from the UV exposure experiment.

It is evident that the parylene pattern sterilised in penicillin/streptomycin is superior to the other two. Parylene stripes in figure 4.26(a) are full of glia and neurons, while only a few glia

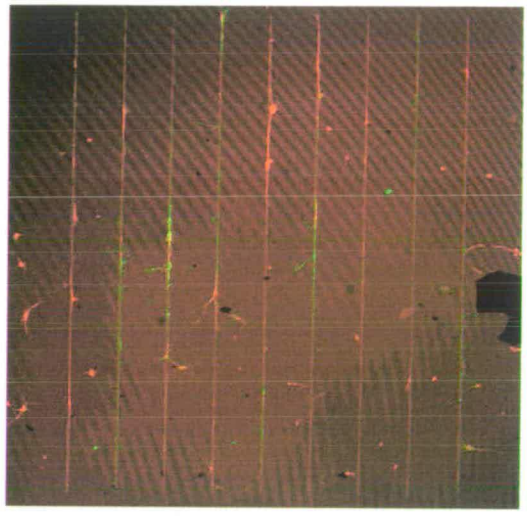

(a) Sterilised by immersion in penicillin/streptomycin for 1 hour (5% parylene, x5 magnification)

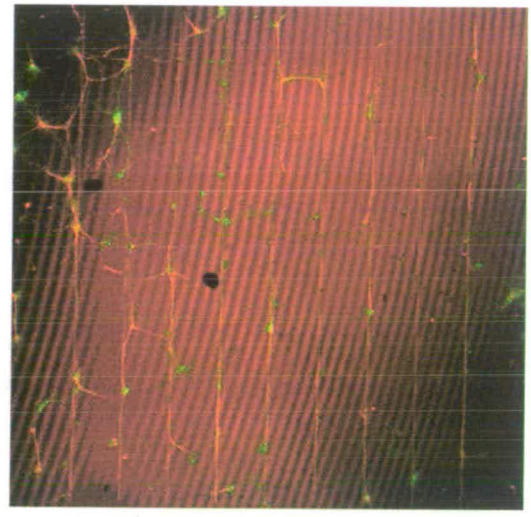

(b) Sterilised by exposure to UV for 1 hour then immersion in penicillin/streptomycin for an additional hour (5% parylene, x5 magnification)

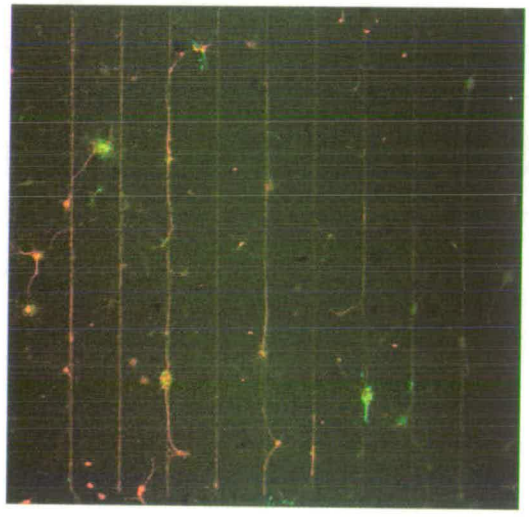

(c) Sterilised by exposure to UV for 1 hour. Glia and neurons only (5% parylene, x5 magnification)

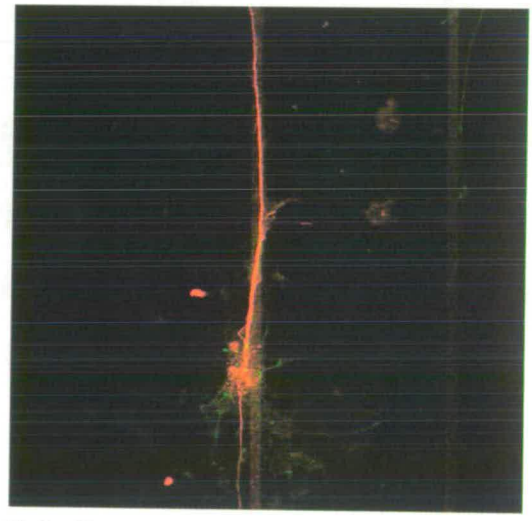

(d) Sterilised by exposure to UV for 1 hour. Zoom in on glia and neurons (5% parylene, x20 magnification)

Figure 4.26: *Examples of cultures from the various sterilisation treatments: exposure to ultraviolet radiation, immersion in penicillin/streptomycin or a combination of both.*

processes have extended to neighbouring stripes. No large glial or neuronal clusters are noticeable. Likewise, glia and neurons adhered and followed the parylene stripes on the substrate that was sterilised by UV radiation (figure 4.26(c)). In this case however, two large glial aggregates are visible, one residing on a parylene stripe (bottom right) and one on the TO background (top left). A few smaller clusters of glia and neurons can be distinguished on two parylene stripes (bottom left and bottom center). Image 4.26(d) illustrates a neuronal processes following a parylene stripe. Finally, cell patterning is obvious on the substrate that was subjected to both UV and pencillin/streptomycin (figure 4.26(b)). The majority of glia and neurons have followed the parylene stripes however, the extension of processes to neighbouring stripes is more predominant compared to the previous two cases. Glia and neuronal clusters are also present and are located both on the parylene stripes and the TO background. The statistical analysis of the images collected is presented below.

Green and red pixel density ratio data were calculated as usual, while a logarithmic (natural) transformation was performed in both groups of data. A two way ANOVA on the green pixel density ratio data, with the sterilisation method as the first factor and the parylene percentage as the second was carried out. Both equal variance and normality tests passed ($P=0.703$ and $P=0.146$ respectively). The means across all three different treatment groups ($(9.818 \pm 1.231$, $n=15)$ for the Pen/Strep group, $(3.872 \pm 0.481$, $n=12)$ for the UV group, $(1.758 \pm 0.361$, $n=12)$ for the UV&Pen/Strep group) were statistically different with each other ($P<0.001$). In contrast, no statistically significant differences were detected between the means of different parylene percentages ($P=0.726$) ($(5.534 \pm 1.494$, $n=13)$ for the 5% group, $(5.633 \pm 1.343$, $n=13)$ for the 10% group, $(5.359 \pm 1.176$, $n=13)$ for the 20% group). There was a statistically significant interaction between the two factors ($P=0.044$).

The two way ANOVA on the red pixel data (normality and equal variance tests passed with $P>0.2$ and $P=0.043$ respectively) revealed statistically signficant differences between the means of the various treatment groups. In particular, the red pixel density ratio means of the UV group (8.473 ± 1.294, $n=12$) and Pen/Strep group (10.444 ± 1.016, $n=15$) were significantly different from the means of the samples which received both treatments (UV&Pen/Strep group (5.36 ± 1.113, $n=12$))($P<0.001$), while the difference between the red pixel density ratio means of UV and Pen/Strep samples was not significant ($P=0.158$). Differences between various percentages were statistically significant ($P<0.001$) ($(10.238 \pm 1.246$, $n=13)$ for the 5% group, $(8.467 \pm 1.12$, $n=13)$ for the 10% group, $(6.115 \pm 1.199$, $n=13)$ for the 20% group). Interactions between

the treatment and percentage factors were statistically significant ($P<0.001$).

The bar graph of figure 4.27 summarises these results.

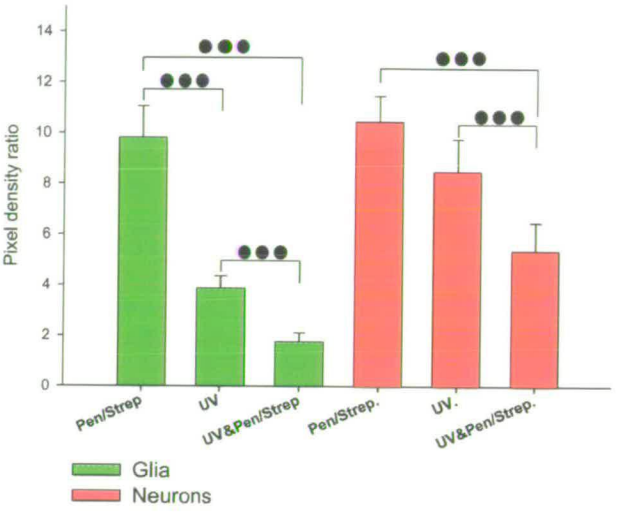

Figure 4.27: *Average colour ratios for UV exposed and penicillin/streptomycin treated patterns. Non UV exposed patterns were immersed in penicillin/streptomycin for 1 hour for sterilisation. UV exposed patterns were subjected to ultraviolet radiation for 1 hour. The last group was exposed to UV and then immersed in penicillin/streptomycin for 1 hour. Error bars represent SEMs.*

4.3.7 Different Serums of Various Concentrations

Twenty four parylene stripe patterns were prepared as per the protocol in section 3.2.3. Half of them were immersed in horse serum while the other half were immersed in foetal bovine serum. Both types of serum were diluted with distilled sterilised water to the following concentrations: 0.1%, 1%, 10% and 100%. Thus, three patterns (one for each parylene percentage) were included per concentration, per serum. The culture protocol of section 3.2.4 was followed and after a week of incubation the cultures were fixed and images were taken on the confocal microscope. The plating cell density was 71 cells/mm^2.

Figures 4.28(a) through 4.28(d) are representative examples of neurons on horse and foetal bovine serum treated patterns.

A comparison between the four images reveals that the substrates immersed in pure serum, horse or bovine, have generated superior neuronal patterns compared to those immersed in

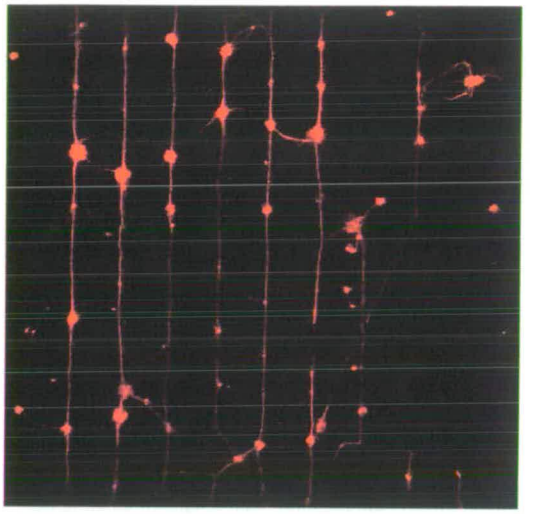

(a) Non diluted (100%) horse serum. Neurons on 10% parylene stripes.

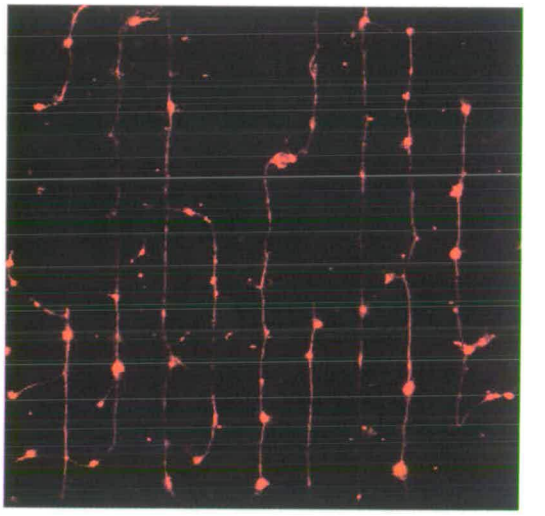

(b) 10% horse serum. Neurons on 10% parylene stripes.

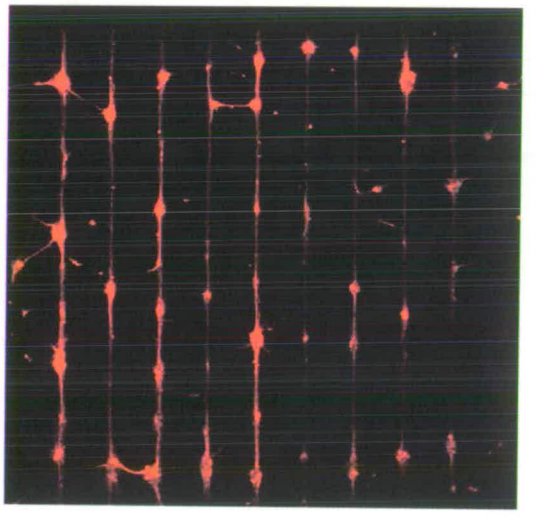

(c) Non diluted (100%) foetal bovine serum. Neurons on 10% parylene stripes.

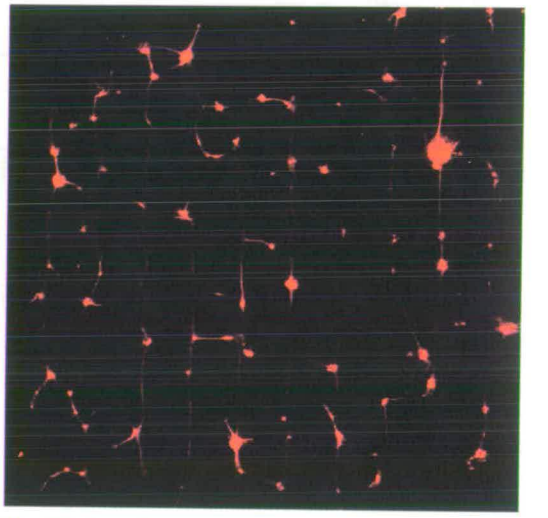

(d) 10% foetal bovine serum. Neurons on 10% parylene stripes.

Figure 4.28: *Neurons on parylene stripe patterns (10%) in pure and 10% horse or foetal bovine serum (x5 magnification).*

10% serum. In figures 4.28(a) and 4.28(c), neurons adhered and extended processes within the parylene stripes. One neuronal process in figure 4.28(a) and two in figure 4.28(c) are extending between stripes however, the overall cell conformity to the underlying pattern is good. In contrast, in figures 4.28(b) and 4.28(d), neurons follow the pattern loosely as a large portion of the total neural mass is located on the TO background. Additionally, the cells have aggregated more and have extended less processes compared to cultures 4.28(a) and 4.28(c). The statistical analysis presented below supports these observations.

A statistical analysis was performed on the green and red pixel density ratios extracted from the images. In particular, a three way ANOVA test on the green pixel data[2] revealed that the difference detected between horse serum (2.178 ± 0.32, n=12) and foetal bovine serum (6.177 ± 1.716, n=12) treated samples was statistically significant (P=0.006). There was also a statistically significant difference (P=0.013) between the samples that were treated with 100% (8.537 ± 3.085, n=6) and 0.1% (1.875 ± 0.498, n=6) serum (whether horse or bovine), as well as the 100% and 10% (2.11 ± 0.423, n=6) groups (P=0.041). In addition, a statistically significant difference was detected between 1% (4.187 ± 0.967, n=6) and 0.1% serum treated samples. All other differences between serum concentrations as well as differences due to different parylene percentages ((3.248 ± 0.068, n=8) for the 5% group, (5.198 ± 0.068, n=8) for the 10% group, (4.084 ± 0.068, n=8) for the 20% group) were not significant (P=0.846).

Similarly, a three way ANOVA was performed on the red ratio data. The difference among the means of the two serums, horse (2.898 ± 0.456, n=12) and bovine (6.127 ± 1.587, n=12), were statistically different (P=0.031), while no statistically significant difference was found between the means of different parylene percentages (P=0.327). In addition, the mean of the 100% (8.53 ± 2.869, n=6) serum concentration was significantly different from the 0.1% (1.728 ± 0.967, n=6) concentration. No other differences were statistically significant ((3.965 ± 0.713, n=6) and (3.825 ± 0.396, n=6) for the 1% and 10% serum concentrations respectively). Also the means and SEMs of the different parylene percentages are as follows: ((5.109 ± 0.113, n=8) for the 5% group, (4.994 ± 0.113, n=8) for the 10% group, (3.430 ± 0.113, n=8) for the 20% group)

The following bargraphs, 4.29 and 4.30 summarise the above results.

[2] Data was transformed through the natural logarithm to conform with normality and equal variance requirements. The same is true for the red colour ratios

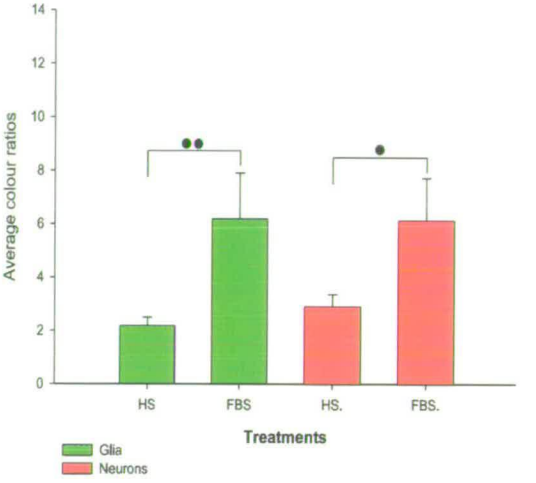

Figure 4.29: *Average green and red pixel density ratios for horse and foetal bovine serum. Error bars represent SEMs.*

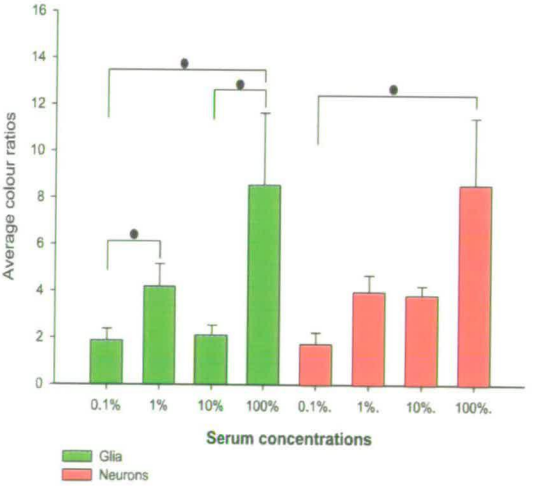

Figure 4.30: *Average green and red pixel density ratios for various serum concentrations. Error bars represent SEMs.*

4.3.8 Variability Across Different Batches of Horse Serum

In order to assess the importance of the horse serum batch on the outcome of the patterning, the following experiment was conducted. Nine parylene stripe patterns (3 from every percentage 5%, 10% and 20%) were immersed in horse serum taken from the current stock that was used in the experiments. Nine more patterns were immersed in horse serum taken from an old stock which had remained frozen for 2 years. The surfaces were cultured the following day, fixed and stained after a week in incubation and imaged in a microscope as per the protocols in sections 3.2.4 and 3.2.5 respectively. The cell plating density was 80 cells/mm^2.

Figures 4.31(a) and 4.31(b) are representative examples of the horse and foetal bovine serum treated patterns.

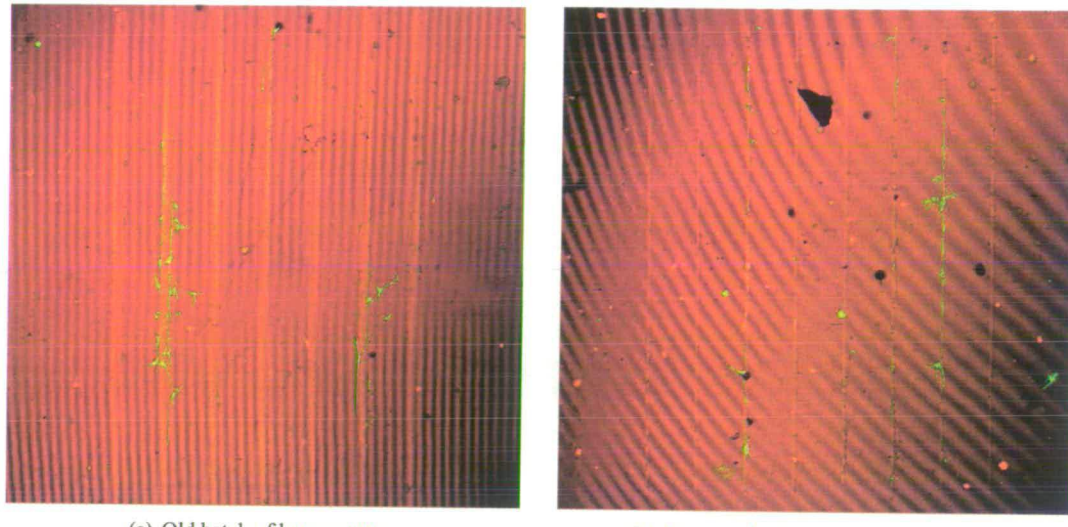

(a) Old batch of horse serum

(b) New batch of horse serum (Neurons)

Figure 4.31: *Parylene stripe patterns treated with two different batches of horse serum (x5 magnification, 5% stripes).*

The two culture examples seem similar. Neurons and glia are present in both and give the impression of following the parylene stripes. Culture 4.31(b) however, appears slightly more populated by both types of cells, while glia seem to be on the stripes, rather than surrounding them as in figure 4.31(a). The statistical analysis is presented below.

A two way ANOVA on the green pixel density ratios (glia) revealed a statistically significant difference between the means of the old (2.897 ± 0.611, n=9) and new (5.619 ± 0.81, n=9) batches of horse serum (P=0.023). No statistically significant differences were found (P=0.087)

between the means of different percentages ((5.463 ± 0.787, n=6) for the 5% group, (4.423 ± 0.787, n=6) for the 10% group, (2.555 ± 0.880, n=5) for the 20% group), while interactions between the two factors were insignificant (P=0.965).

In the red ratios (neurons) results were similar. Differences between the means of old (2.12 ± 0.39, n=9) and new (5.503 ± 1.06, n=9) horse serum were statistically significant (P=0.006). No statistically significant interactions were found between the two factors (P=0.248), while no statistically significant differences were found (P=0.582) between the red pixel density ratio means of different parylene percentages ((5.220 ± 0.753, n=6) for the 5% group, (3.774 ± 0.753, n=6) for the 10% group, (1.953 ± 0.842, n=5) for the 20% group).

The bargraph of figure 4.32 illustrates the difference between the old and the new batches of horse serum.

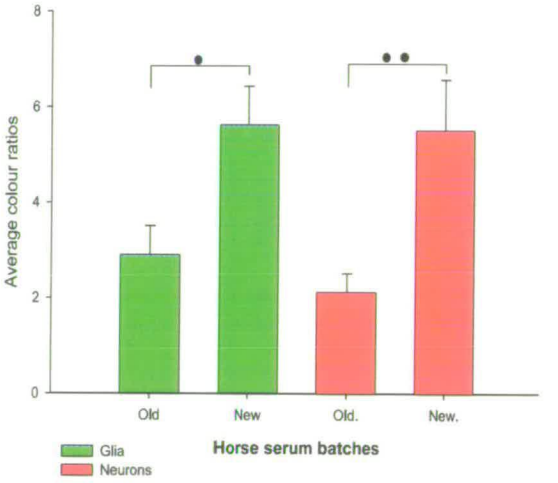

Figure 4.32: *Average green and red pixel density ratios for treatment in two different batches of horse serum, old and new. Error bars represent SEMs.*

4.3.9 The Effects of Fixation

One of the primary concerns regarding the quality of our results was the effect the fixation step had on the cells. Throughout the staining procedure and especially during the PFA application, we would sometimes witness pieces of tissue floating of the surfaces. In order to examine whether this was substantial or trivial, images of the cultures stained with CellTracker Green were taken before and after fixation. As can be seen on figures 4.33 and 4.34 the effect of

fixation is negligible as the cell patterns remain unaffected. There is no significant loss of cells after fixation for both horse serum and control samples, while the majority of cells have maintained their initial positions pre and post-fixation. This was confirmed by capturing and comparing more images of cultures before and after fixation, which are not all shown here. In all cases the number of cells that became unattached was fairly small and would not be cause for concern.

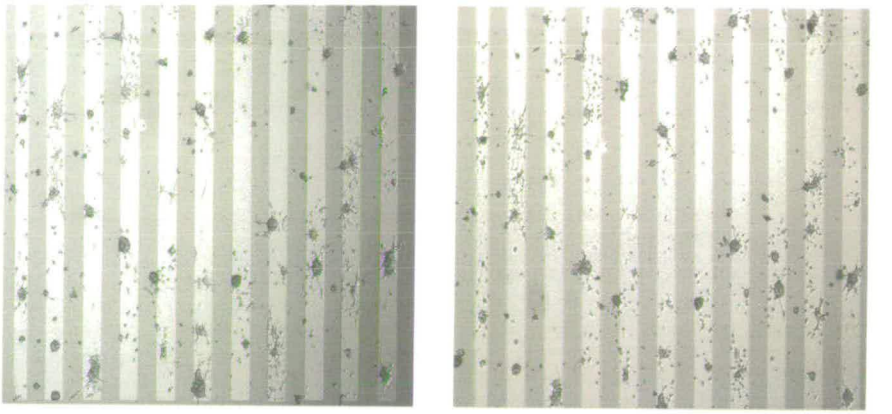

(a) Control pattern before fixation. Cells are still live.

(b) Control pattern after fixation.

Figure 4.33: *Effects of fixation on control samples(50% stripes at x5 magnification).*

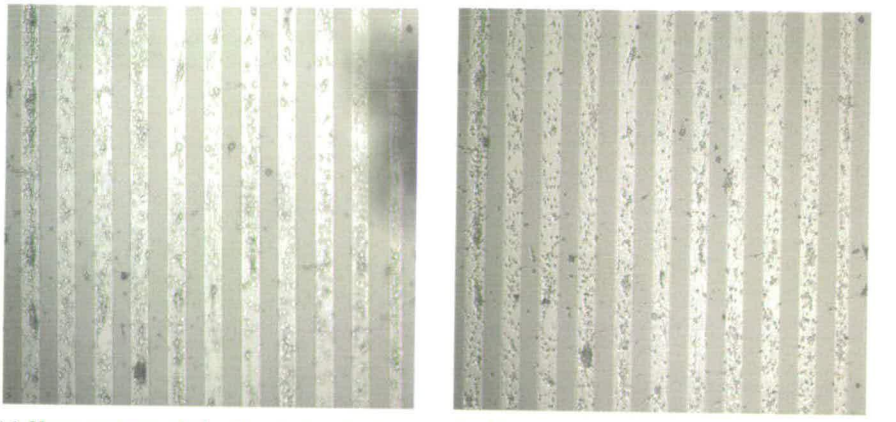

(a) Horse serum treated pattern before fixation. Cells are still live.

(b) Horse serum treated pattern after fixation.

Figure 4.34: *Effects of fixation on horse serum treated samples (50% stripes at x5 magnification).*

4.4 Discussion

4.4.1 Overnight vs 3 Hour Immersion in Horse Serum

The statistical analysis in section 4.3.2 reveals that there is a statistically significant difference between the samples that were immersed in horse serum overnight or 3 hours and the controls. This is true both for the colour and the nuclear density ratios. In addition, the scatter plots of figures 4.7, 4.8, 4.10 and 4.11 clearly indicate that the control data points are segregated from the data points derived from the horse serum treated samples. Finally, in the culture examples of figures 4.4 through 4.6 it is apparent that in the horse serum treated surfaces the cells have remained mostly within the parylene stripes while in the controls they have spread throughout the parylene and thermal oxide substrates. These results reinforce the results of section 3.3.3 and further support the hypothesis that proteins within the horse serum are enhancing the parylene's attractive quality.

Nonetheless, no statistically significant differences were detected in colour and nuclear density ratios between samples immersed in horse serum overnight and samples immersed in horse serum for 3 hours only. Indeed, the two representative examples of the two different immersion times (figures 4.4 and 4.5) look very similar. This result has two important implications. First, it reduces the overall time needed for the protocol and thus leads to a quicker and more robust patterning method. It is possible that the required immersion time is even smaller and this would certainly be an interesting research avenue to explore. In addition, this result suggests that the mechanics underlying the effect horse serum has on the parylene and thermal oxide substrates, are fast. This promotes the protein deposition theory presented in section 5.4.1 [95].

4.4.2 The Theories of Cell Detachment and Cell Migration

The initial success in patterning glia and neurons with parylene and horse serum raised numerous interesting questions with regards to cell behaviour during the incubation time. Hence, the establishment of a cell behavioural model explaining the process of glia and neuronal patterning became a central research objective. In particular, two theories explaining cell patterning were considered.

The theory of cell detachment suggests that as cells land on the surface during plating and the initial incubation period and attach either firmly or loosely depending on the surface they

interact with. Therefore, while cells, and particularly glia, will adhere well on the serum treated parylene, they will attach loosely on the thermal oxide. As a result, when the surfaces are shaken to remove cell debris and unattached cells, all the cells on the thermal oxide will be rinsed away leaving behind only the cells already located on the parylene. Subsequently, the remaining cells will divide and extend processes on the parylene. However, the patterning has already occurred during the first few hours of incubation and the first exchange of culturing media.

In contrast, the theory of cell migration supports that during plating, cells attach to all surfaces, at least to such an extent that they cannot be detached during the shaking step or by a media exchange. Over the course of the incubation, cells slowly migrate from the cell deterrent substrate, thermal oxide in this case, towards the attractive surface, parylene. Once the cells are located on the parylene, they attach firmly on the surface and extend processes.

The two theories are not mutually exclusive, so it is entirely possible for both to be true at the same time. In order to access which of the two aforementioned models is prevalent, the experiment detailed in section 4.3.3 was performed. The results indicate that no statistically significant difference exists between shaken and non shaken surfaces, which in turn implies that cell detachment is not contributing considerably to cell patterning. This leaves cell migration as the principal cell behaviour model. The similarity in cell patterning quality between shaken and non shaken cultures is supported both by the pixel and nuclear density ratios (see figure 4.18). In addition, both neurons (red) and glia (green) seem to behave in the same way.

Nonetheless, the green pixel density ratio bargraph of figure 4.15 implies that cell detachment is present, at least with regards to glia. When the surfaces were shaken, the difference between horse serum and control samples was great enough to be statistically significant. On the other hand when the surfaces were not shaken the difference between horse serum and control samples was mitigated to the point of not being statistically significant anymore. Provided the proteins in the horse serum make parylene more attractive and adhesive, when surfaces treated with horse serum are shaken, some glia get detached from the thermal oxide substrate while the majority of glia located on the parylene remain attached. When this is contrasted to a control sample, where cells have detached almost equally from parylene and thermal oxide, the difference is great enough to be statistically significant. However, when the patterns are not shaken, cell detachment is not as predominant and the difference between horse serum and control samples is attenuated.

The black pixel density ratio bargraphs of figure 4.17 offer some valuable information. It is evident that shaking leads to an overall decrease in the number of both glia and neurons while the application of horse serum increases the number of cells on the surface. However, whereas there is a statistically significant difference in the number of cells between horse serum and control samples regardless of shaking, the same is not true for the shaking factor. The difference in the number of glia and neurons between shaken and non shaken samples is significant only when horse serum is applied, not in the controls. In order to explain this we have to take into account that under normal circumstances (controls), cells are probably unattaching from the surface due to poor adhesion. Therefore, if horse serum is not applied, it makes little difference whether the surfaces are shaken or not. In contrast, when horse serum is applied, both substrates, and in particular parylene, become more adhesive. This is probably due to proteins adsorbing to the substrates. As a result, cells adhere more firmly on the surfaces and require greater mechanical force, or shaking, to detach.

In summary, the conclusions we can draw from this experiment thus far are:

- in control samples cells are detaching from both substrates (parylene and thermal oxide) whether the surfaces are shaken or not
- the application of horse serum makes thermal oxide and in particular parylene more adhesive and attractive to cells
- cell detachment is occurring and is contributing to an extent to cell patterning
- cell migration is assumed to be present, since cell patterning can not be solely justified by cell detachment

Taking into consideration this new information, we can now develop the cell behaviour model suggested previously in section 3.4.2.

Following seeding cells land on the two substrates randomly. They adhere firmly on the protein loaded parylene stripes and loosely on the thermal oxide. Agitation of the surfaces encourages mostly cells located on the thermal oxide to detach. The remaining cells slowly migrate towards the parylene stripes where they adhere and start dividing, in the case of glia. During the course of the week they extend processes which also follow the parylene substrate.

4.4.3 Longevity of the Cell Patterns and Glia Division

An important aspect of any patterning method, especially one that aims to pattern neurons, is the sustainability of the cell patterns. In the case of neural networks it is important, since the objective is usually to record neuronal activity. As activity in cultured neurons is usually detected after 3 weeks in culture [96], it is essential for the neural patterns to last more than 3 weeks. Recently however, there have been examples of activity in such networks, as early as 10 DIV [97].

The experiment of section 4.3.4 was conducted in order to examine whether the cell patterns would last more than a week. It is evident from the nuclear and pixel density ratio bargraphs of figures 4.22 and 4.23 respectively, that glia and neurons stop conforming to the parylene stripes after the first week. This can also be clearly seen in the culture examples fixed at the end of the first, second and third weeks (figures 4.19, 4.20 and 4.21). At the end of the first week (figure 4.19) no glia or neurons reside on the thermal oxide. However, at the end of week 2 (figure 4.20) glia have already started branching out of the stripes with neurons mostly remaining on the parylene. Finally, at the end of the third week (figure 4.21) glia are freely growing on the thermal oxide attracting neurons out of the parylene stripes (noticeable by the red colour spheres located at the center of the majority of the large green masses).

A possible explanation for the loss of patterning could be that the attached horse serum proteins, which make the parylene more attractive and adhesive, are gradually detaching from the substrates after the first week. Alternatively, adhesive proteins secreted by the cells could be attaching to both substrates, diminishing the contrast between parylene and TO [98]. However, under the evidence presented in section 5.3.5, this becomes unlikely, as nitrogen levels which measure the protein load on the surfaces remain stable after the first week.

This leaves glia division as the most probable cause for the loss of patterning. However, in the experiment of section 4.3.4, it is impossible to access the final glia density at the end of each week, as the starting glia density as well as the rate of glia division are unknown (cell plating density is known however, the neuron to glia ratio is not, rendering any conjecture with regards to starting glia density impossible). Thus, in order to investigate the effect of glia density in the longevity of the cell patterns the experiments of section 4.3.5 were conducted. By utilising the F2 fraction, which is rich in glia, and fixing all cultures at the end of the first week, different glia densities can be compared.

The statistical analysis on experimental data over a fixed period of culturing, reveals that there is a correlation between glia density and successful patterning. The pixel and nuclear density ratio bargraphs of figures 4.24 and 4.25 indicate that as long as the starting glia density is adequately low (less than 50 cells/mm^2) glia and neurons successfully grow and remain on the parylene. However, at higher glia densities patterning fails as it does in the case of the two and three week cultures. In fact the means of the green pixel density ratios for weeks 2 and 3 in section 4.3.4 are very similar to the means of the green colour ratios for medium and high density in section 4.3.5.

A glia density of 50 cells/mm^2 might seem a bit low compared to the plating densities of other experiments which are typically 100 cells/mm^2 or more. Nevertheless, in all the other experiments the F3 fraction was used which is rich in neurons and not in glia. Since neurons do not divide during culture, at the end of the first week, the final cell density of experiments involving the F3 fraction should be similar to the final glia density of a glia only culture with a lower plating density.

Taking into consideration the results from sections 4.3.4 and 4.3.5 we can confidently deduce that as glia divide during culturing they can outgrow the patterns. This is probably due to confinement issues. As glia divide, there is progressively less space on the parylene for their somata and processes to adhere to. Eventually, some have to migrate outside the parylene attracting other glia and neurons away from the stripes. This results in the loss of patterning.

Fortunately, loss of patterning due to glia division can easily be resolved. The addition of an anti-mitotic agent such as Cytosine arabinoside (Ara-C) in the media will prevent the glia from dividing and extend the life of the neural patterns. As Ara-C has been reported to be cyto-toxic to neurons [99], various parameters would have to be adjusted, in order to achieve an optimal result. Additionally, an interesting possibility would be to explore the time of Ara-C application in the culturing media (for example at the end of 6^{th} or 7^{th} day of culture) as a function of the neuronal and glial density during plating. This way, if the plating density is undesirable, the application of Ara-C could be either be postponed or brought forward depending on the starting glia density.

4.4.4 Exposure of Parylene to Ultraviolet Radiation

Prior to plating the surfaces with cells, all parylene patterns are sterilised via UV exposure for at least 1 hour. However, it has been substantiated in literature that under ultraviolet radiation, parylene is degraded via oxidation of its methylene groups [100, 101]. As a result, various properties of parylene such as thermal stability or its dielectric constant are altered during or after exposure to UV [102]. It has also been reported that this oxidation results in the formation of aldehyde and carboxylic groups near the surface of the parylene film [103]. These groups may later act as binding sites for various protein molecules. In some cases, UV exposure of polymer surfaces has actually been proposed as a valid method of inducing protein adhesion, which could be utilised to promote cell patterning [104].

Under the light of this information, it was important to ascertain whether protein adhesion and cell patterning in our method was attributable to the UV exposure of the parylene. In the experiment of section 4.3.6, the cell patterning ability of a group of surfaces that were not exposed to UV was contrasted to a group of surfaces which was treated and cultured under the normal protocol. The sterilisation method used on the first group was immersion in penicillin/streptomycin for 1 hour. In order to test whether the use of penicillin and streptomycin had any adverse effects on the parylene patterns, a control group which was sterilised both under UV and immersed in penicillin/streptomycin was also included.

The data presented in section 4.3.6 clearly indicate a statistically significant difference between the various treatment groups with regards to glia patterning capability. According to the pixel density ratio bargraph of figure 4.27 the samples that did not receive UV treatment possess better potential for patterning at least with regards to glia. This result seems to contradict Pruden [103] and Welle [104] as they are suggesting that UV exposure in fact promotes protein adhesion. However, it is possible that the proteins that are attaching due to UV exposure are, in our case, detrimental to cell patterning. Another explanation could be that the UV induced parylene degradation limits the quantity of protein adhesion thus, giving the advantage to the group of surfaces which was sterilised via penicillin/streptomycin. This becomes more likely if protein adhesion in our case occurs via hydrophobic bonding. If this is true, then the formation of carboxylic and aldehyde groups on the parylene which Pruden [103] is proposing, actually deters protein adhesion by reducing the hydrophobicity of the surface (Pruden reports a decrease in the parylene contact angle as exposure to UV increases [103]). Nevertheless, based on these results we can dismiss with enough certainty the theory that cell patterning in

our technique is relying on the UV exposure of the parylene.

The group of surfaces that was exposed to UV and immersed in penicillin/streptomycin for an hour has the worst patterning capability. A possible explanation for this is that the penicillin/streptomycin is binding to the aldehyde and carboxylic groups generated by the ultraviolet radiation. This would also account for the fact that this group is even worse than the group which was only exposed to UV. In the case of the latter, the degraded parylene surface is not ideal for hydrophobic protein adhesion but at least some binding sites remain free, whereas in the former case the parylene surface is loaded with penecillin/streptomycin molecules preventing any protein-parylene interaction.

The neurons seem to be following the glia like they do in the majority of the experiments. Again the trend of the red bars shows that neurons in surfaces not exposed to UV followed the patterns to a greater extent. In addition, the red ratios are generally greater because the number of neurons is usually smaller than the number of glia. It is important to highlight that no statistically significant difference was found between the UV exposed and the penicillin/streptomycin surfaces, in the case of neurons. This seems to suggest that once a certain threshold of glia has been patterned, neurons will follow them in the parylene stripes. Therefore, even though glia in UV exposed surfaces do not seem to pattern as well as glia in the penicillin/streptomycin surfaces, neurons follow the parylene stripes in both cases similarly well.

Finally, a statistically significant interaction was detected between the treatment factor (UV or penicillin/streptomycin) and the stripe width factor (percentage 5%, 10% or 20%). There were also statistically significant differences among various parylene percentage groups in the case of neurons. This interaction can be explained by taking into account that any UV effect on the parylene stripes is going to be proportional on the amount of parylene, or in other words, the size of those stripes. Therefore, as the parylene stripes get progressively wider (5%, 10% or 20%) the effect of ultraviolet radiation on the stripes becomes greater.

4.4.5 Horse Serum and Foetal Bovine Serum at Various Concentrations

Fibronectin (Fn) has been regarded for a long time as a primary cell adhesive protein [105] present in serum. Early research by Grinnell et al. [106] suggested that Fibronectin binds in different conformations and quantities between hydrophobic and hydrophilic surfaces. In particular, immersion of hydrophobic and hydrophilic surfaces in various concentrations of

Fibronectin and subsequent cultures of baby hamster kidney cells on these surfaces revealed that at low concentrations of Fibronectin more Fibronectin binds to the hydrophobic surfaces. However, the hydrophobically bound Fibronectin was not as biologically active as the one bound in hydrophilic surfaces which suggests that in the hydrophobic surfaces Fn was denatured or in other words adsorbed in such a way so that its cell binding domains remain hidden or inactive. Research from other groups further support these results regarding the conformation of Fn and its effects on cell adhesion [107], proliferation [108, 109] and differentiation [110].

Grinnell [106] also discovered that the inclusion of small amounts of serum Albumin (one of the major proteins in serum) in the Fibronectin solutions increased the biological activity of Fibronectin in hydrophobic surfaces. This seems as a rather strange result, as serum albumin and Fibronectin should compete for binding sites on the surface, a behaviour which is reflected in Grinnell's results as a drop in the amount of Fibronectin adsorbed on the hydrophobic substrates. Nonetheless, Grinnell argues that the concurrent application of Fibronectin and low concentrations of Albumin, might "protect" the former even though its binding might be outcompeted by the introduction of Albumin. Of particular interest are Grinnell's cell culture experiments at low concentrations of human serum. At low concentrations of serum, less than 0.1%, Fibronectin binding and cell attachment and spreading are increased while at concentrations higher than 10% virtually no Fn binding and cell proliferation exists. Grinnell explains these results by the Albumin-Fibronectin interaction described previously.

In order to explore whether Grinnell's model could partially explain what is occurring on the parylene and thermal oxide surfaces during their immersion in serum, we performed the experiment of section 4.3.7. From an engineering perspective, we also wanted to investigate the capacity of our method to function properly at the lower end of the spectrum of serum concentrations (possibly allowing us to include the serum in the media during culturing) and see whether our patterning technique was based on a saturation effect. Moreover, we wanted to examine the capability of other types of serum to induce patterning on a combined parylene-thermal oxide substrate or detect whether something unique to horse serum was responsible for the cell patterning.

The pixel density ratio bargraph of figure 4.29 clearly indicates that other types of serum, such as foetal bovine serum, are capable of activating the parylene surface and promoting cell patterning. Therefore, we can deduce that the protein, or group of proteins, responsible for patterning is not unique to horse serum. In addition, the results of section 4.3.7 indicate that sam-

ples treated with 100% serum have superior patterning capabilities compared to those treated with diluted serum. It is interesting however, that in the lower serum concentrations a peak is achieved at 1% serum and not 0.1%, as in Grinnell's case (see figure 4.30). It is uncertain whether this indicates an involvement of Fn and Albumin in a fashion similar to Grinnell's model. However, it is certain that the 100% serum concentration is superior, a finding which does not conform to Grinnell's theory. We can therefore assume that either Fn is not involved in our patterning method at all, or that it somehow manages to out-compete Albumin during binding to the parylene. The latter however, is highly unlikely. According to McFarland et al. [95], Fn present in 10% intact foetal bovine serum fails to adsorb onto either hydrophilic (N-(2-aminoethyl)-3-aminopropyl-trimethoxysilane or EDS) or hydrophobic (dimethyldichlorosilane or DMS) surfaces. In contrast, pure Fn adsorbs to the hydrophilic surface (EDS) normally. Nevertheless, it should be pointed out that the surfaces, cells and conditions employed by McFarland [95] and Grinnell [106] are not identical to ours and as such the possibility of Fn's involvement remains. For example, one possibility could be that Fibronectin is out-competed in the thermal oxide (hydrophilic) region by Albumin, whereas manages to adhere to the parylene (hydrophobic) region, while protected from denaturing by Albumin.

If Fibronectin is not involved in our patterning technique then the question emerges of what protein, or group of proteins, is responsible for encouraging cells to migrate and adhere to parylene. Vitronectin, a serum protein which contains the RGD binding site and similar integrin subunits to Fibronectin [111], is a very good candidate and has been investigated by various research groups [95, 112, 113]. As reported by these groups, Vitronectin is more competitive in the presence of other serum proteins in high serum concentrations and promotes cell adhesion and proliferation. More details on the presence of Vitronectin and its function on our patterning technique are discussed in section 5.4.6.

4.4.6 Different Batches of Horse Serum

After noticing some discrepancies in the quality of the cell patterning between surfaces that were treated with different stocks of horse serum, we decided to investigate whether variability in the origin of horse serum could have an effect in the outcome of the cultures.

The results of section 4.3.8 indicate a significant difference between surfaces treated with different batches of horse serum. The issue of serum variability is well known in literature [90]. This is a serious concern in our patterning method, since it introduces an unwelcome variable in

our protocol, which could compromise any potential commercial applications of our technique. Serum batch testing may be employed as a temporary solution, whereby performing cultures on surfaces treated with samples from different batches of serum may allow one to find the optimal batch and utilise it in all subsequent cultures [90]. However, the identification of the exact proteins and the understanding of the mechanisms involved in our patterning technique is the preferable long term solution, which will allow us to eschew serum altogether, eliminating the variability inherent with its use.

4.4.7 Aged Surfaces

One of the distinct advantages of our patterning technique is parylene's durability and resistance to moisture, the majority of chemicals and most common forms of degradation. As a consequence, it should be feasible to store the parylene patterns for prolonged periods of time, utilising them in cell patterning when it is convenient, rather than having to build the patterns exactly before a cell culture. In order to examine whether this is indeed true we performed the experiment described in section 4.3.1.

This experiment however, served an additional purpose. During early experimentation with parylene as the non adhesive surface, we achieved an inverse result described in section 3.4.1 and shown in figures 3.11 3.12 and 3.13. One of the possible explanations offered for this inverse result was the increased negative charge of the TO due to the presence of silanol groups (Si-OH) on its surface. It was hypothesized that during surface cleaning with piranha acid, the majority of the Si-O-Si bonds on the TO are cleaved, while silanol groups are formed. Consequently, when TO is immersed into the culture medium, the H dissociates leaving negatively charged $Si\text{-}O^-$ groups on the surface [114]. However, as time from the piranha acid cleaning elapses, the silanol groups of TO surfaces on stored patterns will revert back to the normal Si-O-Si groups. Therefore, stored substrates should not produce high quality cell patterns.

The results of section 4.3.1 do not reveal any statistical significance between stored and control patterns. Nevertheless, a trend does exist between stored and control groups, which could indicate the loss of silanol groups from the TO surfaces of the aged patterns. However, the lack of statistical significance implies that the parylene patterns are free from any drastic degradation due to the passage of time. Furthermore, immersion in horse serum will sufficiently activate the parylene in stored patterns and induce cell guidance. Indeed, in all the experiments presented in this and the previous chapters, the parylene patterns utilised had been stored for considerable

time prior to culturing. Nonetheless, they provided superior glial and neuronal guidance after treatment in horse serum. This is an advantage of our patterning method, which can prove very beneficial in any potential commercial application.

4.4.8 Width of the Parylene Stripes

The issue of parylene width or surface area has already been addressed in section 3.4.2. The data from almost all experiments presented in this chapter has been analysed as if the percentage of the parylene stripes was a considerable factor. Even though it would be possible to pool the data from different stripe widths together based on the findings of section 3.3.3, we decided to treat parylene width as a significant variable and allow the statistical tests to reveal, yet again, whether this was true or not. Primarily, this was done in order to prove that even in the newly adopted 5% parylene stripes the width of the attractive area did not affect the quality of the patterning. In addition, the recurring statistical insignificance of the parylene percentage factor re-enforces the deduction that parylene stripes in our method are able to attract glia and neurons equally regardless of their width.

4.5 Conclusions

Various experiments were conducted in order to optimise and to discover the limits of our patterning technique. In this chapter it was demonstrated that activation of the parylene patterns via immersion in horse serum can be accomplished in three hours instead of a full day. This simplifies and accelerates the patterning protocol. In addition, the durability of the parylene patterns was revealed, as it was illustrated that prolonged storage does not compromise their capacity to generate cell patterns. Furthermore, throughout the experiments, the independence of the quality of the cell patterns from the parylene stripe width was verified.

The results of the experiments presented in this chapter also helped us in the formation of a cell behavioural model. We believe that at the first hours of their incubation, glia and neurons detach from the surfaces, specifically from the thermal oxide. However, the principal force behind glial and neuronal patterning in this technique is cell migration. Additionally, glia division during culture was revealed as a contributing factor to the distraction of cells from the parylene stripes after the first week of incubation. The anti-mitotic agent Ara-C may help in prolonging the life span of the cell patterns by prohibiting glia division.

Following the established literature, we investigated whether the oxidative effects of UV radiation on parylene, during sterilisation, were assisting in protein adhesion and thus glial and neuronal patterning. We discovered that UV sterilisation is, in fact, a hindering element in our protocol and results improve when it is excluded. In addition, we showed that the activation of the parylene substrate to cell adhesion can be achieved via other serums, such as foetal bovine serum, and not through horse serum exclusively. Using different dilutions of serums we proved that our patterning technique does not follow Grinnell's established model regarding Fibronectin and therefore, this protein is probably not a key factor in our patterning scheme. Further evidence indicating the absence of Fibronectin from parylene surfaces will be presented in the next chapter. Finally, we tested horse serums from different stock and showed that variations between horse serum batches can affect cell patterning quality.

Chapter 5

Surface Analysis

5.1 Introduction

This chapter describes the experiments performed on blank parylene and thermal oxide surfaces in order to gain some insight into the mechanisms underlying our patterning technique. Included are the results of said experiments as well as a discussion on the theories proposed regarding protein and cell adhesion onto the parylene and thermal oxide surfaces. Once more, our desire to analyse the two substrates (parylene and thermal oxide) and investigate various models of protein and cell adhesion was not based purely on scientific curiosity. Our primary goal has always been to optimise our technique thus, gathering more information regarding the underlying causes of patterning in our method, would allow us to produce a more refined and consistent protocol.

5.1.1 The Four Hypotheses Regarding the Mechanisms of Patterning

It was evident from early patterning experiments that the parylene-thermal oxide contrast could not guarantee high quality cell patterning on its own. In contrast, the addition of horse serum in the protocol resulted in the superior outcome presented in the previous chapters. Based on the established literature [115, 116], we theorised that, like in other methods, the protagonists in our patterning technique are cell adhesive proteins.

The first and simplest model we adopted to explain why cells were attracted to parylene was that proteins were only binding to parylene and not to thermal oxide. In light of evidence from XPS (X-ray Photo-Electron Spectroscopy) experiments disproving this theory, we considered the following three options:

a different amounts of proteins are binding to parylene and thermal oxide

b different proteins are binding to parylene and thermal oxide

c the proteins bound to parylene and thermal oxide have different conformations

Although each of the above hypotheses is sufficient to explain glial and neuronal patterning individually, they are not mutually exclusive. Therefore, they could all be true at the same time and each contributing to the final result to a different extent. However, the sum of the three theories presented above exhausts the possible explanations of our patterning method, at least as far as proteins are involved. Consequently, as one theory gets disproved or becomes unlikely, the probabilities of the remaining being true increase. This has been taken into account during the decision of what experiments to undertake and during the analysis and explanation of the results.

5.1.2 X-Ray Photo-Electron Spectroscopy

X-Ray Photo-Electron Spectroscopy (XPS also known as Electron Spectroscopy for Chemical Analysis ESCA), is a surface analysis method, which identifies the elemental composition of an analysed material. The technique also offers a quantitative measure of the contribution of each element to the material examined, as well as the chemical and electronic state of said elements. It operates by exciting the electrons of various atoms on the surface, via irradiation of the material with a beam of either magnesium or aluminum X-Rays. Subsequently, the electrons escape from their natural state orbits and are collected in an electron detector, which measures their kinetic energy. The binding energy of the electrons can then be calculated via the following equation:

$$E_{binding} = E_{photon} - E_{kinetic}$$

where $E_{binding}$ is the energy of the electron in its orbit before excitation, E_{photon} is the energy of the X-Ray photons and $E_{kinetic}$ is the kinetic energy of the emitted electron measured by the instrument. An XPS spectrum is then plotted of the number of electrons detected (Y-axis) versus their binding energy (X-axis). Depending on the peaks in the spectrum, individual elements can be identified as well as the electron configuration in their atoms.

5.2 Materials and Methods

5.2.1 Blank Substrate Fabrication

The fabrication procedure of the parylene and thermal oxide blanks is identical to the one described in section 3.2.1. However, during the photolithographic printing of the wafers in the Optimetrix 8605 5x stepper, a mask was not employed. Instead, the wafers that would produce the parylene blanks remained unexposed whereas the wafers which would eventually become the thermal oxide chips were flood exposed. This would ensure to an extent that the blank substrate fabrication procedure would resemble the stripe pattern fabrication protocol as much as possible.

5.2.2 Surface Cleaning and Sterilisation

The surface cleaning and sterilisation procedures utilised are identical to the ones described in section 3.2.3. Very briefly, blank chips of thermal oxide and parylene in the cleanroom were immersed for 10 minutes in piranha acid (25ml 30% H_2O_2, 15ml of 98% H_2SO_4). The substrates were then rinsed 3 times in distilled DI water, blown dry with nitrogen and taken out of the cleanroom in plastic dust free cases inside a vacuum desiccator.

The chips were individually placed in 24-well plates and sterilised under UV radiation (2x15W light bulbs) for 1 hour in a class 2 hood. Depending on the experiment, a 15μl serum droplet was pipetted on the blanks, which were then left in the incubator overnight. In the controls, a 15μl sterilised, distilled water droplet was pipetted instead.

5.2.3 Washing the Proteins off with Sodium Dodecyl Sulfate

Following incubation of the blanks in either serum or water, protein de-absorption was performed where necessary. The chips were rinsed once in distilled, sterilised water, relocated into new wells and rinsed again in distilled sterilised water. Finally, they were placed again into new wells and immersed in 1ml of 10% Sodium Dodecyl Sulfate (referred to as SDS from here on) and left on a R100/TW Luckham Rotatest shaker for 3 hours. In order to concentrate the proteins in the eluant, as much as 10 blank surfaces were placed in the same well and rinsed with SDS together. For the same reason, upon completion of the 3 hour rinse, the SDS eluant was collected and allowed to evaporate down to 500μl. All of the above procedures were performed

inside a class 2 hood to avoid contamination of the surfaces and the collected samples.

5.2.4 Analysis of the Surface via X-Ray Photo-Electron Spectroscopy

Control, protein loaded and SDS rinsed chips were placed inside fresh 24-well plates individually and taken to the VG Scientific, Sigma Probe XPS machine, inside a vacuum desiccator. During the water, serum and SDS immersion, as well as during the transfer and loading of the blanks into the XPS device, great care was taken not to contaminate the surfaces. Gloves and a lab coat were worn, while the mouth and nose of the researcher were covered with a white medical mask.

One general (zoom out, low resolution) and 4 element specific (zoom in, high resolution) XPS scans were executed on each blank surface. In the zoom out scan, 7 passes were performed with the pass energy of the beam at 80eV and dwell time at 40msec. In the elemental scans the pass energy was 20eV while the dwell time was again 40msec. The number of passes in the high resolution scans ranged between 60 and 100, depending on the element and the quality of the spectrum. In all cases, the radius, or spot size, of the beam was 400μm. The pressure in the vacuum chamber was always below $2*10^{-}8$ Torr and the energy of the X-ray source was (AlKa) 1486.6eV.

Data was collected as percentages of the contribution of each element in the surface composition.

5.2.5 Protein Acrylamide Gel Electrophoresis

During the procedures described in this and the following section (5.2.5) great care was given into preventing any contamination of the samples with ambient proteins. A lab coat and gloves were worn at all times, while fresh sterile containers were used where necessary. Re-usable hardware, such as electrophoresis boxes, volumetric cylinders and glass beakers were thoroughly rinsed in distilled water multiple times.

After evaporation, 30μl of the SDS eluant from each surface type (eg. parylene treated with horse serum) were added to 10μl of NuPAGE LDS sample buffer in 1ml eppendorfs. The eppendorfs were then immersed in boiling water for 5 minutes in order for the proteins to denature. Meanwhile, 50ml of MES SDS running buffer (for the Tris-Acetate gels, Novex

Tris-Acetate SDS running buffer was used instead) (x20) were added to 950ml of distilled water and the solution was used to fill up an electrophoresis box (Novex Mini Cell). In the majority of the cases, the NuPAGE 4-12% Bis-Tris Gels (1.0mm x 12 well) were used (6-200kDa), although the NuPAGE 3-8% Tris-Acetate Gels were employed in the experiments focusing on the 50-400 kDa band. The gel card was rinsed with distilled water and 15μl from the samples in the eppendorfs were added in each well of the gel comb. Either at one or both ends, 5μl of Invitrogen SeeBlue Plus 2 marker was also added. The gel card was then inserted in the electrophoresis box and a 150V voltage was applied for 1 hour (current 120mA, 30W) at the end of which, the card was taken out of the box and rinsed in distilled water. The gel was taken out of the card and rinsed in distilled water as well, before staining. Initially, staining was performed with immersion of the gel in Coomasie Blue (50ml distilled water, 40ml methanol, 10ml acetic acid, 1ml Coomasie Brilliant Blue) for 30 minutes and subsequent rinses and immersion in Destain (50ml distilled water, 40ml methanol, 10ml acetic acid) overnight. However, as Coomasie staining is not very sensitive we decided to adopt the silver staining technique, which is described below.

Silver Staining

Silver staining is a protein and DNA staining technique, which relies on the attachment of silver ions to a protein band and their subsequent chemical reduction into metallic silver [117]. Most proteins can be seen as dark bands where reduction occurs, as silver staining is 30 times more sensitive than Coomasie Blue staining, allowing detection of proteins at the sub-nanogram level. In our experiments we used the Invitrogen SilverQuest^{TM}Silver Staining Kit.

During the entirety of the silver staining method the use of distilled, ultrapure water, which has a resistance greater than 18 megaohms/cm, is advised. As water of poor quality may increase the background and impair band development, the above advice was adopted. Hence in this protocol "water" shall refer to ultrapure water mentioned above.

Following the removal of the gel from the card and its rinsing in water, the gel was fixed in fixative (40ml ethanol, 10ml acetic acid, 50ml water) for 20 minutes. The gel was then washed (30ml ethanol, 70ml water) for 10 minutes, before the 10 minute sensitization step (30ml ethanol, 10ml sensitizer, 60ml water). Two more washes were applied, both for 10 minutes (first 30ml ethanol, 70ml water, second 100ml water). Afterwards, the gel was stained for 15 minutes (1ml stainer, 99ml water) and washed in 100ml of water for 1 minute. The devel-

opment step (10ml developer, 1 drop developer enhancer, 90ml water) lasted 4 to 8 minutes depending on the desired intensity of the bands. At the end of the developing process 10ml of Stopper were added directly to the developing solution. Finally, the gel was washed in 100ml of water, packed between two transparent acetates and scanned in a HP scanner.

5.3 Results

5.3.1 Chemical Elements on the Surfaces of Horse Serum Treated Blanks and Controls

Seven parylene and eight thermal oxide blanks were cleaned, sterilised and treated with horse serum as explained in section 5.2.2. Five controls for each surface type, which were treated with distilled sterile water instead of horse serum, were included as well. After an overnight incubation in the horse serum or water, the surfaces were rinsed twice with distilled sterile water and subjected to an XPS analysis. The main elements found on the parylene were Nitrogen, Chlorine, Carbon and Oxygen while the main elements on the silicon blanks were Nitrogen, Silicon, Carbon and Oxygen. Figures 5.1 and 5.2 are spectrum examples of two parylene and thermal oxide surfaces, one treated with horse serum and one control. Notice the emergence of a nitrogen peak and the disappearance of the chlorine and silicon peaks, in the spectra of parylene and TO horse serum treated samples (figures 5.1(a) and 5.2(a) respectively).

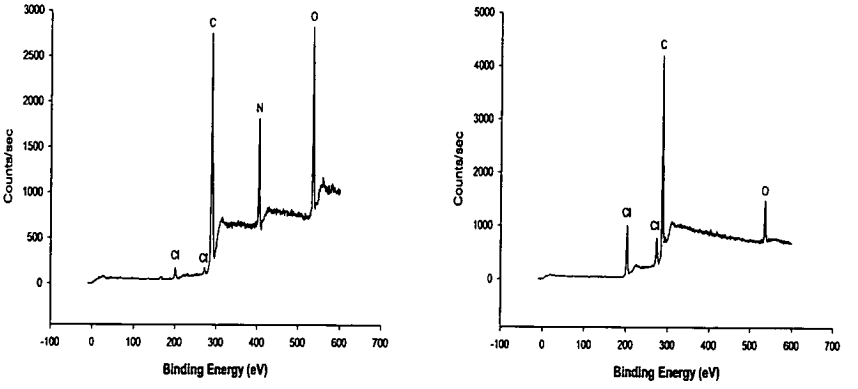

(a) Horse serum treated sample

(b) Control sample

Figure 5.1: *XPS spectra of parylene surfaces. The nitrogen peak is absent in the control spectrum while the chlorine peaks disappear in the horse serum spectrum, probably due to protein covering the surface.*

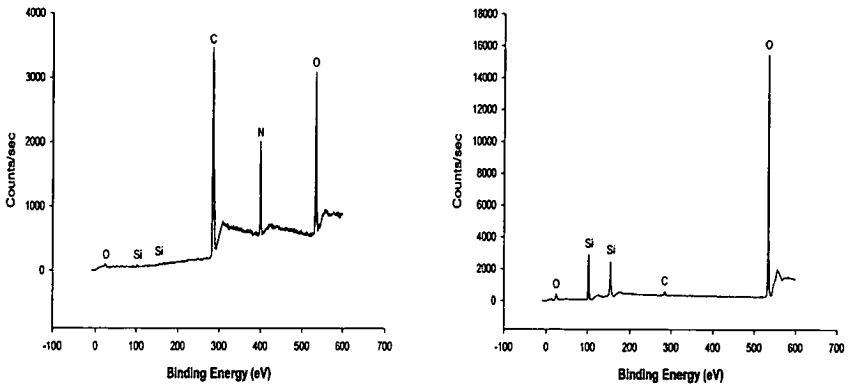

(a) Horse serum treated sample (b) Control sample

Figure 5.2: *XPS spectra of thermal oxide surfaces. The nitrogen peak is absent in the control spectrum while the silicon peaks disappear in the horse serum spectrum, probably due to protein covering the surface.*

Figures 5.3(a) and 5.3(b) is the carbon spectra of horse serum treated parylene and TO surfaces respectively. The small peak to the right denotes the presence of the peptide bond.

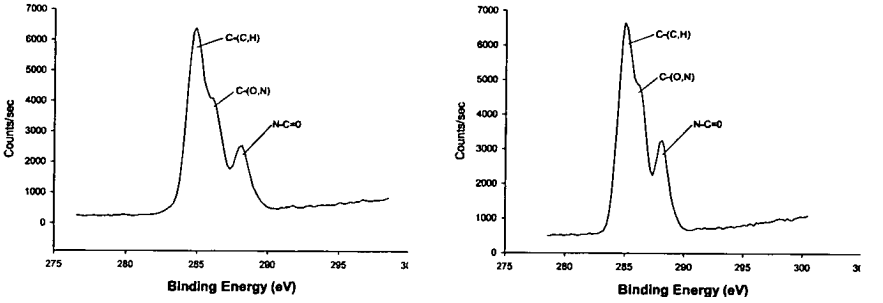

(a) Parylene (b) SiO_2

Figure 5.3: *XPS spectra of carbon on parylene and thermal oxide surfaces that have been incubated in horse serum overnight. The small peak around 288eV represents the peptide bond present in proteins.*

ANOVA tests were performed on the data of all the elements. In the case of nitrogen (normality and equal variance tests passed at P=0.026 and P=0.547 respectively) a two way ANOVA test revealed no statistically significant differences between the means of nitrogen levels on parylene (13.176% ± 0.401, n=7 for horse serum treated or 0.372% ± 0.249, n=5 for control) and TO (13.159% ± 0.277, n=8 for horse serum treated or 0.258% ± 0.258, n=5 for control) (P=0.844). However, differences between horse serum treated and control samples were statis-

tically significant ($P \leq 0.001$). Finally, no statistically significant interactions existed between the treatment and surface type factors ($P=0.884$).

One way ANOVA tests were performed for chlorine and silicon, since they were present only on one of the two surfaces. In the chlorine ANOVA, normality and equal variance tests passed with $P>0.2$ and $P=0.741$ respectively, while the difference between the means of horse serum treated ($1.943\% \pm 0.299$, $n=7$) and control samples ($8.46\% \pm 0.305$, $n=5$) was statistically significant ($P \leq 0.001$). Similarly, in the silicon ANOVA, normality and equal variance tests passed with $P>0.2$ and $P=0.399$ respectively while the difference between the means of horse serum treated ($4.404\% \pm 1.020$, $n=8$) and control samples ($23.536\% \pm 0.586$, $n=5$) was statistically significant ($P \leq 0.001$).

The two way ANOVA for the carbon (normality and equal variance tests passed with $P=0.054$ and $P=0.355$ respectively) revealed statistically significant differences ($P \leq 0.001$) both between the means of horse serum treated ($65.881\% \pm 0.666$, $n=7$ for parylene or $56.896\% \pm 2.403$, $n=8$ for TO) and control samples ($83.45\% \pm 0.466$, $n=5$ for parylene or $7.762\% \pm 2.197$, $n=5$ for TO), and between the average carbon levels of parylene and thermal oxide ($P \leq 0.001$). The interaction between the treatment and surface type factors was statistically significant ($P \leq 0.001$).

Finally, the two way ANOVA for oxygen (normality and equal variance tests passed with $P=0.059$ and $P=0.393$ respectively) revealed statistically significant differences ($P \leq 0.001$) between the means of horse serum treated ($19.003\% \pm 0.41$, $n=7$ for parylene or $25.541\% \pm 1.613$, $n=8$ for TO) and control samples ($7.714\% \pm 0.391$, $n=5$ for parylene or $68.442\% \pm 1.978$, $n=5$ for TO). Differences between the average oxygen levels of parylene and thermal oxide were also statistically significant ($P \leq 0.001$), while the interaction between the treatment and surface type factors was statistically significant ($P \leq 0.001$) as well.

The five bar graphs of figures 5.4 through 5.8 summarise the average percentage contribution of each element on the surface.

5.3.2 XPS Analysis of Piranha Cleaned, Untreated Surfaces

In order to establish the levels of the composing elements of each substrate, we piranha cleaned 4 chips of each material (parylene and TO) and analysed them with XPS. The results are summarised in figure 5.9.

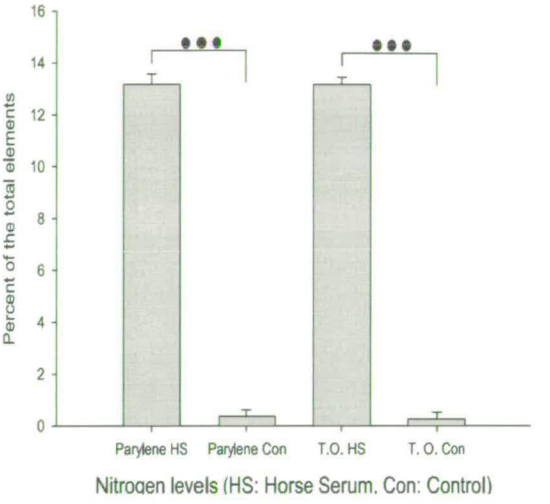

Figure 5.4: *Contribution of nitrogen to the surface (parylene or thermal oxide) as a percentage (controls have been treated with water instead of horse serum). Error bars represent the Standard Error of the Means (SEM). One dot represents statistical significance of $P < 0.05$, two dots represent statistical significance of $P < 0.01$, three dots represent statistical significance of $P < 0.001$.*

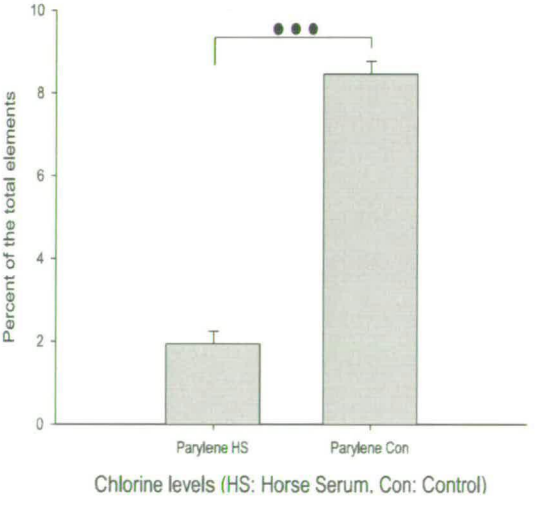

Figure 5.5: *Contribution of chlorine to the parylene surface as a percentage (controls have been treated with water instead of horse serum). Error bars represent SEMs.*

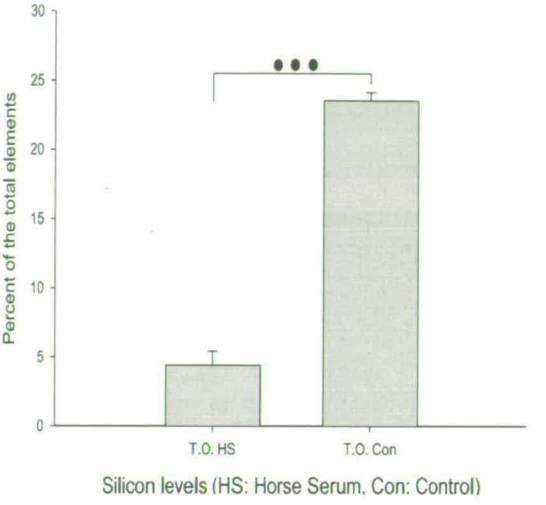

Figure 5.6: *Contribution of silicon to the surface of the thermal oxide as a percentage (controls have been treated with water instead of horse serum). Error bars represent SEMs.*

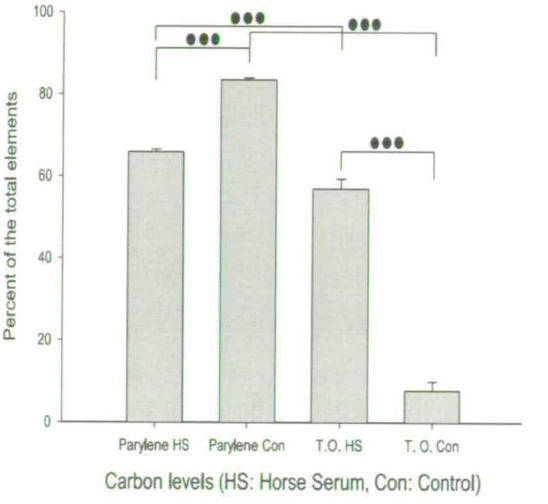

Figure 5.7: *Contribution of carbon to the surface (parylene or thermal oxide) as a percentage (controls have been treated with water instead of horse serum). Error bars represent SEMs.*

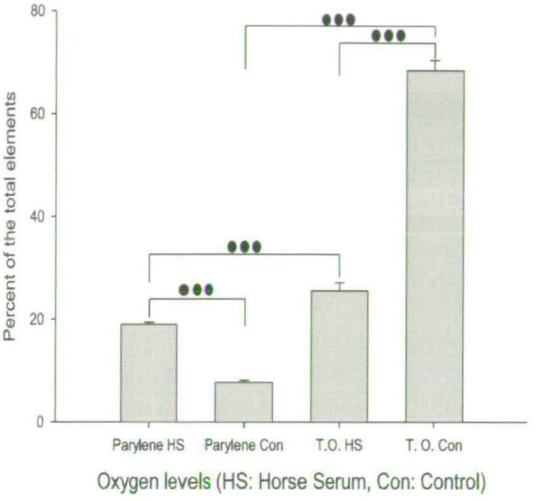

Figure 5.8: *Contribution of oxygen to the surface (parylene or thermal oxide) as a percentage (controls have been treated with water instead of horse serum). Error bars represent SEMs.*

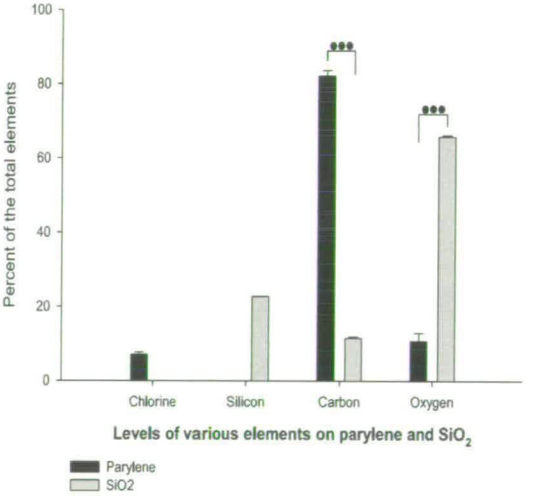

Figure 5.9: *Main elements on parylene (Cl, C, O) and thermal oxide (Si, C, O). Surfaces were only cleaned with piranha acid. Traces of nitrogen detected. Error bars represent SEMs.*

As usual, statistical significance was determined via one way ANOVA tests. As expected, the carbon ANOVA (normality and equal variance tests passed with P=0.156 and P=0.211 respectively) revealed a statistically significant difference ($P \leq 0.001$) between the average parylene (82.163% ± 1.514, n=4) and the average thermal oxide (11.5% ± 0.342, n=4) carbon levels. Similarly, average oxygen levels on parylene (10.758% ± 2.144, n=4) were significantly different from the thermal oxide ones (65.787% ± 0.397, n=4) ($P \leq 0.001$).

In addition, the oxygen levels on the parylene and thermal oxide piranha cleaned surfaces were contrasted to the oxygen level of corresponding surfaces that were cleaned with piranha and subjected to UV radiation. A two way ANOVA demonstrates (normality and equal variance tests passed with P=0.066 and P=0.471 respectively) that the difference between oxygen levels on non UV (10.757% ± 1.572, n=4) and UV (7.714% ± 1.406, n=5) radiated parylene is insignificant (P=0.171). Likewise, the oxygen levels of non UV (65.788% ± 1.572, n=4) and UV (68.442% ± 1.406, n=5) radiated thermal oxide are similar (P=0.229). Oxygen levels of parylene and thermal oxide were significantly different ($P \leq 0.001$) regardless of treatment. No statistically significant interactions were detected between the treatment and surface type factors (P=0.077).

Similar comparisons were drawn between carbon, chlorine and silicon levels. A two way ANOVA test (normality and equal variance tests passed with P=0.097 and P=0.470 respectively) of carbon levels on the same parylene and thermal oxide surfaces revealed no significant differences (P=0.539) between average carbon levels on of piranha cleaned (82.163% ± 1.522, n=4) and UV radiated (83.45% ± 1.362, n=5) parylene. Similarly, differences in average carbon levels of piranha cleaned (11.5% ± 1.522, n=4) and UV radiated (7.762% ± 1.362, n=5) thermal oxide were insignificant (P=0.089). Carbon levels of parylene and thermal oxide were significantly different ($P \leq 0.001$) regardless of treatment. No statistically significant interactions were detected between the treatment and surface type factors (P=0.104).

One way ANOVA tests were performed on the chlorine (normality and equal variance tests passed with P=0.087 and P=0.566 respectively) and silicon (normality and equal variance tests passed with P=0.147 and P=0.040 respectively) data. Average chlorine levels on piranha cleaned parylene (7.083% ± 0.638, n=4) were not significantly different (P=0.075) from chlorine levels on UV treated parylene (8.46% ± 0.305, n=5). On the thermal oxide surfaces, average silicon levels on piranha cleaned surfaces (22.715% ± 0.056, n=4) were not significantly different (P=0.258) from the silicon levels of UV radiated substrates (23.536% ± 0.586,

n=5).

Figures 5.10 and 5.11 illustrate these results, while image 5.12 is the high resolution XPS spectrum of carbon on parylene which has and has not been subjected to ultraviolet radiation.

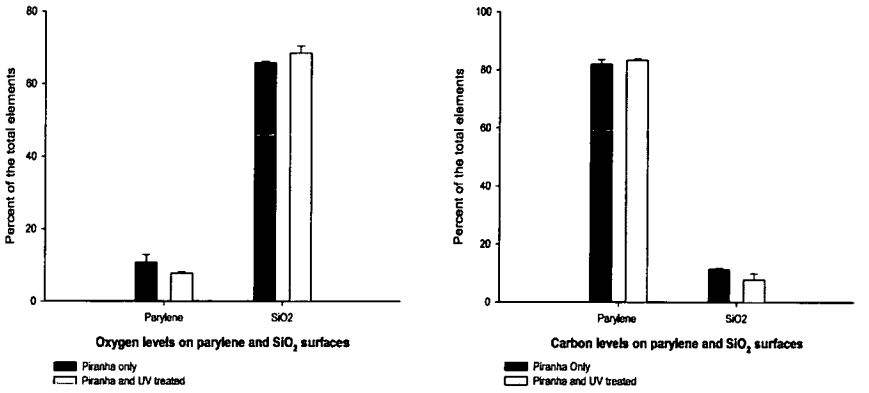

(a) Oxygen (b) Carbon

Figure 5.10: *The effect of ultraviolet radiation on parylene and thermal oxide. Differences in oxygen and carbon levels between the two treatments are insignificant. Error bars represent SEMs.*

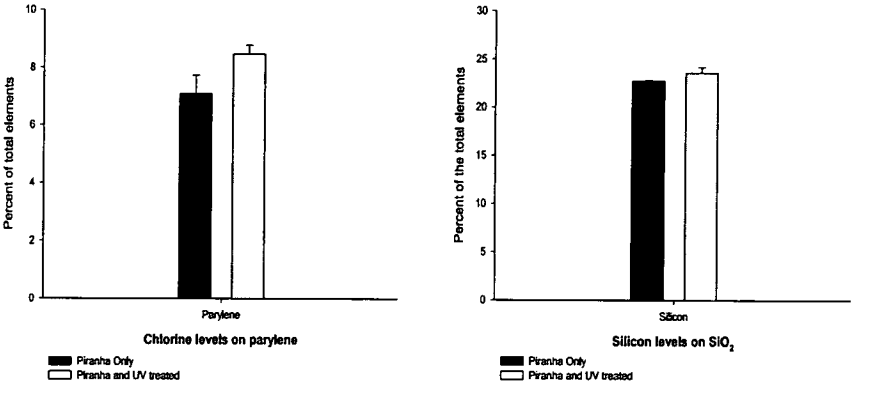

(a) Chlorine (only parylene) (b) Silicon (only thermal oxide)

Figure 5.11: *The effect of ultraviolet radiation on parylene and thermal oxide. Differences in chlorine and silicon levels between the two treatments are insignificant. Error bars represent SEMs.*

It is evident from figure 5.12 that O-C=O groups appear on the UV radiated parylene. The significance of these groups is explained in the discussion.

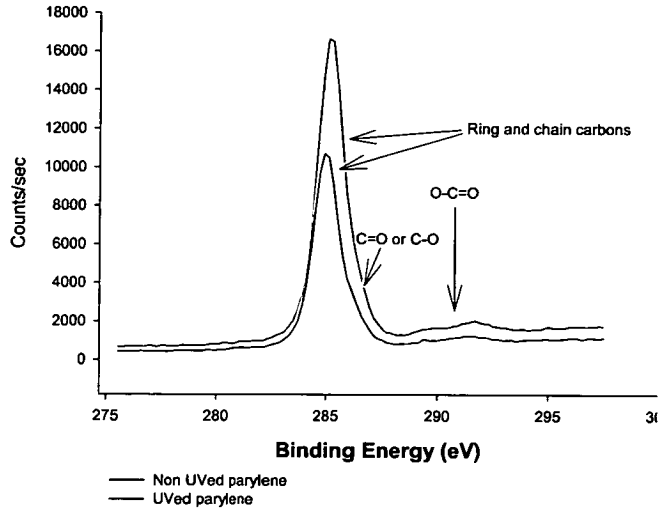

Figure 5.12: *High resolution XPS spectrum of carbon on a parylene surface that has only been cleaned with piranha acid and a parylene surface that has additionally been subjected to UV radiation for 1 hour.*

5.3.3 Protein de-Adsorption via the Use of SDS

In order to gain insight into protein-surface interactions on the two substrates and investigate whether SDS was capable of removing the proteins from the surfaces completely, we piranha cleaned and sterilised under UV 14 parylene and 14 thermal oxide blanks. Three chips from each substrate were incubated in sterile distilled water overnight and acted as a control group (**no horse serum** control). Three more surfaces from each substrate were incubated in horse serum overnight and also acted as controls (**horse serum** controls). In the experimental groups, 3 parylene and 3 thermal oxide surfaces were incubated in horse serum overnight and then rinsed once in SDS. A final experimental group, comprised of 5 blanks for each surface type, was incubated in horse serum overnight and rinsed 3 times in SDS.

All surfaces prior to SDS rinsing were rinsed first with sterile distilled water to remove any unstuck proteins from the surface and any residual horse serum. The horse serum controls were not rinsed with SDS and were used to determine the average maximum amount of nitrogen on the surfaces. Finally, the first, second and third SDS rinses in the last experimental group lasted for 150, 90 and 60 minutes respectively. The surfaces were rinsed with distilled sterile water in between SDS rinses, while the SDS from each rinse was collected and fresh SDS was used for each rinse. All the experimental surfaces were rinsed twice in distilled sterile water before

being analysed.

One way ANOVA tests were performed for every element on each surface type. A one way ANOVA test on the nitrogen levels on parylene (normality and equal variance tests passed with $P>0.2$ and $P=0.051$ respectively) revealed a statistically significant difference between average nitrogen levels of all pair wise combinations of the **no horse serum** control group (0.08% $\pm$ 0.031, n=3), the **horse serum** control group (13.89% $\pm$ 0.421, n=3), the **1 SDS rinse** experimental group (9.877% $\pm$ 0.228, n=3) and the **3 SDS rinses** experimental group (9.776% $\pm$ 0.159, n=5), ($P\leq0.001$). However, the difference among the average nitrogen levels of the 1 SDS and 3 SDS rinses experimental groups was not statistically significant ($P=0.988$). A similar one way ANOVA test on the thermal oxide nitrogen levels (normality and equal variance tests passed with $P>0.2$ and $P=0.097$ respectively) revealed that average nitrogen levels of the **no horse serum** control group (0.063% $\pm$ 0.024, n=3) and the **horse serum** control group (12.953% $\pm$ 0.298, n=3) were statistically different ($P\leq0.001$). Likewise, the average nitrogen levels of the **horse serum** control group were significantly different from the average nitrogen levels of both the **1 SDS rinse** (0.4% $\pm$ 0.108, n=3) and the **3 SDS rinses** (0.208% $\pm$ 0.082, n=5) experimental groups ($P\leq0.001$). In contrast, differences between the two experimental groups ($P=0.771$) and between the **no horse serum** control group and the **1 SDS rinse** ($P=0.465$) and the **3 SDS rinses** experimental groups ($P=0.884$) were not statistically significant. These results are summarised by the bar graph of figure 5.13.

The one way ANOVA test for the chlorine on parylene (normality and equal variance tests passed with $P>0.2$ and $P=0.894$ respectively) revealed a statistically significant difference between average chlorine levels of all pair wise combinations of the **no horse serum** control group (8.84% $\pm$ 0.196, n=3), the **horse serum** control group (0.417% $\pm$ 0.250, n=3), the **1 SDS rinse** experimental group (2.44% $\pm$ 0.146, n=3) and the **3 SDS rinses** experimental group (2.628% $\pm$ 0.137, n=5), ($P\leq0.001$). However, the difference among the average chlorine levels of the **1 SDS** and **3 SDS** rinses experimental groups was not statistically significant ($P=0.865$). Similarly, for the silicon levels of the thermal oxide (normality and equal variance tests passed with $P=0.100$ and $P=0.395$ respectively) the **horse serum** control group (5.827% $\pm$ 0.337, n=3) was found significantly different from the **no horse serum** control group (18.49% $\pm$ 0.244, n=3), the **1 SDS rinse** experimental group (20.47% $\pm$ 1.333, n=3) and the **3 SDS rinses** experimental group (20.7% $\pm$ 0.456, n=5) ($P\leq0.001$ for all). However, differences between the two experimental groups ($P=0.994$) and between the **no horse serum** control group and the

two experimental groups (P=0.278 and P=0.140 for 1 and 3 SDS rinses respectively) were not statistically significant. The bar graph of figure 5.14 illustrates these results.

A one way ANOVA test was performed on the carbon levels on parylene (normality and equal variance tests passed with P=0.041 and P=0.428 respectively). Differences between average nitrogen levels of the **no horse serum** control group (80.847% ± 1.422, n=3), the **horse serum** control group (64.953% ± 0.418, n=3), the **1 SDS rinse** experimental group (66.74% ± 0.372, n=3) and the **3 SDS rinses** experimental group (67.796% ± 0.253, n=5) were significant ($P \leq 0.001$). The difference between the **horse serum** control group and the **3 SDS rinses** experimental group was also statistically significant (P=0.044). On the other hand differences between the carbon levels of the two experimental groups (P=0.658) and differences between the **horse serum** control group and the **1 SDS rinse** experimental group (P=0.341) were not statistically significant. A similar one way ANOVA test on the thermal oxide carbon levels (normality and equal variance tests passed with P=0.092 and P=0.250 respectively) revealed that average carbon levels of the **no horse serum** control group (23.923% ± 0.454, n=3) and the **horse serum** control group (52.47% ± 0.555, n=3) were statistically different ($P \leq 0.001$). Likewise, the average carbon levels of the **horse serum** control group were significantly different from the average carbon levels of both the **1 SDS rinse** (19.02% ± 4.749, n=3) and the **3 SDS rinses** (18.278% ± 1.535, n=5) experimental groups ($P \leq 0.001$). In contrast, differences between the two experimental groups (P=0.995) and between the **no horse serum** control group and the **1 SDS rinse** (P=0.53) and the **3 SDS rinses** experimental groups (P=0.33) were not statistically significant. These results are summarised by the bar graph of figure 5.15.

A one way ANOVA test was performed on the average oxygen levels on parylene (normality and equal variance tests passed with P=0.025 and P=0.379 respectively). Average oxygen levels on the **no horse serum** control group (10.223% ± 1.598, n=3) were statistically different from average oxygen levels on the **horse serum** control group (20.707% ± 0.195, n=3), the **1 SDS rinse** experimental group (20.367% ± 0.228, n=3) and the **3 SDS rinses** experimental group (19.212% ± 0.247, n=5) ($P \leq 0.001$ for all). However, differences between the two experimental groups (P=0.635) and between the **horse serum** control group and the two experimental groups (P=0.988 and P=0.438 for 1 and 3 SDS rinses respectively) were not statistically significant. On silicon (normality and equal variance tests passed with P=0.066 and P=0.216 respectively), average oxygen levels of the **horse serum** control group (28.743% ± 0.494, n=3) were significantly different from average oxygen levels of the **no horse serum** control group (56.377%

$\pm$ 0.141, n=3), the **1 SDS rinse** experimental group (59.503% $\pm$ 3.824, n=3) and the **3 SDS rinses** experimental group (60.114% $\pm$ 1.243, n=5) ($P \leq 0.001$ in all cases). On the other hand, differences between the two experimental groups (P=0.995) and between the **no horse serum** control group and the two experimental groups (P=0.695 and P=0.485 for 1 and 3 SDS rinses respectively) were not statistically significant. The bar graph of figure 5.16 illustrates these results.

Finally, one way ANOVA tests were carried out on the average sulphur levels on the parylene and thermal oxide (normality and equal variance tests of the parylene passed with P>0.2 and P=0.523 and of the thermal oxide with P>0.2 and P=0.523 respectively). Differences between the **1 SDS rinse** (0.577% $\pm$ 0.103, n=3) and **3 SDS rinses** (0.544% $\pm$ 0.046, n=5) experimental groups were not statistically significant (P=0.973). Additionally, differences between the two control groups, **no horse serum** (0.007% $\pm$ 0.003, n=3) and **horse serum** (0.033% $\pm$ 0.033, n=3), were not statistically significant (P=0.989). However, all other pair wise comparisons were statistically significant ($P \leq 0.001$ in all cases). In the case of silicon, average sulphur level differences between the **no horse serum** (1.147% $\pm$ 0.07, n=3) and the **horse serum** (0.007% $\pm$ 0.007, n=3) controls were statistically significant (P=0.009). All other differences, including the difference between the two experimental groups ((0.610% $\pm$ 0.307, n=3) and (0.700% $\pm$ 0.160, n=5) for **1 SDS rinse** and **3 SDS rinses** groups respectively) (P=0.982), were not statistically significant. The bar graph of figure 5.17 summarises these results.

5.3.4 Protein de-Adsorption via the Use of Various Solvents

Four other solvents, besides SDS, were tested in order to see whether any would rinse the proteins off the parylene and the thermal oxide surfaces. These solvents were sodium hydroxide (referred to as NaOH from here on), methanol, trifluoroacetic acid (referred to as TFA from here on) and toluene. The choice of these solvents is explained in the discussion.

As with other experiments, two control groups were included. The "**no horse serum**" control group consisted of 5 blank substrates for each surface type (parylene and thermal oxide), which were piranha cleaned and sterilised according to normal protocol and then incubated overnight in sterile distilled water. These substrates did not come into contact with horse serum or with any of the solvents. The "**horse serum**" control group consisted of 5 blank substrates for each surface type (parylene and thermal oxide), which were piranha cleaned, sterilised and incubated overnight in horse serum according to normal protocol. These substrates were rinsed twice in

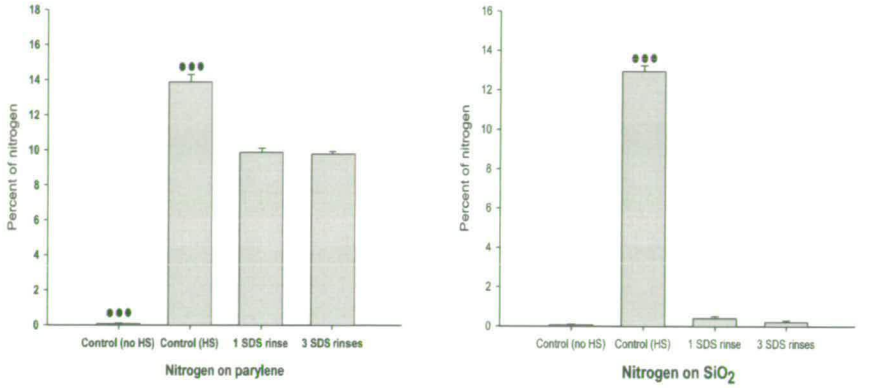

(a) Parylene (b) Thermal oxide

Figure 5.13: *Nitrogen on parylene and thermal oxide that have been treated with horse serum, after 1 and 3 rinses with SDS. The (HS) control was not rinsed with SDS and reveals the average maximum nitrogen load on the surface. The (no HS) control was not treated with horse serum but was rinsed with SDS and reveals the minimum nitrogen load on the surface, as well the contribution of SDS to said load. Error bars represent SEMs.*

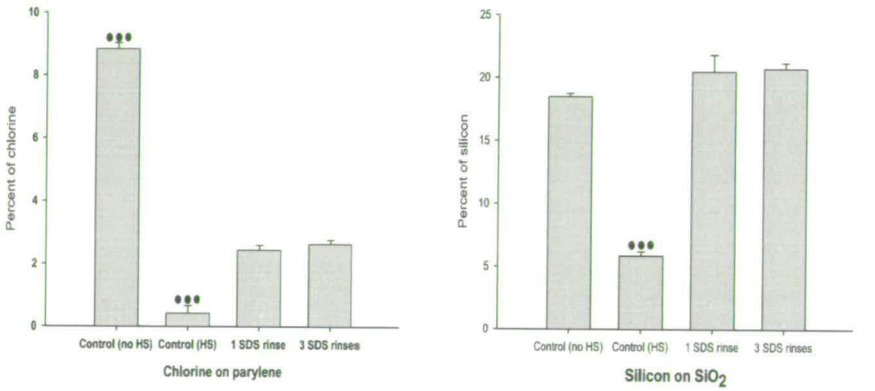

(a) Parylene (b) Thermal oxide

Figure 5.14: *Chlorine on parylene and silicon on thermal oxide that have been treated with horse serum, after 1 and 3 rinses with SDS. The (HS) control was not rinsed with SDS and reveals the average minimum chlorine or silicon load on the surface. The (no HS) control was not treated with horse serum but was rinsed with SDS and reveals the maximum chlorine or silicon load on the surface, as well the contribution of SDS to said load. Error bars represent SEMs.*

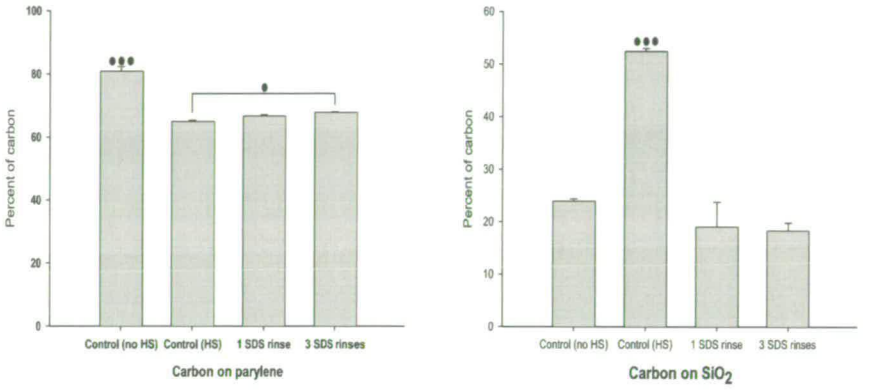

(a) Parylene (b) Thermal oxide

Figure 5.15: *Carbon on parylene and thermal oxide that have been treated with horse serum, after 1 and 3 rinses with SDS. The (HS) control was not rinsed with SDS and reveals the average maximum carbon load on the surface. The (no HS) control was not treated with horse serum but was rinsed with SDS and reveals the minimum carbon load on the surface, as well the contribution of SDS to said load. Error bars represent SEMs.*

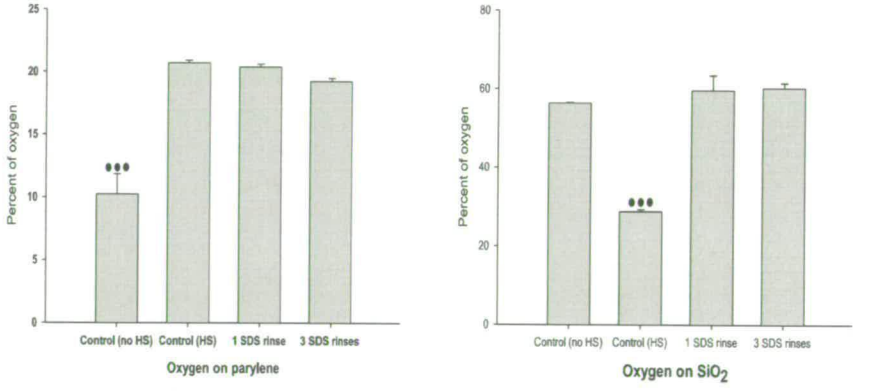

(a) Parylene (b) Thermal oxide

Figure 5.16: *Oxygen on parylene and thermal oxide that have been treated with horse serum, after 1 and 3 rinses with SDS. The (HS) control was not rinsed with SDS and reveals the average maximum (parylene) or minimum (thermal oxide) oxygen load on the surface. The (no HS) control was not treated with horse serum but was rinsed with SDS and reveals the minimum (parylene) or maximum (thermal oxide) oxygen load on the surface, as well the contribution of SDS to said load. Error bars represent SEMs.*

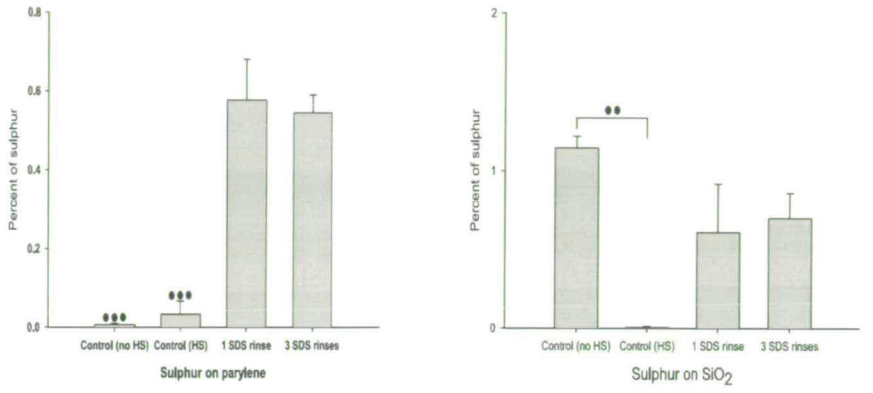

(a) Parylene (b) Thermal oxide

Figure 5.17: *Sulphur on parylene and thermal oxide that have been treated with horse serum, after 1 and 3 rinses with SDS. The (HS) control was not rinsed with SDS and reveals the average minimum (thermal oxide) sulphur load on the surface. The (no HS) control was not treated with horse serum but was rinsed with SDS and reveals the maximum (thermal oxide) sulphur load on the surface, as well the contribution of SDS to said load. Error bars represent SEMs.*

sterile distilled water before scanning, but did not come into contact with any of the solvents.

Five blank substrates for each surface type (parylene and thermal oxide) were used in each of the experimental (solvent) groups. All substrates were piranha cleaned, sterilised and incubated overnight in horse serum according to normal protocol. Substrates in the NaOH group were rinsed 15 minutes in 1M NaOH then rinsed with sterile distilled water. This cycle was repeated two more times. Substrates in the methanol group were rinsed for 15 minutes in 100% methanol then rinsed with sterile distilled water. This cycle was repeated two more times however, 50% and 33% methanol was used in the second and third cycles. Substrates in the TFA group were rinsed in 200mM TFA then rinsed with sterile distilled water. This was repeated once more. Substrates in the toluene group were rinsed in 100% toluene then rinsed with sterile distilled water. This was repeated once more.

All experimental surfaces were rinsed with sterile distilled water once more and were allowed to dry before scanning in the XPS. Between cycles, fresh solvent was always used while used solvent was collected.

A two way ANOVA was performed on the average nitrogen levels on parylene and thermal oxide (normality and equal variance tests passed with P=0.184 and P=0.065 respectively). Within

the **no horse serum** and **horse serum** control groups no significant difference was detected (P=0.106 and P=0.081 respectively) between nitrogen levels of parylene (0.108% ± 0.059, n=5), (14.286% ± 0.532, n=5) and thermal oxide (0.026% ± 0.011, n=5), (12.986% ± 0.926, n=5). However, within the experimental groups differences in average nitrogen levels were statistically significant. In particular, in the NaOH group nitrogen levels on parylene (10.86% ± 0.201, n=5) were significantly different ($P \leq 0.001$) from those on thermal oxide (0.246% ± 0.111, n=5). Likewise, in the methanol group nitrogen levels on parylene (15.974% ± 0.177, n=5) and on thermal oxide (13.81% ± 0.461, n=4) were statistically different (P=0.013). In the TFA group parylene (12.814% ± 0.375, n=5) and thermal oxide (2.026% ± 0.203, n=5) nitrogen levels were also significantly different ($P \leq 0.001$). Finally, in the toluene group differences between parylene (14.178% ± 0.148, n=4) and thermal oxide (11.104% ± 0.499, n=5) were also significant ($P \leq 0.001$). The bar graph of figure 5.22 summarises these results.

One way ANOVA tests were also performed on every element of both surfaces for different solvent treatments. With the exception of a few cases, differences between various solvents were statistically significant. Due to the quantity of the results and the indirect nature of their significance, actual numbers are not included. However, the bar graphs of figures 5.18 through 5.21 illustrate the mentioned results. In some cases, statistical significance has been included in the graphs.

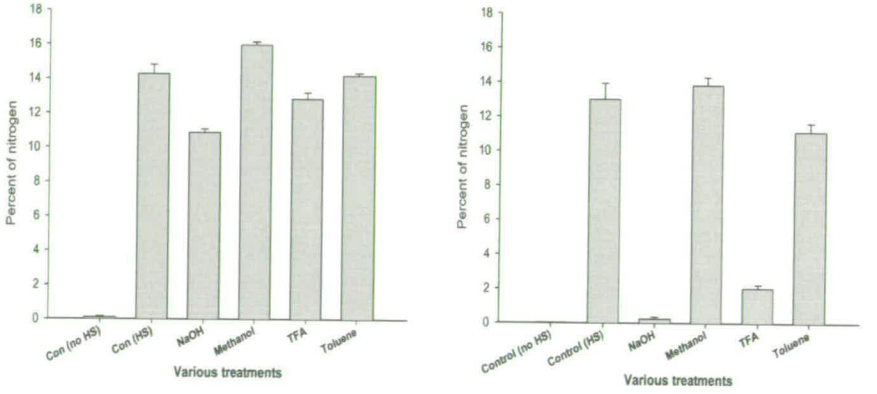

(a) Parylene (b) Thermal oxide

Figure 5.18: *Nitrogen on parylene and thermal oxide that have been treated with horse serum, after rinses with various solvents. The (HS) control was not rinsed with any solvent and reveals the average maximum nitrogen load on the surface. The (no HS) control was not treated with horse serum and reveals the average minimum nitrogen load on the surface. Error bars represent SEMs.*

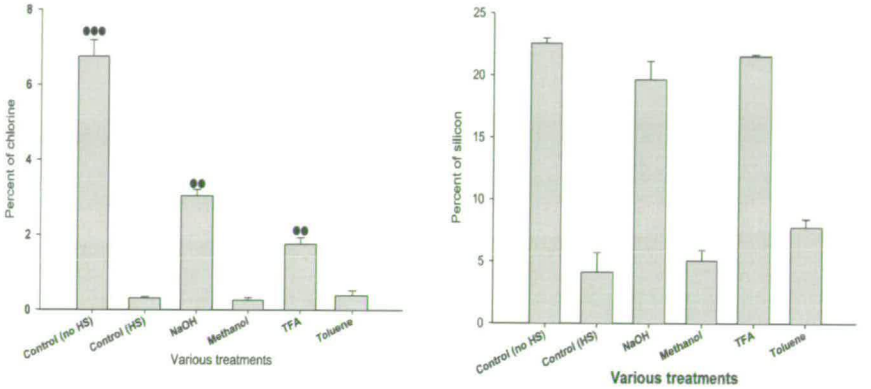

(a) Parylene (b) Thermal oxide

Figure 5.19: *Chlorine on parylene and silicon on thermal oxide that have been treated with horse serum, after rinses with various solvents. The (HS) control was not rinsed with any solvent and reveals the average minimum chlorine or silicon load on the surface. The (no HS) control was not treated with horse serum and reveals the average maximum chlorine or silicon load on the surface. Error bars represent SEMs.*

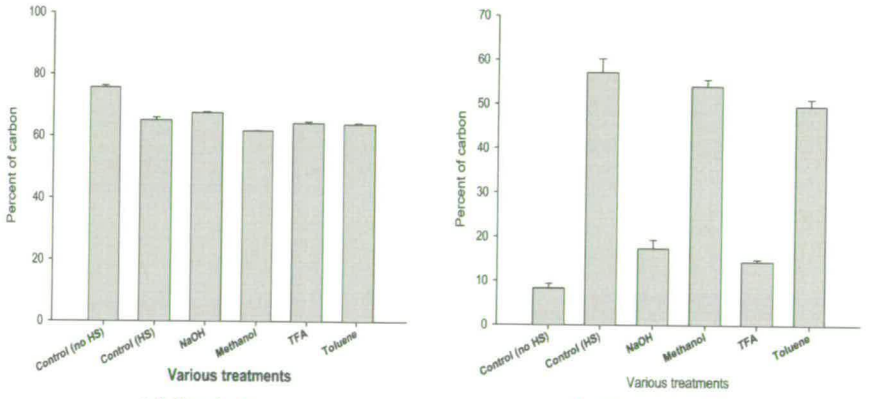

(a) Parylene (b) Thermal oxide

Figure 5.20: *Carbon on parylene and thermal oxide that have been treated with horse serum, after rinses with various solvents. The (HS) control was not rinsed with any solvent and reveals the average maximum carbon load on the surface. The (no HS) control was not treated with horse serum and reveals the average minimum carbon load on the surface. Error bars represent SEMs.*

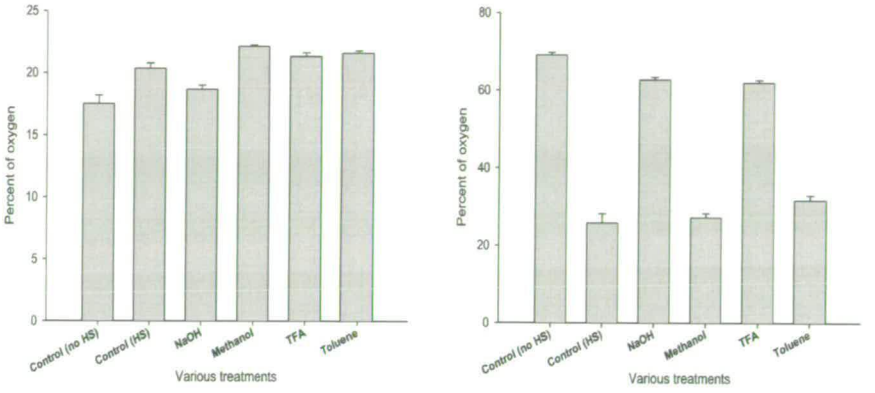

(a) Parylene (b) Thermal oxide

Figure 5.21: *Oxygen on parylene and thermal oxide that have been treated with horse serum, after rinses with various solvents. The (HS) control was not rinsed with any solvent and reveals the average maximum (parylene) or minimum (thermal oxide) oxygen load on the surface. The (no HS) control was not treated with horse serum and reveals the average minimum (parylene) or maximum (thermal oxide) oxygen load on the surface. Error bars represent SEMs.*

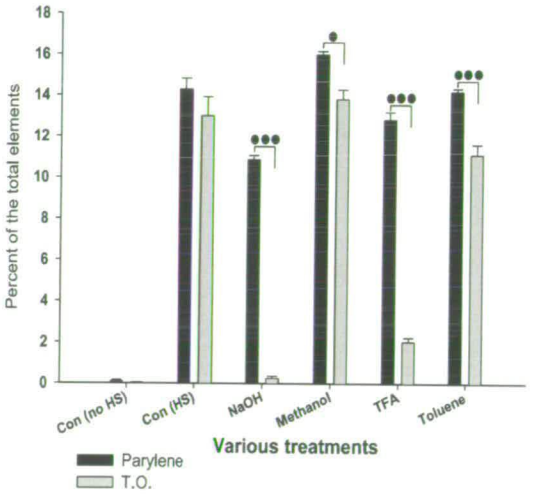

Figure 5.22: *Comparison of nitrogen levels between parylene and thermal oxide. The surfaces have been subjected to rinses with various solvents. The (HS) control was not rinsed with any solvent and reveals the average maximum nitrogen load on the surface. The (no HS) control was not treated with horse serum and reveals the average minimum nitrogen load on the surface. Notice how some solvents rinse nitrogen away of the thermal oxide completely while failing to do the same on the parylene. Error bars represent SEMs.*

5.3.5 Monitoring Nitrogen Levels Over the Course of 3 Weeks

Data in section 4.3.4 in page 85 suggested that patterning was lost over the course of 3 weeks. In order to explore the cause of this behaviour, we monitored the levels of nitrogen and other elements on the surfaces over the course of 3 weeks, by incubating blank surfaces in normal culture media, under normal culturing conditions and then scanning them in the XPS. Specifically, blank chips were divided into three experimental groups, **week1**, **week2** and **week3**. Within each group some surfaces were incubated in sterile distilled water overnight (they did not come into contact with horse serum) and were considered as controls, while the rest were incubated in horse serum overnight as per the protocol in section 5.2.2. Following the overnight incubation, the surfaces of groups **week1**, **week2** and **week3** were incubated in Neurobasal-A growth media over the course of one, two and three weeks respectively. The media was changed as per the protocol of section 3.2.4 in page 36. Overnight data from the experiment of section 5.3.1 were also included in order to be aware of average starting nitrogen levels as well as the starting levels of other elements.

Two way ANOVA tests were conducted on the data of each element on parylene and on thermal oxide. In every case the average overnight elemental levels were significantly different from the average elemental levels of weeks 1, 2 and 3. However, the average levels of weeks 1, 2 and 3 were never statistically different.

In particular, overnight levels of nitrogen on parylene controls (0.372% $\pm$ 0.247, n=5) were significantly different from levels of week 1 (11.498% $\pm$ 0.155, n=5), week 2 (11.468% $\pm$ 0.339, n=5) and week 3(11.228% $\pm$ 0.338, n=4) ($P \leq 0.001$ in all cases). Similarly, on horse serum parylene samples, overnight nitrogen levels (13.176% $\pm$ 0.401, n=7) were statistically different from average nitrogen levels of week 1 (10.009% $\pm$ 0.376, n=8), week 2 (9.236% $\pm$ 0.298, n=10) and week 3 (8.508% $\pm$ 1.114, n=6) ($P \leq 0.001$ in all cases). On thermal oxide controls, average overnight nitrogen levels (0.258% $\pm$ 0.258, n=5) were also different from levels of week 1 (9.242% $\pm$ 0.206, n=5), week 2 (9.158% $\pm$ 0.474, n=4) and week 3 (9.513% $\pm$ 0.607, n=4) ($P \leq 0.001$ in all cases). Finally, on horse serum thermal oxide samples, differences between overnight nitrogen levels (13.159% $\pm$ 0.277, n=8) and levels of week 1 (9.166% $\pm$ 0.722, n=7) week 2 (8.646% $\pm$ 0.258, n=9) and week 3 (8.683% $\pm$ 0.270, n=6) were statistically significant ($P \leq 0.001$ in all cases). Differences in nitrogen levels between week 1, week 2 and week 3 in controls and horse serum samples of parylene and thermal oxide were never statistically significant. There results are summarised in figure 5.23.

Overnight levels of chlorine on parylene controls (8.46% ± 0.305, n=5) were significantly different from levels of week 1 (3.258% ± 0.381, n=5), week 2 (3.686% ± 0.188, n=5) and week 3(3.638% ± 0.121, n=4) ($P \leq 0.001$ in all cases). Similarly, on horse serum parylene samples, overnight chlorine levels (1.943% ± 0.299, n=7) were statistically different from average chlorine levels of week 1 (4.201% ± 0.358, n=8), week 2 (4.403% ± 0.223, n=10) and week 3 (3.538% ± 0.612, n=6) ($P \leq 0.001$ in all cases except overnight vs week 3 in which P=0.011). On thermal oxide controls, average overnight silicon levels (23.536% ± 0.586, n=5) were also different from levels of week 1 (12.442% ± 0.334, n=5), week 2 (12.528% ± 0.920, n=4) and week 3 (12.220% ± 1.132, n=4) ($P \leq 0.001$ in all cases). Finally, on horse serum thermal oxide samples, differences between overnight silicon levels (4.404% ± 1.020, n=8) and levels of week 1 (11.876% ± 1.224, n=7) week 2 (12.602% ± 0.565, n=9) and week 3 (12.712% ± 0.389, n=6) were statistically significant ($P \leq 0.001$ in all cases). Differences in chlorine and silicon levels between week 1, week 2 and week 3 in controls and horse serum samples of parylene and thermal oxide were never statistically significant. Figure 5.24 illustrates these results.

Overnight levels of carbon on parylene controls (83.45% ± 0.466, n=5) were significantly different from levels of week 1 (67.094% ± 0.616, n=5), week 2 (67.146% ± 0.417, n=5) and week 3 (67.833% ± 0.688, n=4) ($P \leq 0.001$ in all cases). Similarly, on horse serum parylene samples, overnight carbon levels (65.881% ± 0.666, n=7) were statistically different from average carbon levels of week 1 (69.48% ± 0.698, n=8), week 2 (70.377% ± 0.361, n=10) and week 3 (71.138% ± 1.577, n=6) ($P \leq 0.001$ in all cases except overnight vs week 1 in which P=0.004). On thermal oxide controls, average overnight carbon levels (7.762% ± 2.197, n=5) were also different from levels of week 1 (36.254% ± 0.935, n=5), week 2 (36.165% ± 1.681, n=4) and week 3 (36.35% ± 1.798, n=4) ($P \leq 0.001$ in all cases). Finally, on horse serum thermal oxide samples, differences between overnight carbon levels (56.896% ± 2.403, n=8) and levels of week 1 (37.793% ± 3.086, n=7) week 2 (35.948% ± 1.445, n=9) and week 3 (34.935% ± 0.642, n=6) were statistically significant ($P \leq 0.001$ in all cases). Differences in carbon levels between week 1, week 2 and week 3 in controls and horse serum samples of parylene and thermal oxide were never statistically significant. There results are summarised in figure 5.25.

Overnight levels of oxygen on parylene controls (7.720% ± 0.388, n=5) were significantly different from levels of week 1 (18.150% ± 0.917, n=5), week 2 (17.696% ± 0.511, n=5) and

week 3 (17.295% ± 0.493, n=4) ($P \leq 0.001$ in all cases). Similarly, on horse serum parylene samples, overnight oxygen levels (19.003% ± 0.410, n=7) were statistically different from average oxygen levels of week 1 (16.310% ± 0.586, n=8), week 2 (15.982% ± 0.394, n=10) and week 3 (16.817% ± 0.691, n=6) ($P=0.002$, $P \leq 0.001$ and $P=0.029$ respectively). On thermal oxide controls, average overnight oxygen levels (68.442% ± 1.978, n=5) were also different from levels of week 1 (42.062% ± 0.94, n=5), week 2 (42.150% ± 1.267, n=4) and week 3 (41.913% ± 1.304, n=4) ($P \leq 0.001$ in all cases). Finally, on horse serum thermal oxide samples, differences between overnight oxygen levels (25.541% ± 1.613, n=8) and levels of week 1 (41.164% ± 2.585, n=7) week 2 (42.808% ± 1.139, n=9) and week 3 (43.667% ± 0.498, n=6) were statistically significant ($P \leq 0.001$ in all cases). Differences in oxygen levels between week 1, week 2 and week 3 in controls and horse serum samples of parylene and thermal oxide were never statistically significant. There results are summarised in figure 5.26.

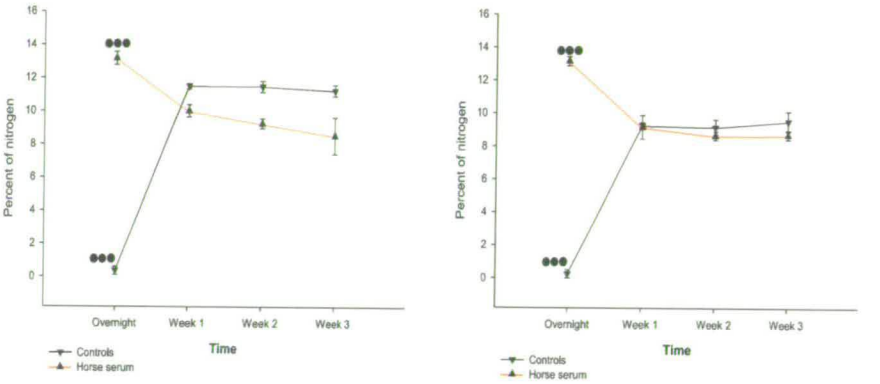

(a) Parylene (b) Thermal oxide

Figure 5.23: *Nitrogen on parylene and thermal oxide that have been treated with horse serum over the course of 3 weeks. The controls were not incubated in horse serum overnight but were incubated, like the horse serum samples, in Neurobasal-A culture media from 1 to 3 weeks. The controls reveal the effect of the culture media on the average nitrogen levels on the surface. Error bars represent SEMs.*

5.3.6 Protein Analysis Using Electrophoresis

In order to investigate what proteins adhered to the parylene and thermal oxide surfaces, blank substrates were incubated in horse serum overnight and rinsed with SDS as described in section 5.2.3. The eluant was then subjected to electrophoresis and the gel was stained. Both procedures are explained in sections 5.2.5 and 5.2.5 respectively.

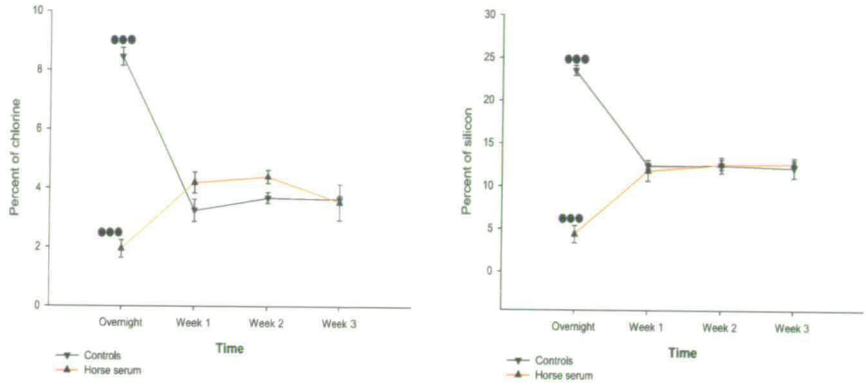

(a) Parylene (b) Thermal oxide

Figure 5.24: *Chlorine on parylene and silicon on thermal oxide surfaces that have been treated with horse serum over the course of 3 weeks. The controls were not incubated in horse serum overnight but were incubated, like the horse serum samples, in Neurobasal-A culture media from 1 to 3 weeks. The controls reveal the effect of the culture media on the average chlorine and silicon levels on the surface. The statistical significance of the difference between overnight and week 3 levels of chlorine on horse serum parylene is only 1 star (P=0.011). Error bars represent SEMs.*

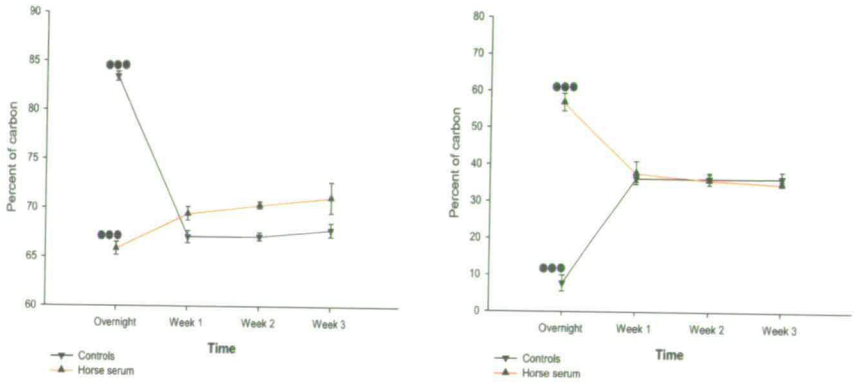

(a) Parylene (b) Thermal oxide

Figure 5.25: *Carbon on parylene and thermal oxide that have been treated with horse serum over the course of 3 weeks. The controls were not incubated in horse serum overnight but were incubated, like the horse serum samples, in Neurobasal-A culture media from 1 to 3 weeks. The controls reveal the effect of the culture media on the average carbon levels on the surface. The statistical significance of the difference between overnight and week 1 levels of carbon on horse serum parylene is only 2 stars (P=0.004). Error bars represent SEMs.*

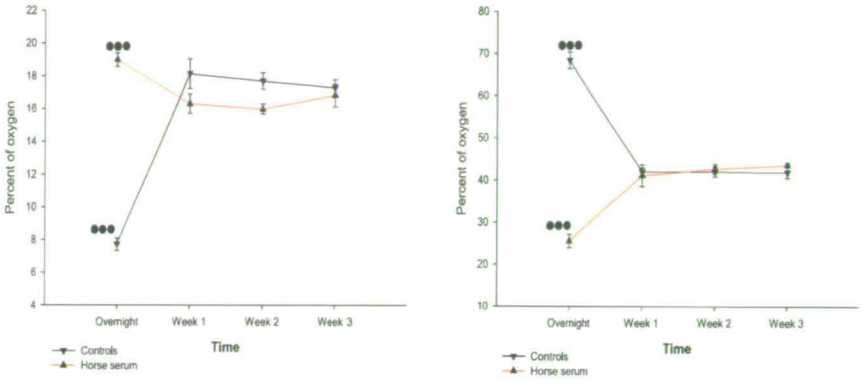

(a) Parylene (b) Thermal oxide

Figure 5.26: *Oxygen on parylene and thermal oxide that have been treated with horse serum over the course of 3 weeks. The controls were not incubated in horse serum overnight but were incubated, like the horse serum samples, in Neurobasal-A culture media from 1 to 3 weeks. The controls reveal the effect of the culture media on the average oxygen levels on the surface. The statistical significance of the difference between overnight and week 1 and overnight and week 3 levels of oxygen on horse serum parylene is only 2 stars (P=0.002) and 1 star (P=0.029) respectively. Error bars represent SEMs.*

Two NuPAGE 4-12% Bis-Tris Gels focusing on the 6-200kDa band are depicted in figures 5.27 and 5.28. As it was difficult to distinguish whether fibronectin was present, since the fibronectin band is high up in the lane and beyond the capabilities of these gels, two NuPAGE 3-8% Tris-Acetate Gels were also used. The 3-8% Tris-Acetate Gels focus on the 50-400kDa band and can be seen in figures 5.29 and 5.30. An image with the apparent molecular weights of the SeeBlue Plus2 Pre-Stained Standard marker is given in figure 5.31.

For the gel of figure 5.27 going from left to right the lanes are: marker, parylene in horse serum, gap, parylene in foetal bovine serum, gap, TO in horse serum, gap, TO in foetal bovine serum, gap, vitronectin, fibronectin and marker. The amount of vitronectin loaded onto the lane was 250ng while the amount of fibronectin was 150ng.

For the gel of figure 5.28 going from left to right the lanes are: marker, parylene in horse serum, gap, TO in horse serum, gap, parylene in foetal bovine serum, gap, TO in foetal bovine serum, gap, fibronectin, vitronectin and bovine serum albumin. 60ng of vitronectin, fibronectin and BSA were loaded onto the lanes.

For the gel of figure 5.29 going from left to right the lanes are: marker, vitronectin, gap, fi-

bronectin, gap, gap, TO in horse serum, gap, gap, parylene in horse serum, gap and bovine serum albumin. 100ng of vitronectin and fibronectin and 30ng of BSA were loaded onto the lanes.

Finally, in figure 5.30 going from left to right the lanes are: marker, fibronectin, gap, vitronectin, gap, gap, parylene in horse serum, gap, gap, TO in horse serum, gap and bovine serum albumin. The amount of fibronectin and vitronectin loaded onto the lanes was 150ng while the amount of BSA was 80ng.

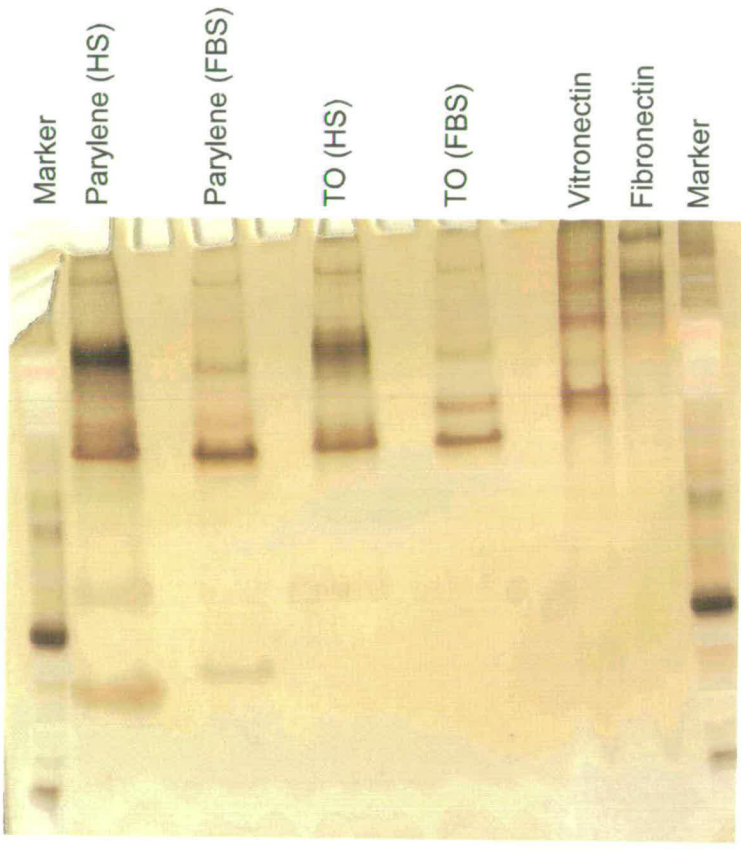

Figure 5.27: *A NuPAGE 4-12% Bis-Tris Gel: this gel focuses on the 6-200kDa region. Notice the presence of two bands in both parylene lanes (HS and FBS, lanes 2 and 4) at approximately the 14kDa region. These bands are not present in the thermal oxide lanes. Also the horse serum lanes (parylene and thermal oxide) are darker, and thus loaded with more protein, than the foetal bovine serum lanes.*

A close inspection of the figures will reveal the following important observations.

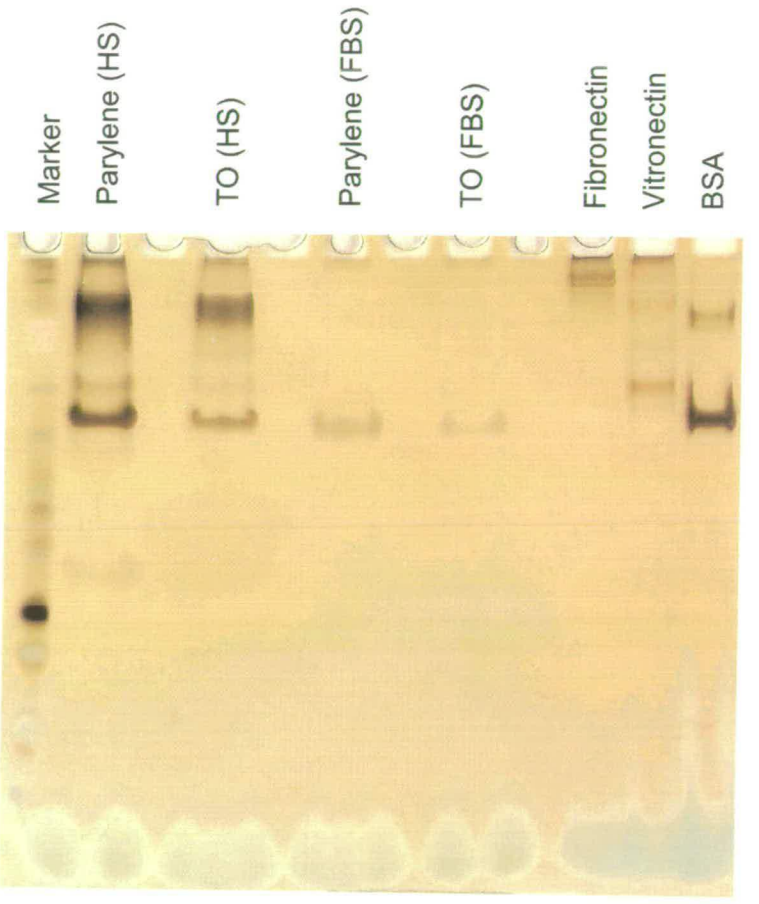

Figure 5.28: *A NuPAGE 4-12% Bis-Tris Gel: this gel focuses on the 6-200kDa region. Notice how in both horse and foetal bovine serum cases, parylene are darker than the thermal oxide lanes. Also, the BSA band is aligned with both parylene and thermal oxide bands. The same is true for the vitronectin band.*

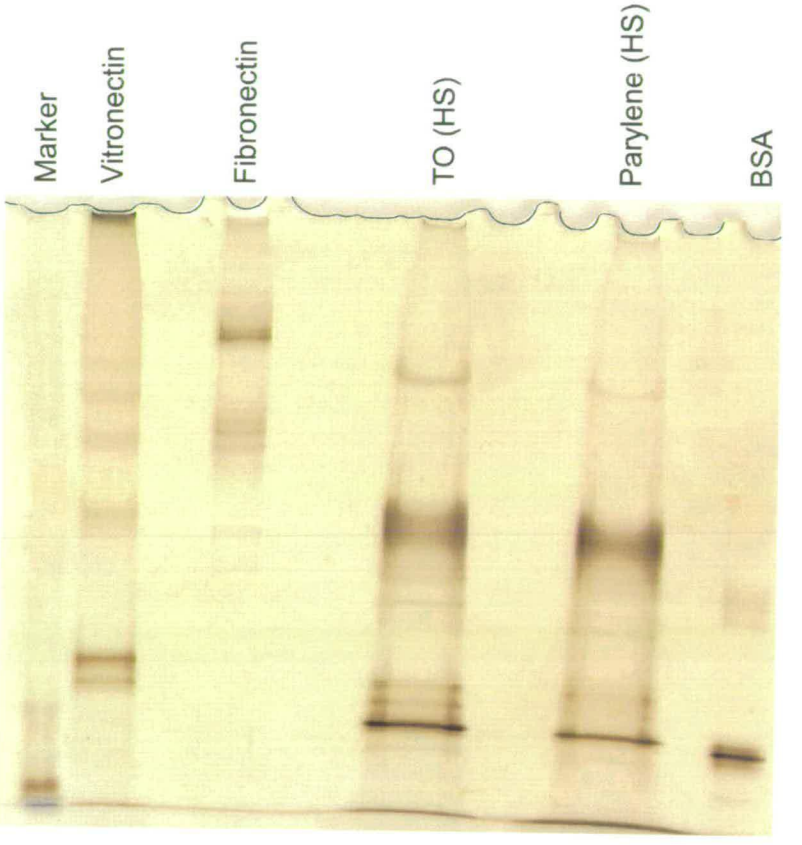

Figure 5.29: *A NuPAGE 3-8% Tris-Acetate Gel: this gel focuses on the 50-400kDa region. The BSA band is aligned with both parylene and thermal oxide bands. In contrast, none of the fibronectin bands are aligned to any bands in the parylene and thermal oxide lanes. The multiple lower fibronectin bands (in the 200-300kDa range) are probably due to its two 250kDa subunits. In the vitronectin lane there are bands that align to bands in the parylene and thermal oxide lanes however, it is difficult to distinguish how exact this alignment is.*

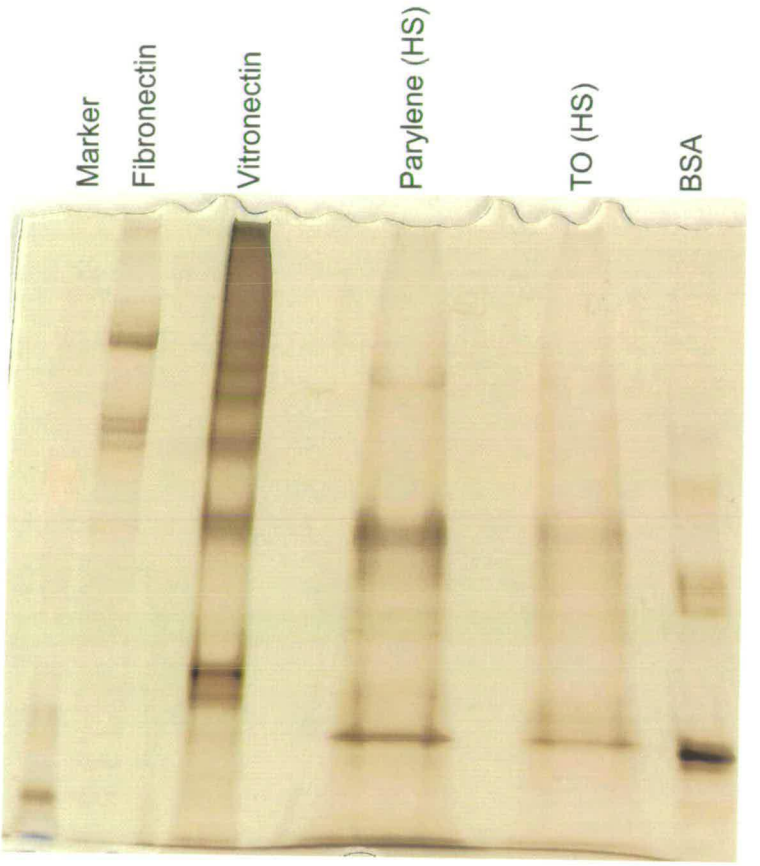

Figure 5.30: *A NuPAGE 3-8% Tris-Acetate Gel: this gel focuses on the 50-400kDa region. Notice how again the parylene lane is darker (loaded with more protein) than the thermal oxide lane. The BSA band is aligned to both parylene and thermal oxide bands, while fibronectin is not. In the vitronectin lane there are bands that align to bands in the parylene and thermal oxide lane.*

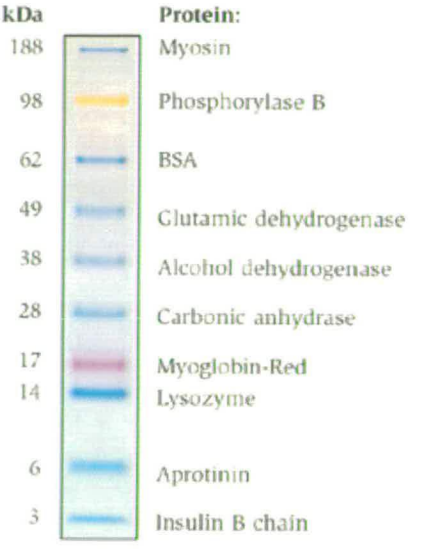

Figure 5.31: *"Apparent molecular weights of SeeBlue Plus2 Pre-Stained Standard on a NuPAGE 4-12% Bis-Tris Gel." Image and text taken from Invitrogen site.*

- the lanes of samples treated with foetal bovine serum are always fainter than lanes of samples treated with horse serum.
- the lanes of parylene substrates are similar or darker than thermal oxide substrate lanes
- parylene and thermal oxide lanes are identical with the exception of one low band in the parylene lane, approximately at 14kDa (figure 5.27)
- BSA bands are found in both parylene and thermal oxide samples
- fibronectin bands are not found in either parylene or thermal oxide
- vitronectin bands can be found in both parylene and thermal oxide lanes

The significance of these observations is explained in the discussion.

5.3.7 Cultures on Patterns Incubated in Bovine Serum Albumin

As BSA was detected on both parylene and thermal oxide surfaces, a culture experiment was performed in order to investigate whether albumin was responsible for glia and neuronal patterning in our technique. Six different patterns were incubated overnight in BSA (concentration

44mg/ml). The plating cell density was 67 cells/mm^2. Figures 5.32(a) and 5.32(b) are two representative examples of the cultures.

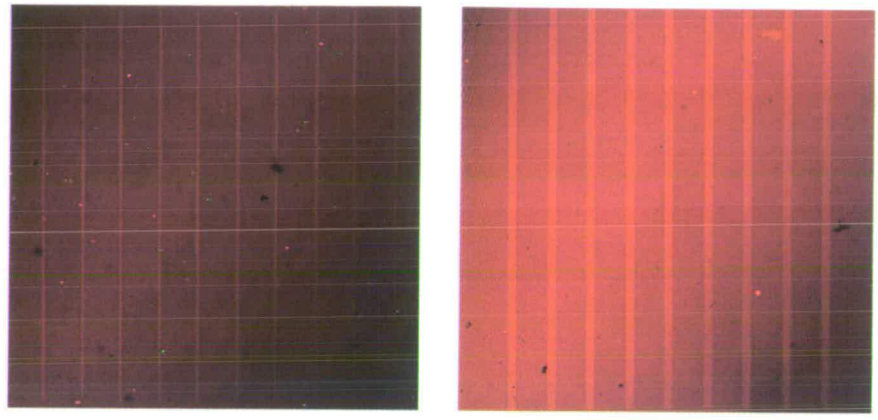

(a) 5% parylene stripes, x5 magnification

(b) 20% parylene stripes, x5 magnification

Figure 5.32: *Two representative examples of a neuronal and glia culture on patterns that were incubated in bovine serum albumin overnight. Both patterns are empty of cells while the green and red dot-like stains on the background are stained debris and false positives.*

As we can see both sample patterns are empty of cells. The minor green and red stains in figure 5.32(a) are probably due to cellular debris or background staining.

5.4 Discussion

5.4.1 Involvement of Proteins in our Patterning Method

As mentioned previously, our first hypothesis as to why glia and neurons are attracted to parylene and not thermal oxide serum treated surfaces, was that proteins adhere exclusively to parylene during the horse serum incubation step. Since proteins (fibrous and globular) are one of the main contents of serum, and their role in cell adhesion has been recurrently established in literature [118, 119], it was reasonable to assume they were contributing to our patterning method as well. The presence of proteins on the surfaces can easily be detected via the existence of nitrogen, which is present in the peptide bond.

The XPS spectra of figures 5.1 and 5.2 clearly reveal the presence of nitrogen and hence proteins, on the surfaces that have been treated with horse serum. It is also evident, that nitrogen is present on both parylene and thermal oxide substrates that have been incubated in horse serum.

Figures 5.5 and 5.7 suggest that serum incubation of the parylene leads to a coating of the surface with a layer of proteins, as levels of chlorine and carbon drop significantly after serum application. The same is true for the thermal oxide as figures 5.6 and 5.8 illustrate a statistically significant decrease in the thermal oxide silicon and oxygen levels respectively, when the samples are treated with horse serum.

Although the involvement of proteins in cell patterning cannot be conclusively proven via the presence of nitrogen alone, the masking effect of serum on certain surface elements (such as chlorine and silicon) is a very good indication that proteins are present. In addition, the carbon (C_{1s}) spectra of figure 5.3 exhibits characteristic contributions of adsorbed protein as in Dewez's case [120]. Furthermore the gels of images 5.27, 5.28, 5.29 and 5.30 in section 5.3.6 strongly indicate the existence of bovine serum albumin on the surfaces, as well as vitronectin, although the first cannot be responsible for cell patterning. Between the nitrogen and carbon spectra, the masking effect of chlorine and silicon and the protein gels of section 5.3.6 there can be little doubt that proteins are involved in our patterning technique.

The presence of nitrogen on both surface types dismisses our initial theory, leaving the three options mentioned in the introduction:

a a higher quantity of proteins binds to parylene thus attracting the cells

b specific proteins that cells are attracted to are bound only to parylene

c proteins bind in different conformations to parylene and thermal oxide and are biologically active only on parylene

With regards to the amount of proteins on the two surface types, the lack of statistical significance between nitrogen levels of horse serum treated parylene and thermal oxide (see also figure 5.4) implies that similar quantities of proteins adsorb to both substrates. However, as the XPS analysis is limited to the top 10nm of the examined surface [121], it is perilous to dismiss the hypothesis that different quantities of proteins bind to the two substrates, based solely on this result.

The XPS analysis did not reveal any differences in the elemental composition of the two substrates beyond those we would normally expect. Carbon and chlorine are both elements that exist in parylene, as are silicon and oxygen in thermal oxide. As such, we cannot conclude whether option b above is true and different proteins adsorb to parylene and SiO_2. What is

more, the images of the gels (5.27, 5.28, 5.29 and 5.30) reveal an almost identical protein composition of the two surfaces. However, in image 5.27 a dark band exclusive to parylene is detectable at the 14kDa range. The nature of this band is yet unknown to us. A family of binding proteins that are known to be involved in cell proliferation, chemotaxis and migration are the Insulin-like Growth Factor (IGF) binding proteins [122]. Since, the molecular weight of their subunits can be as low as 18kDa it is possible that they are somehow involved in the cell patterning process. However, a western blot experiment is needed to obtain a conclusive result.

The correlation of the conformation of proteins and their biological function is well established in literature [115, 123, 124]. It is possible that the same proteins bind differently to parylene and thermal oxide. This could render the SiO_2 bound proteins biologically inert thus leaving parylene bound proteins to attract the glia and neurons. It is unlikely that this can be proven from the XPS results. However, the protein de-adsorption experiment in section 5.3.3 reveals that whereas protein is completely rinsed off the SiO_2 surface with SDS, a significant protein residue remains on the parylene. This may be due to a different binding mechanism of the proteins to parylene and SiO_2 surfaces.

5.4.2 Nitrogen Levels Over the Course of Three Weeks

The experiment of section 4.3.4 revealed that glial and neuronal patterning was lost after the first week of incubation. Based on the results of experiments in sections 4.3.5 and 5.3.5 it was supported that this loss of patterning was due to glia division and not due to natural detachment of the proteins from the surface. Indeed, average levels of nitrogen between weeks 1 through 3 are not significantly different to each other (figure 5.23) indicating the preservation of the protein load on the surfaces throughout this period. In contrast, overnight levels of nitrogen are statistically different from nitrogen levels in weeks 1, 2 and 3 in both parylene and TO which implies the elution of some protein into the media during the first week. However, if this limited loss of protein influenced patterning we should be noticing its effects from the first week and not at the end of weeks 2 and 3 only. The levels of the rest of the elements (figures 5.24 through 5.26) are in agreement with the nitrogen trend. For example, small quantities of chlorine (figure 5.24(a)) and carbon (figure 5.25(a)) are revealed on parylene at week 1 and remain constant throughout the following 2 weeks, whereas oxygen (figure 5.26(a)) drops at week 1 and remains at the same levels until week 3. The same is true for silicon (figure 5.24(b)), carbon on TO (figure 5.25(b)) and oxygen on TO (figure 5.26(b)).

It is of particular interest that nitrogen is present on both parylene and TO controls, which were incubated only in Neurobasal media. In fact, the levels of nitrogen on parylene controls at weeks 1, 2 and 3 are higher than their respective levels of nitrogen on serum treated parylene. However, patterns of parylene on TO that have not been treated with horse serum and were incubated only in Neurobasal growth media have repeatedly failed to pattern glia and neurons. This indicates the involvement of a specific protein or set of proteins in our patterning method, which exist in the horse serum but not in the Neurobasal growth media.

5.4.3 Piranha Cleaned, Untreated Surfaces

The experiment of section 5.3.2 allows us to establish a baseline of the elements constituting the two surfaces. Figure 5.9 for example, reveals that chlorine, carbon and oxygen are elements which already exist on untreated parylene, whereas silicon, carbon and oxygen are present on untreated TO. The occurrence of carbon on TO is a result of atmospheric contamination and cannot be prevented, while the oxygen on parylene probably emerges due to minor oxidation of the latter. It is also important to point out that nitrogen is not present on either of the untreated surfaces. Therefore, we can be certain that the appearance of nitrogen on parylene and SiO_2 surfaces that have been incubated in horse serum is a consequence of protein adhesion and not a constituent element of the aforementioned substrates.

Figures 5.10 and 5.11 portray the effects of ultraviolet (UV) radiation on the two surfaces. It is evident that no significant differences exist in the elemental composition of either parylene or TO before and after ultraviolet exposure. This result is consistent with the results of section 4.3.6 and our claim in section 4.4.4 that cell patterning in our case is not attributable to oxidation of parylene and the creation of carboxylic and aldehyde groups on the surface. Additionally, image 5.12 illustrates the spectral difference between carbon on parylene that has been radiated under UV and carbon on parylene that has not. A minor peak is noticeable on the spectrum of the parylene that has been radiated. Taking into account Pruden's results on parylene-N and parylene-C photooxidation [103], this could signify the emergence of carboxylic groups (-COOH) on the parylene surface. Moreover, the attenuated decline of ring and chain carbon curve (bell shaped curve) implies the presence of single or double bonds between carbon and oxygen or carbon and nitrogen. In any case, the differences between the two spectra are not as prevalent as in Pruden's case. Besides, the statistical analysis of the elemental levels failed to detect any significant differences attributable to UV, while the culture results clearly indicate

that UV radiation is not assisting in patterning.

5.4.4 The Use of SDS and Protein de-Adsorption

SDS is a common dissociating agent, frequently used to denature proteins that are going to be electrophoresised [125]. It has also been used in the de-adsorption of proteins from polymeric surfaces [126]. As such, we decided to utilise SDS to rinse the protein load off the parylene and thermal oxide. In order to establish whether SDS was successful in encouraging proteins to de-adsorb from the surfaces, we conducted the experiment of section 5.3.3. As previous pilot experiments had already revealed that 1 rinse in SDS was not adequate to elute all the proteins off the parylene, we decided to experiment not only with 1 but with 3 rinses as well.

It is evident from figure 5.13 that SDS fails to rinse the entire protein load off the parylene. In contrast, even one rinse in SDS is enough to elute all the proteins off the thermal oxide. The rest of the elements (figures 5.14 through 5.17) follow a similar trend. For example, whereas average chlorine levels increase after 1 or 3 rinses with SDS (figure 5.14(a)), they never reach the average levels of the control samples that have not been treated with horse serum. On the other hand, silicon on thermal oxide is covered with the application of horse serum and the adsorption of proteins, only to be revealed again fully after 1 or 3 rinses with SDS (figure 5.14(b)). Carbon levels on parylene (figure 5.15(a)) flunctuate similarly to chlorine levels, while oxygen, like silicon, on thermal oxide (figure 5.16(b)) is restored after 1 and 3 SDS rinses.

The emergence of sulphur on parylene (figure 5.17(a)) and on thermal oxide (figure 5.17(b)) after the SDS rinses is of particular interest. The highest level of sulphur is detected on the thermal oxide "no horse serum" control. Since sulphur is not a constituent element of silicon thermal oxide and as it does not appear on pristine, piranha cleaned SiO_2 surfaces (see section 5.3.2), its presence on the TO control and the experimental samples must be due to adhesion of the SDS on the oxide surface. Conversely, SDS did not bind to parylene control but only to experimental samples. This implies that in parylene, unlike thermal oxide, SDS attaches to proteins, which is the expected behaviour of a dissociating solvent.

In conclusion, we can deduce the following from this experiment:

1 We can elute 100% of the proteins adhering to silicon thermal oxide surfaces. As such, any PAGE on the SDS eluant will reveal the full spectrum of proteins on the TO surfaces

2 SDS can rinse proteins off the parylene surfaces however, fails to do so completely, leaving protein and SDS residue behind

3 Because of conclusions 1 and 2, proteins are adhering differently to parylene and thermal oxide. In fact, proteins adhere more strongly on the parylene since SDS cannot dissolve them

4 A solvent which can rinse all the proteins off the parylene surfaces must be found, before we can be sure that none of the proteins on the parylene is absent from our PAGE experiments

5.4.5 Protein de-Adsorption with other Solvents

In search of a solvent which would rinse all proteins off the parylene surface, we decided to experiment with the following four solvents: Sodium Hydroxide (NaOH), Trifluoroacetic acid (TFA), Methanol and Toluene. Both NaOH and TFA, as a base and an acid, have been used before as solvents in the elution of proteins from silicon based materials [127]. Furthermore, TFA is commonly used to separate proteins in column chromatography [128, 129].

In addition, to the acid-base comparison, we wanted to explore the hydrophobic-hydrophilic contrast, as we suspected that the difference in surface energies between the two substrates might have an important role into how the proteins bind to the surface [130]. We chose methanol as a polar (hydrophilic) protic solvent, as it has a high dielectric constant[1] of 33, while toluene with a dielectric constant of 2.4 acted as the non polar (hydrophobic) solvent.

Figures 5.18 through 5.21 depict the effect of the four solvents on the various elements detected on the surfaces. As in previous experiments, nitrogen levels indicate the presence, absence or partial elution of proteins from the surface while the rest of the elements get concealed or exposed depending on the top protein layer. Figure 5.22 illustrates the effects of each solvent in a pairwise comparison between parylene and TO. By comparing the nitrogen levels of the surfaces treated with the solvents to the nitrogen levels of surfaces incubated in horse serum it becomes evident that, as in SDS, NaOH and TFA manage to completely strip the protein away from the TO, while methanol and toluene fail. In parylene, only two solvents, NaOH and TFA, were capable of marginally reducing nitrogen levels, whereas methanol and toluene fail to do so.

[1] an index which measures polarity

The failure of methanol and toluene is not that surprising. The first is very hydrophilic, while the last is extremely hydrophobic. As such, they would dissolve only strongly polar and non-polar compounds respectively. Therefore, their failure to rinse the proteins off the surfaces implies that in both substrates the prevalent surface-protein interactions are neither strongly hydrophilic nor extremely hydrophobic. Perhaps a less polar hydrophilic solvent such as butanol (dielectric constant 18), or a slightly more polar hydrophobic solvent such as ethyl acetate (dielectric constant 6) might be more successful.

Although the acidic (TFA) and basic (NaOH) solvents were more successful than the other two, they still did not manage to de-adsorb the protein from the parylene surface. What is more, only NaOH reduced nitrogen levels in both parylene and thermal oxide to an extent similar to that of SDS (see also figure 5.13). TFA left more protein residue than SDS, on both parylene and TO. It is somewhat intriguing that both SDS and NaOH consist of Na (sodium) connected to oxygen via an ionic bond. Whether this bares any significance in their ability to dissociate proteins from the parylene better than other solvents is unknown, however it is certainly an interesting research avenue to explore as it might contribute to the comprehension of the protein-surface bonds in our patterning technique.

Nevertheless, based on the above results we can deduce that with the exception of NaOH, SDS has been the superior solvent. We believe that the hydrophobic chain of 12 carbon atoms allows SDS to out-compete some hydrophobic protein-protein interactions, while its hydrophilic sulfate group permits it to be miscible in water. However, the hydrophobic protein-surface interactions in parylene must be too potent for SDS to overcome.

5.4.6 Analysis of the Proteins Using Electrophoresis

The experiment of section 5.3.6 was conducted in order to investigate the range of proteins present on blank parylene and thermal oxide surfaces that had been treated with serum. It was expected that a comparison of the proteins on the two surfaces in the form of an acrylamide gel would reveal whether different proteins bind to parylene and thermal oxide. Additionally, since equal amounts of eluant from each surface were loaded into the gel, the intensity of the staining of each lane would indicate whether the quantity of proteins on each surface is similar or more protein is adsorbing onto one of the two substrates.

A careful examination of the gels in figures 5.27, 5.28, 5.29 and 5.30 will reveal that in all

four gels parylene lanes are stained to a similar if not greater extent than thermal oxide lanes. However, the results of the experiment in section 5.3.3 indicated that SDS does not rinse all the protein off the parylene. This fraction of the parylene bound proteins, that is de-adsorbed via SDS, appears equal to, if not greater than, the full amount of proteins bound on the thermal oxide surfaces. Therefore, we can conclude that quantitatively more protein is present on the parylene than on thermal oxide.

Qualitatively, the parylene and thermal oxide lanes appear very similar, as the protein bands that are present in the former are also present in the latter. However, in figure 5.27 an additional band can be seen on both horse and foetal bovine serum parylene lanes (lanes 2 and 4). It is located near the lysozyme band at the 14kDa region. Whether this protein, which is present only on parylene, contributes to glia and neuronal patterning is unknown. This band could be an indication that insulin-like growth factor (IGF) binding proteins are involved, as mentioned previously 5.4.1. If this is the case, then that could explain the preferential adhesion of glia and neurons to the parylene.

Fibronectin and vitronectin are two glycoproteins commonly found in serum. Reasons as to why fibronectin is probably not involved in our patterning method have already been discussed in section 4.4.5. Additionally, in the gels of figures 5.29 and 5.30 it is clearly evident that none of the fibronectin bands can be aligned to the bands present in the parylene and thermal oxide lanes. Therefore, fibronectin is absent from the SDS eluant of both parylene and thermal oxide surfaces, which supports the argument made earlier against this protein's involvement in our patterning technique. However, due to the outcome of the SDS protein de-adsorption experiment (section 5.3.3) the minor possibility remains that fibronectin is present on the parylene surface but cannot be rinsed with SDS. Nevertheless, it is unlikely that fibronectin would behave in such a way, as previous studies on various surfaces have showed that after elution in SDS, only a small fraction of the initially adsorbed fibronectin remained on the surfaces [131]. In fact most of the other proteins examined, and especially vitronectin, exhibited higher adsorption strength than fibronectin.

On the other hand, vitronectin is present on both parylene and thermal oxide as indicated by the four gels in figures 5.27, 5.28, 5.29 and 5.30. However, the bands on the thermal oxide appear fainter signifying a smaller quantity of vitronectin bound to that surface. As mentioned previously, vitronectin is a highly competitive binding protein present in serum. Its integrin-mediated role in astrocytic migration and attachment has been substantiated and explored in

literature [132, 133]. What is more, a comparison between fibrinogen, fibronectin and vitronectin revealed that vitronectin not only adheres to biosurfaces more strongly than the other two, but as the serum concentration or exposure of the polymer substrates to serum increases, vitronectin becomes more competitive and resistant to displacement by other proteins [134]. Additionally, Fath has established that in the presence of serum, cell adhesion involves primarily vitronectin and its integrin [135], while Steele shows that serum Vitronectin adsorbs to surfaces and prevails over other serum components [136]. Therefore, it is very likely that vitronectin, present on both parylene and thermal oxide, is playing a pivotal role in our patterning technique. The preference of glia and neurons to parylene and not the thermal oxide could be attributed to either the higher quantity of vitronectin present on the parylene or the loss of vitronectin's binding ability on the thermal oxide due to a denaturation effect [137].

It is also clear from both figures (5.27, 5.28, 5.29 and 5.30) that BSA is present on both parylene and SiO_2. However, as shown in figure 5.32 in section 5.3.7 BSA is not cell adhesive but cell repellent. In the experiment of section 5.3.7, all patterns were empty of cells as glia and neurons were probably not able to attach onto the surfaces due to the presence of albumin. As such albumin cannot be the protein responsible for patterning. Nevertheless, it is possible that it contributes to patterning by protecting other proteins, especially vitronectin, from denaturation [106].

Finally, a comparison between the horse serum and foetal bovine serum treated lanes in the gels of figures 5.27 and 5.28 reveals that the lanes corresponding to the former are darker than the ones corresponding to the latter. This indicates that more proteins are deposited on the surfaces during horse serum incubation, which could be due to a limited quantity of proteins in the foetal bovine serum. Despite its cause, this result indicates that, at high serum concentrations, patterning is not linearly correlated to the amount of proteins on the surface, which means that our current protocol is operating in the saturated end of the spectrum.

5.5 Conclusions

Experiments in this chapter focused on examining the two substrates, parylene and thermal oxide, that are utilised in our patterning technique. The use of XPS was employed, in order to investigate the elemental composition of pristine and horse serum treated surfaces, while material bound to the substrates was eluted and analysed with PAGE. Results from XPS experi-

ments clearly indicate the presence of nitrogen on both parylene and thermal oxide horse serum treated samples. Since nitrogen is not a constituent element of either parylene or thermal oxide, its occurrence can only be attributed to proteins present on the two aforementioned surfaces. This result is also verified and supported by the PAGE experiments.

The levels of nitrogen on parylene and thermal oxide horse serum treated surfaces were monitored over the course of three weeks. No significant decrease was detected, which indicates that the protein load remains constant on the two substrates over extended periods of time. This supports our claim in section 4.4.3 that loss of patterning after the first week is due to glia division and not due to protein de-adsorption.

We also reaffirmed our hypothesis in section 4.4.4 that UV radiation of the parylene during sterilisation can not be responsible for cell patterning. XPS experiments illustrate that differences in the elemental composition of UV radiated and control samples are insignificant, in both parylene and TO cases.

The protein dissociating ability of SDS and four other solvents was scrutinised. It was revealed that SDS and NaOH can rinse proteins off TO substrates completely while leaving protein residue on parylene surfaces. This discrepancy suggests that proteins bind differently to the two substrates and was also employed in conjunction with data from the protein gels to prove that more protein is adhering on the parylene.

Finally, the PAGE experiments reveal that BSA and vitronectin are present on parylene and TO, while fibronectin is absent from both surfaces. This result confirms our claim in section 4.4.5 that fibronectin is not involved in our patterning method. As we demonstrated that BSA is cell repellent and cannot induce cell patterning on its own, vitronectin remains as the most probable adhesive protein, responsible for glial and neuronal guidance in our technique. However, before drawing a definite conclusion, the presence of the additional band at the 14kDa range in the parylene lanes and the elution of the total protein load from the parylene surfaces have to be addressed.

Chapter 6

Summary, Conclusions and Future Work

6.1 Summary

This study aimed to produce a novel glial and neuronal patterning method, which would be compatible with an existing planar patch-clamp device and MEA technology. Due to the parameters set out by the planar patch-clamp project, photolithographic patterning techniques where adopted. Experimentation with boron doped SiO_2 tracks on a photoresist and subsequently on a plain SiO_2 background were not successful. We suspect that the contrast in cell adhesiveness between boron doped SiO_2 and photoresist, as well as, boron doped SiO_2 and plain SiO_2 is simply not potent enough to overcome the cell-cell attraction forces and induce cell patterning.

Parylene-C, a polymer of xylylene, was selected as an alternative cell repellent material due to its extreme hydrophobic nature. Unexpectedly, a culture of hippocampal neurons and glia adhered to the cell inhibiting parylene background and avoided the cell permissive boron doped SiO_2 grid pattern. This result encouraged us to re-evaluate the role of parylene and use it as a cell attractive material. Subsequent cultures of hippocampal neurons and glia proved that parylene patterns on plain SiO_2 backgrounds can induce high quality patterning, after a simple dip-and-rinse activation of the patterns in horse serum.

A variety of experiments was performed to optimise the parylene based patterning method. It was discovered that muliple aspects of this patterning technique, such as pattern quality and longevity, consistency and protocol speed can be optimised. Unlike other cases, where parylene is modified by UV radiation to become more adhesive to proteins, parylene in our method remains largely unaffected by the small doses of UV it is exposed to. In addition, our parylene patterns are storable and they do not degrade over time, as numerous successful patterning experiments with stored substrates have revealed.

Surface analysis experiments were also executed, in order to investigate the underlying mechanisms of cell patterning in our method. We are confident that different quantities of proteins adhere to parylene and thermal oxide. The larger amount of proteins present on the parylene is a possible cause of neuronal and glial guidance in our cultures. In addition, we believe that vitronectin is playing a crucial role in the preference of neurons and glia towards parylene.

6.2 Conclusions

The aim of this project as presented on the first chapter is:

Develop the simplest possible photolithographic technique for patterning neurons and glia, that can be integrated with silicon microchip/MEMs technology, MEAs and planar patch-clamp structures.

To a large extent this goal has been achieved. The patterning method proposed in this thesis utilises photolithography and is fully compatible with microfabrication techniques and cleanroom facilities. Furthermore, it is simple and easier than all existing photolithographic patterning methods as it entails fewer steps. Finally, our patterning scheme is compatible with MEA technology.

Nevertheless, the use of horse serum brings into question the compatibility of our patterning technique with the planar patch-clamp device, as it is commonly accepted that the presence of proteins hinders seal formation. This issue needs to be addressed before this method is employed in conjunction with the planar patch-clamp device.

Due to the involvement of organic molecules, such as proteins, our patterning method can also be classified as a Selective Molecular Assembly Patterning-like technique. Nonetheless, our patterning method is superior to the existing SMAP schemes for the following reasons:

- one fewer dip-and-rinse process is required
- there is no likelihood of disassembling previously assembled molecules as our technique does not involve a second dip-and-rinse process
- no gold (unusable in a standard cleanroom) is utilised

- parylene is a cheap and biocompatible material
- parylene deposition is conducted at room temperatures

Compared to most other established patterning techniques our method produces patterns of higher resolution and quality. In addition, it is suitable for mass manufacturing, due to the low fabrication costs and can be commercially exploited.

6.3 Future Work

Early on in this work the following interesting question was raised:

Do the spatial specifications of the pattern affect in any way the quality of cell patterning?

This issue has been addressed to an extent in sections 3.4.2 and 4.4.8. Parylene stripes of widths ranging from 10μm to 100μm generate cell patterns of equal quality. However, the question still remains as to whether different pattern geometries will perform equally well under our proposed patterning technique. Future work should investigate the capacity of various parylene schemas on a plain SiO_2 background to induce glial and neuronal patterning. Example geometries include square and hexagonal grids. The cell patterning quality of grid patterns and parylene stripes can then be contrasted, in order to arrive at a general conclusion with regards to the effect of the parylene schema on cell guidance.

The proposed patterning technique can be optimised further. The activation time of the parylene patterns has been reduced to 3 hours from a full day. However, additional experimentation can abbreviate this time even further. Moreover, future research can aim towards the extension of the cell pattern stability. The inclusion of Ara-C in the culture media will prohibit glia division and will assist in the longevity of the patterned neuronal networks.

The surface analysis experiments in this project strongly suggest the involvement of proteins in our patterning method, while protein electrophoresis indicates the absence of fibronectin from the surfaces. Further work can isolate the protein or proteins responsible for patterning in our case. This can be accomplished by the activation of parylene patterns in horse serum that has been sequentially depleted of certain adhesive proteins, such as vitronectin and fibronectin, until our method fails to pattern cells. This work has already provided a useful lead in this direction as the presence of vitronectin on the two surfaces has been proven. Future work can

prove the direct involvement of vitronectin in cell guidance and examine whether its quantity or its conformation is more important in inducing cell patterning. The identification of the key factors in our patterning method will allow us to eschew the use of horse serum and its complications in cell cultures. Moreover, the use of a single or a limited number of proteins could perhaps ameliorate the problems with seal formation, that emerge through the use of serum thus, allowing us to use our technique in conjunction with the planar patch-clamp device.

Finally, our method may be used in future neurophysiological studies that record activity in structured neuronal networks. The effect of the network pattern on neuronal activity, survivability and morphology can be examined. Alternatively, the extension of our patterning method to other types of cells, such as cardiac and stem cells would be a worthwhile achievement. In particular, if stem cells can be patterned under our regime, they could later be induced to differentiate to specific cells, allowing researchers great flexibility in fields such as tissue engineering and regeneration.

Appendix A
Protocol Details and Parylene Specifications

A.1 Protocol Details

Papain Stock Solution

	Final Concentration	12.45ml
Papain	20 units/ml	25mg
L-cysteine	1mM	6.06mg
EDTA	0.5mM	9.31mg

Table A.1: *Papain stock solution made in EBSS. Papain was purchased from Sigma-Aldrich cat. no. 7462*

DNASE Stock Solution

	Final Concentration	7.5ml
DNASE-I	2000 units/ml	15,000 units

Table A.2: *DNASE stock solution made in EBSS. DNASE-I was purchased from Worthington Labs*

Nycoprep Gradients and Low Concentration BSA/Ovomucoid Solution

	Final Concentration	35ml of EBSS
Bovine Serum Albumin 96%	20mg/ml	700mg
Ovomucoid (papain inhibitor)	20mg/ml	700mg

Table A.3: *High concentration BSA/Ovomucoid solution. BSA purchased from Sigma cat. no. A4503, Ovomucoid purchased from Sigma cat. no. 93621*

Dilute remaining high concentration BSA/Ovomucoid solution by 1:10 to obtain low concentration BSA/Ovomucoid solution. The pH of the Nycopreps and the low concentration BSA/Ovomucoid solution is adjusted by the addtion of NaOH.

% Nycoprep	High BSA Ovomucoid	Nycoprep
F4 or 35%	4.76ml	10.24ml
F3 or 25%	7.69ml	7.31ml
F2 or 20%	9.15ml	5.85ml
F1 or 15%	10.61ml	4.39ml

Table A.4: *Nycoprep gradients.*

bFGF Stock Solution

Reconstitute 10μg basic Fibroblast Growth Factor in 100μl of 10mM Tris, pH 7.6 and 0.1% BSA, to obtain a stock solution of 0.1mg/ml of bFGF.

Neurobasal-A Growth Media

	Final Concentration	100ml
Neurobasal-A	(solvent)	100ml
L-glutamine (100x)	0.5mM	0.25ml
B-27 supplement (50x)	1ml/50ml	2ml
Penicillin-streptomycin	125units/ml	1.25ml
bFGF	10ng/ml	10μl

Table A.5: *Neurobasal-A growth media.*

Tris Buffer Solution

	Concentration	1 litre
Tris-HCl, pH=8.0	10mM	1.418g
NaCl	150mM	8.016g

Table A.6: *Tris buffer solution*

Triton-X100 Permeation Solution

Add 1ml of Triton-X100 to 500ml of Tris buffer solution.

Donkey Serum Solution

Add 1.2ml of donkey serum to 22.8ml of Triton-X100 permeation solution.

Primary Antibody Solution

Add 2μl anti-β-tubulin (dilution 1:500) and 20μl anti-GFAP (dilution 1:50) to 978μl of donkey serum solution.

Secondary Antibody Solution

Add 2μl anti-mouse 594 Alexa Fluor^{TM} (dilution 1:500) and 20μl anti-goat 488 Alexa Fluor^{TM} (dilution 1:50) to 978μl of donkey serum solution.

TO-PRO 3 Antibody Solution

Add 0.2μl TO-PRO 3 (dilution 1:5000) to 1ml of Tris buffered saline solution.

Mowoil Mounting Agent

1	Add 2.4g Poly Vinyl Alcohol to 6g (or 4.8ml) of Glycerol in 50ml conical flask
2	Stir with pipette to mix
3	Add 12ml of distilled water and leave overnight at room temperature
4	Add 12ml 0.2M Tris pH=8.5 (26.28mg/ml) solution
5	Heat to 50°C for 2 hours while stirring gently
6	Centrifuge at 2000rpm for 15 minutes
7	Add 0.72g or (2.5%) DABCO Sigma Antifade
8	Aliquot and store at -20°C

Table A.7: *Mowoil mounting agent*

A.2 Parylene Specifications

Properties	Parylene N	Parylene C	Parylene D
Typical Physical & Mechanical Properties			
Tensile strength, psi	65,000	10,000	11,000
Tensile strength, MPa	45	69	76
Yield strength, psi	6,300	8,000	9,000
Yield strength, MPa	2,400	3,200	2,800
Elongation at break, %	40	200	10
Density, g/cm^3	1.110	1.289	1.418
Coefficient of friction: static	0.25	0.29	0.33
Coefficient of friction: dynamic	0.25	0.29	0.31
Water absorption, % (24 hr)	0.01 (0.019")	0.06 (0.029")	
Index of refraction, $\mathbf{n}_D^{23}$	1.661	1.639	1.669
Typical Electrical Properties			
Dielectric strength, short time (Volts/mil at 1 mil)	7,000	6,800	5,500
Volume resistivity, 23°C, 50% RH (Ohm-cm)	1x1017	6x1016	2x1016
Surface resistivity, 23°C, 50% RH (Ohm-cm)	1015	1015	5x1016
Dielectric constant: 60 Hz	2.65	3.15	2.84
Dielectric constant: 1,000 Hz	2.65	3.10	2.82
Dielectric constant: 1,000,000 Hz	2.65	2.95	2.80
Dissipation factor: 60Hz	0.0002	0.020	0.004
Dissipation factor: 1,000Hz	0.0002	0.019	0.003
Dissipation factor: 1,000,000Hz	0.0006	0.013	0.002
Gas Permeability			
Nitrogen	7.7	0.95	4.5
Oxygen	30	7.1	32
Carbon dioxide	214	7.7	13
Hydrogen sulfide	795	13	1.45
Sulphur dioxide	1,890	11	4.75
Chlorine	74	0.35	0.55
Moisture Vapor Transmission	1.5	0.14	0.25
* cm3-mil/100 in2-24hr-atm (23°C)			
** g-mil/100 in2-24hr, 37°C, 90% RH 1 mil = 1/1000 in = 25.4 microns			
Typical Thermal Properties	7.7	0.95	4.5
Metling Temperature (°C)	410	290	380
Linear Coefficient of expansion (10-5 °C)	6.9	3.5	
Thermal Conductivity 10-4 (cal/sec)/(cm^2 °C/cm)	3	2	

Table A.8: *Typical physical, mechanical and electrical parylene specifications (adjusted from: www.vp-scientific.com/parylene_properties.htm).*

References

[1] M. F. Bear, B. W. Connors, and M. A. Paradiso, *Neuroscience Exploring the Brain.* Lippincott Williams & Wilkins, 2001.

[2] P. Baker, T. Shaw, and A. Hodgkin, "Replacement of axoplasm of giant nerve fibres with artificial solutions," *Journal of Physiology-London*, vol. 164 (2), p. 330, 1962.

[3] A. Hodgkin, A. Huxley, and B. Katz, "Ionic currents underlying activity in the giant axon of the squid," *Archives des Sciences Physiologiques*, vol. 3 (2), pp. 129–150, 1949.

[4] A. Hodgkin, A. Huxley, and B. Katz, "Measurement of current-voltage relations in the membrane of the giant axon of loligo," *Journal of Physiology-London*, vol. 116 (4), pp. 424–448, 1952.

[5] B. Katz, "Nerve, muscle, and synapse," *McGraw-Hill, London.*, 1966.

[6] K. Kitamura, B. Judkewitz, M. Kano, W. Denk, and M. Husser, "Targeted patch-clamp recordings and single-cell electroporation of unlabeled neurons in vivo," *Nature Methods*, vol. 5, pp. 61–67, 2007.

[7] G. Banker and K. Goslin, eds., *Culturing Nerve Cells.* The MIT Press, 1998.

[8] M. Steriade, "Impact of network activities on neuronal properties in corticothalamic systems," *The Journal of Neurophysiology*, vol. 86(1), pp. 1–39, 2001.

[9] G. Krause, S. Lehmann, M. Lehmann, I. Freund, E. Schreiber, and W. Baumann, "Measurement of electrical activity of long-term mammalian neuronal networks on semiconductor neurosensor chips and comparison with conventional microelectrode arrays," *Biosensors and Bioelectronics*, vol. 21(7), pp. 1272–1282, 2006.

[10] A. Lacmann, D. Hess, G. Gohla, E. Roussa, and K. Krieglstein, "Activity-dependent release of transforming growth factor-beta in a neuronal network in vitro," *Neuroscience*, vol. 150(3), pp. 247–257, 2007.

[11] M. J. Gutnick, B. W. Connors, and D. A. Prince, "Mechanisms of neocortical epileptogenesis invitro," *Journal of Neurophysiology*, vol. 48 (6), pp. 1321–1335, 1982.

[12] A. Kirkwood and M. F. Bear, "Hebbian synapses in visual-cortex," *Journal of Neuroscience*, vol. 14 (3), pp. 1634–1645, 1994.

[13] A. Urazaev, S. Arganda, K. Muller, and C. Sahley, "Lasting changes in a network of interneurons after synapse regeneration and delayed recovery of sensitization," *Neuroscience*, vol. 150(4), pp. 915–925, 2007.

[14] D. Wagenaar, R. Madhavan, J. Pine, and S. Potter, "Controlling bursting in cortical cultures with closed-loop multi-electrode stimulation.," *Journal of Neuroscience*, vol. 25(3), pp. 680–688, 2005.

[15] T. DeMarse, D. Wagenaar, A. Blau, and S. Potter, "The neurally controlled animat: Biological brains acting with simulated bodies," *Autonomous Robots*, vol. 11, pp. 305–310, 2001.

[16] W. Nakamura, S. Honma, T. Shirakawa, and K. Honma, "Clock mutation lengthens the circadian period without damping rhythms in individual scn neurons," *Nature Neuroscience*, vol. 5 (5), pp. 399–400, 2002.

[17] R. M. Fitzsimonds, H. J. Song, Poo, and MM, "Propagation of activity-dependent synaptic depression in simple neural networks," *Nature*, vol. 388 (6641), pp. 439–448, 1997.

[18] B. Dworak, *The Integration and Miniaturisation of the Patch-Clamp Technique into Planar Silicon-based Microstructures for the Electrophysiological Study of Network Behaviour*. PhD thesis, School of Engineering and Electronics, University of Edinburgh, February 2005.

[19] K. Baldwin, *MEMS devices for neuronal recording: Mimicking the Physical Properties of Patch-Clamp Pipettes*. PhD thesis, School of Engineering and Electronics, University of Edinburgh, October 2006.

[20] E. J. Furshpan, P. R. MacLeish, P. H. O'Lague, and D. D. Potter, "Chemical transmission between rat sympathetic neurons and cardiac myocytes developing in microcultures: evidence for cholinergic, adrenegic and dual-function neurons.," *Proceedings of the National Academy of Sciences of the United States of America*, vol. 73, pp. 4225–9, 1976.

[21] J. C. Chang, G. J. Brewer, and B. C. Wheeler, "Modulation of neural network activity by patterning," *Biosensors and Bioelectronics*, vol. 16(7-8), pp. 527–533, 2001.

[22] T. Leng, P. Wu, N. Z. Mehenti, S. F. Bent, M. F. Marmor, M. S. Blumenkranz, and H. A. Fishman, "Direceted retinal nerve cell growth for use in a retinal prosthesis interface.," *Investigative Ophthalmology & Visual Science*, vol. 45(11), pp. 4132–37, 2004.

[23] R. Weis and P. Fromherz, "Frequency dependent signal transfer in neuron transistors," *Physical Review E*, vol. 55, pp. 877–89, 1997.

[24] G. Zeck and P. Fromherz, "Noninvasive neuroelectronic interfacing with synaptically connected snail neurons immobilized on a semiconductor chip," *Proceedings of the National Academy of Sciences*, vol. 98(18), pp. 10457–10462, 2001.

[25] W. A. Franks, *Towards Monolithic CMOS Cell-based Biosensors*. PhD thesis, Swiss Federal Institute of Technology Zurich, 2005.

[26] S. Brittain, K. Paul, X.-M. Zhao, and G. Whitesides, "Soft lithography and microfabrication," *Physics World*, vol. 11, pp. 31–36, 1998.

[27] A. Bernard, E. Delamarche, H. Schmid, B. Michel, H. R. Bosshard, and H. Biebuyck, "Printing patterns of proteins," *Langmuir*, vol. 14(5), pp. 2225–2229, 1998.

[28] M. Mrksich, L. E. Dike, J. Tien, D. E. Ingber, and G. M. Whitesides, "Using microcontact printing to pattern the attachment of mammalian cells to self-assembled monolayers of alkanethiolates on transparent films of gold and silver," *Experimental cell research*, vol. 235, pp. 305–313, 1997.

[29] G. Lopez, H. Biebuyck, R. Harter, A. Kumar, and G. M. Whitesides, "Fabrication and imaging of two-dimensional patterns of proteins adsorbed on self-assembled monolayers by scanning electron microscopy," *Journal of the American Chemical Society*, vol. 115(23), pp. 10774–10781, 1993.

[30] J. C. Chang, G. J. Brewer, and B. C. Wheeler, "A modified microstamping technique enhances polylysine transfer and neuronal cell patterning," *Biomaterials*, vol. 24, pp. 2863–2870, 2003.

[31] R. S. Kane, S. Takayama, E. Ostuni, D. E. Ingber, and G. M. Whitesides, "Patterning proteins and cells using soft lithography," *Biomaterials*, vol. 20, pp. 2363–2376, 1999.

[32] N. E. Sanjana and S. B. Fuller, "A fast flexible ink-jet printing method for patterning dissociated neurons in culture," *Journal of Neuroscience Methods*, vol. 136, pp. 151–163, 2004.

[33] F. Turcu, K. Tratsk-Nitz, S. Thanos, W. Schuhmann, and P. Heiduschka, "Ink-jet printing for micropattern generation of laminin for neuronal adhesion," *Journal of Neuroscience Methods*, vol. 131, pp. 141–148, 2003.

[34] M. P. Maher, J. Pine, J. Wright, and Y.-C. Tai, "The neurochip: a new multielectrode device for stimulating and recording from cultured neurons," *Journal of Neuroscience Methods*, vol. 87, pp. 45–56, 1999.

[35] N. M. Dowell-Mesfin, M.-A. Abdul-Karim, A. M. P. Turner, S. Schanz, H. G. Craighead, B. Roysam, J. N. Turner, and W. Shain, "Topographically modified surfaces affect orientation and growth of hippocampal neurons," *Journal of Neural Engineering*, vol. 2, pp. 78–90, 2004.

[36] S. Britland, C. Perridge, M. Denyer, H. Morgan, A. Curtis, and C. Wilkinson, "Morphogenetic guidance cues can interact synergistically and hierarchically in steering nerve cell growth," *Experimental Biology Online*, vol. 1(2), pp. 1–12, 1996.

[37] Y. W. Fan, F. Z. Cui, S. P. Hou, Q. Y. Xu, L. N. Chen, and I. S. Lee, "Culture of neural cells on silicon wafers with nano-scale surface topograph," *Journal of Neuroscience Methods*, vol. 120(1), pp. 17–23, 2002.

[38] L. Erskine and C. McCaig, "Integrated interactions between chondroitin sulphate proteoglycans and weak dc electric fields regulate nerve growth cone guidance in vitro," *Journal of Cell Science*, vol. 110, pp. 1957–1965, 1997.

[39] R. B. Borgens, "Electrically mediated regeneration and guidance of adult mammalian spinal axons into polymeric channels," *Neuroscience*, vol. 91(1), pp. 251–264, 1999.

[40] T. J. Goodwin, "Physiological and molecular genetic effects of time-varying electromagnetic fields on human neuronal cells," *NASA/TP*, vol. 212054, 2003.

[41] B. Kaehr, R. Allen, D. J. Javier, J. Currie, and J. B. Shear, "Guiding neuronal development with in situ microfabrication," *Proceedings of the National Academy of Sciences*, vol. 101(46), pp. 16104–16108, 2004.

[42] S. Takayama, J. C. McDonald, E. Ostuni, M. N. Liang, P. J. A. Kenis, R. F. Ismagilov, and G. M. Whitesides, "Patterning cells and their environments using multiple laminar fluid flows in capillary networks," *Proceedins of the National Academy of Science, USA*, vol. 96(10), pp. 5545–5548, 1999.

[43] S. Martinoia, M. Bove, M. Tedesco, B. Margesin, and M. Grattarola, "A simple microfluidic system for patterning populations of neurons on silicon micromachined substrates," *Journal of Neuroscience Methods*, vol. 87(1), pp. 35–44, 1999,.

[44] E. Kim, Y. Xia, and G. M. Whitesides, "Polymer microstructures formed by moulding in capillaries," *Nature*, vol. 376(17), pp. 581–584, 1995.

[45] L. Griscom, P. Degenaar, B. LePioufle, E. Tamiya, and H. Fujita, "Techniques for patterning and guidance of primary culture neurons on micro-electrode arrays," *Sensors and Actuators B: Chemical*, vol. 83, pp. 15–21, 2002.

[46] D. Kleinfeld, K. H. Kahler, and P. E. Hockberger, "Controlled outgrowth of dissociated neurons on patterned substrates," *The Journal of Neuroscience*, vol. 8(11), pp. 4098–4120, 1988.

[47] S. Rohr, R. Flckiger-Labrada, and J. P. Kucera, "Photolithographically defined deposition of attachment factors as a versatile method for patterning the growth of different cell types in culture," *Pflgers Archiv European Journal of Physiology*, vol. 446, pp. 125–132, 2003.

[48] J. M. Corey and E. L. Feldman, "Substrate patterning: an emerging technology for the study of neuronal behavior," *Experimental Neurology*, vol. 184, pp. S89–S96, 2003.

[49] C. Wyart, C. Ybert, L. Bourdieu, C. Herr, C. Prinz, and D. Chatenay, "Constrained synaptic connectivity in functional mammalian neuronal networks grown on patterned surfaces," *Journal of Neuroscience Methods*, vol. 117(2), pp. 123–131, 2002.

[50] H. Sorribas, C. Padeste, and L. Tiefenauer, "Photolithographic generation of protein micropatterns for neuron culture applications," *Biomaterials*, vol. 23(3), pp. 893–900, 2001.

[51] D. Falconnet, A. Koenig, F. Assi, and M. Textor, "A combined photolithographic and molecular-assembly approach to produce functional micropatterns for applications in the biosciences," *Advanced Functional Materials*, vol. 14(8), pp. 749–756, 2004.

[52] D. Falconnet, *Molecular-Assembly Patterning by Lift-off at the Micro- and Nanoscale for Applications in the Biosciences*. PhD thesis, Swiss Federal Institute of Technology Zurich, March 2005.

[53] R. Michel, J. W. Lussi, G. Csucs, I. Reviakine, G. Danuser, B. Ketterer, J. A. Hubbell, M. Textor, and N. D. Spencer, "Selective molecular assembly patterning: A new approach to micro- and nanochemical patterning of surfaces for biological applications," *Langmuir*, vol. 18(8), pp. 3281–3287, 2002.

[54] J. W. Lussi, R. Michel, I. Reviakine, D. Falconnet, A. Goessl, G. Csucs, J. A. Hubbell, and M. Textor, "A novel generic platform for chemical patterning of surfaces," *Progress in Surface Science*, vol. 76(3-5), pp. 55–69, 2004.

[55] W. Franks, S. Tosatti, F. Heer, P. Seif, M. Textor, and A. Hierlemann, "Patterned cell adhesion by self-assembled structures for use with a cmos cell-based biosensor," *Biosensors and Bioelectronics*, vol. 22(7), pp. 1426–1433, 2007.

[56] J. P. Trinkaus, *Biology of the Nerve Growth Cone*, ch. Further Thoughts on Directional Cell Movement During Morphogenesis, pp. 1–19. Alan R. Liss, 1985.

[57] M. J. Katz and R. J. Lasek, "Guidance cue patterns and cell migration in multicellular organisms," *Cell Motility and the Cytoskeleton*, vol. 1(1), pp. 141–157, 1980.

[58] P. H. Patterson, *Cellular and molecular biology of neuronal development*, ch. Surface-Bound and Released Neuronal Glycoconjugates, pp. 87–94. Plenum Press, 1984.

[59] F. Collins and J. E. Garrett, "Elongating nerve fibers are guided by a pathway of material released from embryonic nonneuronal cells," *Proceedings of the National Academy of Sciences*, vol. 77(10), pp. 6226–6228, 1980.

[60] P. C. Letourneau, *Neuronal Development*, ch. Nerve Fiber Growth and Its Regulation by Extrinsic Factors, pp. 213–254. Plenum Press, 1982.

[61] W. Ma, Q.-Y. Liu, D. Jung, P. Manos, J. J. Pancrazio, A. E. Schaffner, J. L. Barker, and D. A. Stenger, "Central neuronal synapse formation on micropatterned surfaces," *Developmental Brain Research*, vol. 111(2), pp. 231–243, 1998.

[62] E. R. Kandel, *Principles of Neural Science*. Elsevier Science Publishing Co, 1985.

[63] M. S. Cooper and M. Schliwa, "Electrical and ionic controls of tissue cell locomotion in dc electric fields," *Journal of Neuroscience Research*, vol. 13, pp. 223–244, 1985.

[64] N. Patel, Z. p. Xie, S. Young, and M. m. Poo, "Response of nerve growth cone to focal electric currents," *Journal of Neuroscience Research*, vol. 13, pp. 245–256, 1985.

[65] B. Liu, J. Ma, Q. Xu, and F. Cui, "Regulation of charged groups and laminin patterns for selective neuronal adhesion," *Colloids and Surfaces B: Biointerfaces*, vol. 53(2), pp. 175–178, 2006.

[66] P. Rakic, "Neuronal-glial interaction during brain development," *Trends in Neurosciences*, vol. 4, pp. 184–187, 1981.

[67] A. Bez, E. Corsini, D. Curti, M. Biggiogera, A. Colombo, R. F. Nicosia, S. F. Pagano, and E. A. Parati, "Neurosphere and neurosphere-forming cells: morphological and ultrastructural characterization," *Brain Research*, vol. 993(1-2), pp. 18–29, 2003.

[68] D. V. Nicolau, T. Taguchi, H. Taniguchi, H. Tanigawa, and S. Yoshikawa, "Patterning neuronal and glia cells on light-assisted functionalised photoresists," *Biosensors and Bioelectronics*, vol. 14, pp. 317–325, 1999.

[69] D. V. Nicolau, T. Taguchi, H. Tanigawa, and S. Yoshikawa, "Control of the neuronal cell attachment by functionality manipulation of diazo-naphtho-quinone/novolak photoresist surface," *Biosensors and Bioelectronics*, vol. 11, pp. 1237–1252, 1996.

[70] W. He, C. R. Halberstadt, and K. E. Gonsalves, "Lithography application of a novel photoresist for patterning of cells," *Biomaterials*, vol. 25, pp. 2055–2063, 2004.

[71] E. Delivopoulos, "Patterned cultures of neurons and glia on silicon with the use of lithography and photo-resist materials," Master's thesis, School of Informatics, August 2004.

[72] *Parylene Knowledge Specifications and Properties*, 2007.

[73] E. M. Schmidt, M. J. Bak, and P. Christensen, "Laser exposure of parylene-c insulated microelectrodes," *Journal of Neuroscience Methods*, vol. 62, pp. 89–92, 1995.

[74] S. Takeuchi, D. Ziegler, Y. Yoshida, K. Mabuchi, and T. Suzuki, "Parylene flexible neural probes integrated with microfluidic channels," *Lab chip*, vol. 5, pp. 519–523, 2005.

[75] P. Patino, M. Garcia-Munoz, and C. R. Freed, "Electrophysiology of ventromedial striatal neurons during movement," *Brain Research Bulletin*, vol. 37 (5), pp. 481–486, 1995.

[76] M. Diana, M. Garcia-Munoz, and C. R. Freed, "Wire electrodes for chronic single unit recording of dopamine cells in substantia nigra pars compacta of awake rats," *Journal of Neuroscience Methods*, vol. 21, pp. 71–79, 1987.

[77] A. Tooker, E. Meng, J. Erickson, Y.-C. Tai, and J. Pine, "Biocompatible parylene neurocages," *IEEE Engineering in Medicine and Biology*, 2005.

[78] E. Meng, Y. Tai, J. Erickson, and J. Pine, "Parylene technology for mechanically robust neurocages," *MicroTAS*, pp. 1109–1112, 2003.

[79] Q. He, E. Meng, Y. Tai, C. Rutherglen, J. Erickson, and J. Pine, "Parylene neurocages for live neural networks study," in *12th IEEE International Conference Solid-State Sensors, Actuators and Microsystems*, pp. 995–998, 2003.

[80] T. Stieglitz, S. Kammer, K. Koch, S. Wien, and A. Robitzki, "Encapsulation of flexible biomedical mircoimplants with parylene-c," in *7th Annual Conference of the International Functional Electrical Stimulation Society*, 2002.

[81] K. S. Hwang, J. H. Park, J. H. Lee, D. S. Yoon, T. S. Kim, I. Han, and J. H. Noh, "Effect of atmospheric-plasma treatments for enhancing adhesion of au on parylene-coated protein chips," *Journal of Korean Physical Society*, vol. 44 (5), pp. 1168–1172, 2004.

[82] G. J. Brewer, "Isolation and culture of adult rat hippocampal neurons," *Journal of Neuroscience Methods*, vol. 71, pp. 143–155, 1997.

[83] J. Huettner and R. Baughman, "Primary culture of identified neurons from the visual cortex of postnatal rats," *Journal of Neuroscience*, vol. 6 (10), pp. 3044–3060, 1986.

[84] Y. Nam and B. C. Wheeler, "Imaging locations of neurons vs. glia in low density culture," in *Proceedings of the 2nd International IEEE EMBS, Conference on Neural Engineering, Arlington, Virginia*, 2005.

[85] S. Totterdell, C. A. Ingham, and J. P. Bolam, *Experimental Neuroanatomy, A practial approach*, ch. Immunocytochemistry I: pre-embedding staining, pp. 103–128. Oxford University Press, 1992.

[86] A. Banerjee, M. Roach, K. Wall, M. Lopata, D. Cleveland, and R. Luduea, "A monoclonal antibody against the type ii isotype of β-tubulin. preparation of isotypically altered tubulin," *Journal of Biological Chemistry*, vol. 263, p. 30293034, 1988.

[87] E. Debus, K. Weber, and M. Osborn, "Monoclonal antibodies specific for glial fibrillary acidic (gfa) protein and for each of the neurofilament triplet polypeptides," *Differentiation*, vol. 25(2), pp. 193–203, 1983.

[88] R. P. Haugland, *Handbook of Fluorescent Probes and Research Chemicals*. Molecular Probes, sixth edition ed., 1996.

[89] K. E. Healy, C. H. Thomas, A. Rezania, J. E. Kim, P. J. McKeown, B. Lom, and P. E. Hockberger, "Kinetics of bone cell organization and mineralization on materials with patterned surface chemistry," *Biomaterials*, vol. 17(2), pp. 195–208, 1996.

[90] L. A. Greene, S. E. Farinelli, M. E. Cunnigham, and D. S. Park, *Culturing Nerve Cells*, ch. Culture and Experimental Use of the PC12 Rat Pheochromocytoma Cell Line, pp. 163–164. The MIT Press, 1998.

[91] J. M. Corey, B. C. Wheeler, and G. J. Brewer, "Micrometer resolution silane-based patterning of hippocampal neurons: Critical variables in photoresist and laser ablation processes for substrate fabrication," *IEEE Transactions on Biomedical Engineering*, vol. 43(9), pp. 944–955, 1996.

[92] L. Lauer, C. Klein, and A. Offenhusser, "Spot compliant neuronal networks by structure optimized micro-contact printing," *Biomaterials*, vol. 22(13), pp. 1925–1932, 2001.

[93] S. Britland, H. Morgan, B. Wojiak-Stodart, M. Riehle, A. Curtis, and C. Wilkinson, "Synergistic and hierarchical adhesive and topographical guidance of bhk cells," *Experimental cell research*, vol. 228, pp. 313–325, 1996.

[94] K. McCarthy and L. Partlow, "Preparation of pure neuronal and non-neuronal cultures from embryonic chick sympathetic ganglia: A new method based on both differential cell adhesiveness and the formation of homotypic neuronal aggregates," *Brain Research*, vol. 114(3), pp. 391–414, 1976.

[95] C. D. McFarland, C. H. Thomas, C. DeFilippis, J. G. Steele, and K. E. Healy, "Protein adsorption and cell attachment to patterned surfaces," *Journal of Biomedical Material Research*, vol. 49, pp. 200–210, 2000.

[96] J. C. Chang, G. J. Brewer, and B. C. Wheeler, "Neuronal network structuring induces greater neuronal activity through enhanced astroglial development," *Journal of Neural Engineering*, vol. 3, pp. 217–226, 2006.

[97] Y. Nam, D. W. Branch, and B. C. Wheeler, "Epoxy-silane linking of biomolecules is simple and effective for patterning neuronal cultures," *Biosensors and Bioelectronics*, vol. 22(5), pp. 589–597, 2006.

[98] D. W. Branch, B. C. Wheeler, G. J. Brewer, and D. E. Leckband, "Long-term stability of grafted polyethylene glycol surfaces for use with microstamped substrates in neuronal cell culture," *Biomaterials*, vol. 22, pp. 1035–1047, 2001.

[99] T. Wallace and E. Johnson, "Cytosine arabinoside kills postmitotic neurons: evidence that deoxycytidine may have a role in neuronal survival that is independent of dna synthesis," *Journal of Neuroscience*, vol. 9, pp. 115–124, 1989.

[100] M. Bera, A. Rivaton, C. Gandon, and J. L. Gardette, "Photooxidation of poly(para-xylylene)," *European Polymer Journal*, vol. 36, pp. 1753–1764, 2000.

[101] M. Bera, A. Rivaton, C. Gandon, and J. L. Gardette, "Comparison of the photodegradation of parylene c and parylene n," *European Polymer Journal*, vol. 36, pp. 1765–1777, 2000.

[102] J. B. Fortin and T. M. Lu, "Ultraviolet radiation induced degradation of poly-para-xylylene (parylene) thin films," *Thin Solid Films*, vol. 397, pp. 223–228, 2001.

[103] K. G. Pruden, K. Sinclair, and S. Beaudoin, "Characterization of parylene-n and parylene-c photooxidation," *Journal of Polymer Science: Part A: Polymer Chemistry*, vol. 41, pp. 1486–1496, 2003.

[104] A. Welle and E. Gottwald, "Uv-based patterning of polymeric substrates for cell culture applications," *Biomedical Microdevices*, vol. 4:1, pp. 33–41, 2002.

[105] M. Pierschbacher and E. Ruoslahti, "The cell attachment activity of fibronectin can be duplicated by small synthetic fragments of the molecule," *Nature*, vol. 309, pp. 30–33, 1984.

[106] F. Grinnell and M. K. Feld, "Fibronectin adsorption on hydrophilic and hydrophobic surfaces detected by antibody binding and analyzed during cell adhesion in serum-containing medium," *The journal of biogical chemistry*, vol. 259(9), pp. 4888–4893, 1982.

[107] B. G. Keselowsky, D. M. Collard, and A. J. Garcia, "Surface chemistry modulates fibronectin conformation and directs integrin binding and specificity to control cell adhesion," *Journal of Biomedical Material Research*, vol. 66A, pp. 247–259, 2003.

[108] A. Garcia, P. Ducheyne, and D. Boettiger, "Effect of surface reaction stage on fibronectin-mediated adhesion of osteoblast-like cells to bioactive glass," *Journal of Biomedical Material Research*, vol. 40, pp. 48–56, 1998.

[109] A. Garcia, M. Vega, and D. Boettiger, "Modulation of cell proliferation and differentiation through substrate-dependent changes in fibronectin conformation," *Molecular Biology of the Cell*, vol. 10(3), pp. 785–798, 1999.

[110] S. N. Stephansson, B. A. Byers, and A. J. Garcia, "Enhanced expression of the osteoblastic phenotype on substrates that modulate fibronectin conformation and integrin receptor binding," *Biomaterials*, vol. 23, pp. 2527–2534, 2002.

[111] R. O. Hynes, "Integrins: Versatility, modulation and signaling in cell adhesion," *Cell*, vol. 69(1), pp. 11–25, 1992.

[112] M. Bale, L. Wohlfahrt, D. Mosher, B. Tomasini, and R. Sutton, "Identification of vitronectin as a major plasma protein adsorbed on polymer surfaces of different copolymer composition.," *Blood*, vol. 74, pp. 2698–2706, 1989.

[113] C. H. Thomas, C. D. McFarland, M. L. Jenkins, A. Rezania, J. G. Steele, and K. E. Healy, "The role of vitronectin in the attachment and spatial distribution of bone-derived cells on materials with patterned surface chemistry," *Journal of Biomedical Material Research*, vol. 37, pp. 81–93, 1997.

[114] D. Arcos, D. C. Greenspan, and M. Vallet-Regi, "A new quantitative method to evaluate the in vitro bioactivity of melt and sol-gel-derived silicate glasses," *Journal of Biomedical Materials Research Part A*, vol. 65A(3), pp. 344 – 351, 2003.

[115] W. J. Parak, M. George, M. Kudera, H. E. Gaub, and J. C. Behrends, "Effects of semiconductor substrate and glia-free culture on the development of voltage-dependent currents in rat striatal neurons," *European Biophysics Journal*, vol. 29, pp. 607–620, 2001.

[116] M. Nakajima, T. Ishimuro, K. Kato, I.-K. Ko, I. Hirata, Y. Arima, and H. Iwata, "Combinatorial protein display for the cell-based screening of biomaterials that direct neural stem cell differentiation," *Biomaterials*, vol. 28(6), pp. 1048–1060, 2006.

[117] T. Rabilloud, L. Vuillard, C. Gilly, and J. Lawrence, "Silver-staining of proteins in polyacrylamide gels: a general overview," *Cellular and Molecular Biology*, vol. 40, pp. 57–75, 1994.

[118] G. K. Toworfe, R. J. Composto, C. S. Adams, I. M. Shapiro, and P. Ducheyne, "Fibronectin adsorption on surface-activated poly(dimethylsiloxane) and its effect on cellular function," *Journal of Biomedical Material Research*, vol. 71A (3), pp. 449–461, 2004.

[119] J.-L. Dewez, A. Doren, Y.-J. Schneider, and P. G. Rouxhet, "Competitive adsorption of proteins: Key of the relationship between substratum surface properties and adhesion of epithelial cells," *Biomaterials*, vol. 20, pp. 547–559, 1999.

[120] J.-L. Dewez, J.-B. Lhoest, E. Detrait, V. Berger, C. Dupont-Gillain, L.-M. Vincent, Y.-J. Schneider, P. Bertrand, and P. Rouxhet, "Adhesion of mammalian cells to polymer surfaces: from physical chemistry of surfaces to selective adhesion on defined patterns," *Biomaterials*, vol. 19, pp. 1441–1445, 1998.

[121] D. Teare, N. Emmison, C. Ton-That, and R. H. Bradley, "Effects of serum on the kinetics of cho attachment to ultraviolet-ozone modified polystyrene surfaces," *Journal of Colloid and Interface Science*, vol. 234, pp. 84–89, 2001.

[122] J. I. Jones and D. R. Clemmons, "Insulin-like growth factors and their binding proteins: Biological actions," *Endocrine Reviews*, vol. 16(1), pp. 3–34, 1995.

[123] J. Chinn, T. Horbett, and B. Ratner, "Baboon fibrinogen adsorption and platelet adhesion to polymeric materials," *Journal of thrombosis and haemostasis*, vol. 65, pp. 608–617, 1991.

[124] K. Healy, B. Lom, and P. Hockberger, "Spatial distribution of mammalian cells dictated by material surface chemistry," *Biotechnology and Bioengineering*, vol. 43, pp. 792–800, 1994.

[125] S.-M. Kim, J.-S. Lee, Y.-H. Lee, W.-J. Kim, S.-I. Do, Y.-K. Cho, and Y.-I. Park, "Increased a2,3-sialylation and hyperglycosylation of n-glycans in embryonic rat cortical neurons during camptothecin-induced apoptosis," *Mollecules and Cells*, vol. 24(3), pp. 416–423, 2007.

[126] D. K. Macario, I. Entersz, D. Bolikal, J. Kohn, and G. B. Nackman, "Iodine inhibits antiadhesive effect of peg: Implications for tissue engineering," *Journal of Biomedical Materials Research Part B: Applied Biomaterials*, vol. Online, 2007.

[127] M.-A. Glasier, A. Keech, H. Sheardown, L. N. Subbaraman, and L. Jones, "Conformational and quantitative characterization of lysozyme extracted from galyfilcon and senofilcon silicone hydrogel contact lenses," *Current eye research*, vol. 33(1), pp. 1–11, 2008.

[128] P. Kubn and P. C. Hausera, "High-performance liquid chromatography with contactless conductivity detection for the determination of peptides and proteins using a monolithic capillary column," *Journal of Chromatography A*, vol. 1176, pp. 185–191, 2007.

[129] V. Manyanga, O. Grishina, Z. Yun, J. Hoogmartens, and E. Adams, "Comparison of liquid chromatographic methods with direct detection for the analysis of gentamicin," *Journal of Pharmaceutical and Biomedical Analysis*, vol. 45(2), pp. 257–262, 2007.

[130] A. Sethuraman, M. Han, R. S. Kane, and G. Belfort, "Effect surface wettability on the adhesion of proteins," *Langmuir*, vol. 20, pp. 7779–7788, 2004.

[131] C. R. Jenney and J. M. Anderson, "Adsorbed serum proteins responsible for surface dependent human macrophage behavior," *Journal of Biomedical Materials Research*, vol. 49(4), pp. 435–447, 1999.

[132] C. L. Gladson, J. E. StewartJr, M. A. Olman, P.-L. Chang, L. M. Schnapp, J. R. Grammer, and E. N. Benveniste, "Attachment of primary neonatal rat astrocytes to vitronectin is mediated by integrins $\alpha v\beta 5$ and $\alpha 8\beta 1$: modulation by the type 1 plasminogen activator inhibitor," *Neuroscience Letters*, vol. 283(2), pp. 157–161, 2000.

[133] M. Buhusi, B. R. Midkiff, A. M. Gates, M. Richter, M. Schachner, and P. F. Maness, "Close homolog of l1 is an enhancer of integrin-mediated cell migration," *Journal of Biological Chemistry*, vol. 278(27), pp. 25024–25031, 2003.

[134] D. Fabrizius-Homan and S. Cooper, "A comparison of the adsorption of three adhesive proteins to biomaterial surfaces," *Journal of Biomaterials Science (Polymer edition)*, vol. 3(1), pp. 27–47, 1992.

[135] K. R. Fath, C.-J. S. Edgell, and K. Burridge, "The distribution of distinct integrins in focal contacts is determined by the substratum composition," *Journal of Cell Science*, vol. 92, pp. 67–75, 1989.

[136] J. G. Steele, G. Johnson, and A. Underwood, "Role of serum vitronectin and fibronectin in adhesion of fibroblasts following seeding onto tissue culture polystyrene," *Journal of Biomedical Materials Research*, vol. 26(7), pp. 861–884, 1991.

[137] M. T. Bernards and S. Jiang, "Ph-induced conformation changes of adsorbed vitronectin maximize its bovine aortic endothelial cell binding ability," *Journal of Biomedical Materials Research Part A*, vol. Online, 2008.